U.PORTO

DOUTORAMENTO

BIOLOGIA MOLECULAR E CELULAR

Functional characterization of the microtubule motor dynein in the *C. elegans* epidermis

Cátia Vieira de Carvalho

D

2024

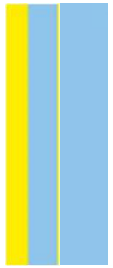

U.PORTO

Cátia Vieira de Carvalho . Functional characterization of the microtubule motor dynein in the *C. elegans* epidermis

D.ICBAS **2024**

Functional characterization of the microtubule motor dynein in the *C. elegans* epidermis

Cátia Filipa Vieira de Carvalho

INSTITUTO CIÊNCIAS BIOMÉDICAS ABEL SALAZAR

FACULDADE DE CIÊNCIAS

CÁTIA FILIPA VIEIRA DE CARVALHO

Functional characterization of the microtubule motor dynein in the *C. elegans* epidermis

Tese de Candidatura ao grau de Doutor em Biologia Molecular e Celular submetida ao Instituto de Ciências Biomédicas Abel Salazar da Universidade do Porto.

Orientador – Doutor Reto Gassmann

Categoria – Investigador Principal

Afiliação – i3S – Instituto de Investigação e Inovação em Saúde, Universidade do Porto

Coorientador – Doutor Daniel José da Costa Barbosa

Categoria – Professor Auxiliar

Afiliação – Unidade de Investigação em Toxicologia e Uma Só Saúde (1H-Toxrun) – Instituto Universitário de Ciências da Saúde (IUCS) - CESPU

The PhD Program and Institutions involved in the development of this thesis work are:

IBMC – Instituto de Biologia Molecular e Celular

I3S – Instituto de Investigação e Inovação em Saúde, Universidade do Porto

Cell Division Mechanisms

Rua Alfredo Allen, 208

4200-135 Porto, Portugal

www.i3s.up.pt

Funding Institutions

This work was funded by:

- The European Research Council under the European Union's Seventh Framework Programme (ERC-2013-StG-338410-DYNEINOME).
- The Fundação para a Ciência e a Tecnologia (FCT)/ Ministério da Ciência, Tecnologia e Ensino Superior (PTDC/BIA-CEL/1321/2021).
- Support from tuition fees was also provided by the academic institution ICBAS – Instituto de Ciências Biomédicas Abel Salazar da Universidade do Porto.
- Cátia Carvalho is supported by an FCT PhD fellowship (SFRH/BD/144877/2019).
- Reto Gassmann is supported by FCT Principal Investigator positions (CEECIND/00333/2017).
- Daniel J. Barbosa is supported by an FCT Junior Researcher position (DL57/2016/CP1355/CT0007).

No competing financial interests

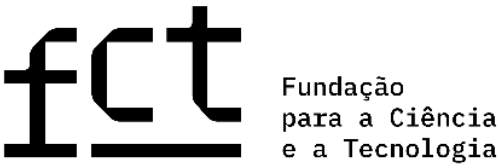

Declaração de Honra

Declaro que a presente tese é de minha autoria e não foi utilizada previamente noutro curso ou unidade curricular, desta ou de outra instituição. As referências a outros autores (afirmações, ideias, pensamentos) respeitam escrupulosamente as regras da atribuição, e encontram-se devidamente indicadas no texto e nas referências bibliográficas, de acordo com as normas de referenciação. Tenho consciência de que a prática de plágio e auto-plágio constitui um ilícito académico.

Porto, May de 2024

"The only true wisdom is in knowing you know nothing"

Socrates

Agradecimentos/ Acknowledgements

A todos os que acreditaram antes de eu acreditar e a todos os que me fizeram companhia no caminho. Foi menos solitário graças a vocês – o meu obrigada!

Firstly, I would like to thank my supervisor Reto Gassmann. I was lucky to be guided by a truly curious scientist who allowed me to be one too. I am grateful for his enthusiasm and ideas, for his understanding, confidence and optimism. I sincerely wish him all the best that life and science can bring.

I thank my co-supervisor, Daniel Barbosa. From the beginning, I have been following his advice to better navigate this challenge. I thank him for the enthusiasm and precious example of dedication that will accompany me throughout my life.

Everyone from the Cell Division Mechanisms and Cytoskeleton Dynamics labs:
To Ana X. Carvalho, I thank her for the enthusiasm and trust. I am very grateful for it.
To Daniel Osório, Marta Silva, Fun Y. Chang, Hélder Rocha, and Vanessa Ferreira, I thank for all daily stories that filled my days with laughter and joy. To Matilde Moreira, and Mariana Sousa, “my” first students: they were the reason I re-learnt so many things. I wish them an happy and successful future!
To my dear *alumnni* colleagues: Cláudia Pereira, Tânia Silva, Rita Reis, Bernardo Gama, Patricia Simões, Adriana Mendes, Filipa Sobral and Inês Santos, I thank them for always keeping in touch.

To the Dantas lab - Tiago Dantas, Carla Abreu, Diogo Rodrigues, the *Twins*, and Tiago Xavier. I am thankfull for their support and enthusiasm. I hope they all succeed in science and in life. Dynein-2 rocks!

I thank to Luís Cirnes, my past molecular biology teacher and now my dear friend. I am truly gratefull for his teachings and I truly admire his profound sense of mission that I intend to honour, obrigada!

I will always be grateful to Ricardo Celestino, the man who trusted me enough to bring me to this lab. His mentorship through these years, professionally and personally, made me

capable of larger dreams and gave me confidence to fight for them. I will always celebrate his victories and be there as his female "*male friend*" from Guimarães.

I thank Beatriz Dias for the friendship and enthusiasm that she always showed. I admire her courage and I deeply missed her company on the long lab hours during these last years.

I want to acknowledge my unwritten *et al*, Vanessa Teixeira. We did this together by sharing more coffees that I can count, while growing and blooming. I am grateful that I was gifted with such a tuned partner to accompany me during this time. I wish to see her suceed in the life that she aspires, obrigada!

Estou grata aos meus queridos amigos: Catarina Machado, Ana Claúdia Gomes, Francisca Silva, João Paulo Fernandes, João Paulo Salgado, João Monteiro, Pedro Simões. Agradeço-lhes a motivação, apoio e paciência. É com eles que eu quero festejar todas as alegrias da minha vida e é também com eles que eu conto nos dias mais negros. Obrigada por tudo.

Agradeço aos meus avós, aos meus primos e primas, e restantes familiares: a riqueza dos percursos deles enriquece todos os dias os meus sonhos e a minha vida. Estou-lhes muito grata pela companhia, amizade e ajuda em todos os momentos. Espero tê-los em todos os momentos da minha vida.

Resta agradecer ao meu Pai e à minha Mãe, Manuel Carvalho e Ana Maria Vieira. Eles são a maior sorte da minha vida e não posso esquecer todos os sacríficios que fizeram para que eu chegasse aqui. Agradeço-lhes o amor e apoio em todas as coisas que eu faço. Tenho muito orgulho em ser tão parecida com eles (*até nos defeitos*).
Agradecer ao meu querido Irmão, Tiago Miguel: ser irmã dele é um privilégio, assistir ao esforço e dedicação que investe em fazer melhor inspira-me a fazer o mesmo. Iremos, *a discutir claro*, juntos para todos os desafios da vida.

Termino a agradecer ao Tiago Macedo: meu companheiro de todas as horas, minha primeira chamada nas boas e nas más notícias, minha gargalhada de todos os dias. Obrigada por me motivares e me apoiares em todos os momentos desta tese. Depois de dois doutoramentos, acho que estamos prontos para mais *desaf*…férias!

A todos, o meu mais sincero obrigada!

Peer Reviewed Publications

A tese de Doutoramento aqui apresentada é uma compilação de resultados, parte dos quais se encontram publicados ou em fase de preparação para submissão em revistas internacionais indexadas. O autor declara que teve participação ativa na conceção e execução dos trabalhos que estiveram na origem das publicações referidas, assim como na sua análise, interpretação, discussão e redação.

Faz parte integrante desta tese o seguinte artigo já publicado:

Cátia Carvalho, Daniel J Barbosa, Ricardo Celestino, Esther Zanin, Ana Xavier Carvalho, Reto Gassmann (2024). *Dynein directs prophase centrosome migration to control the stem cell division axis in the developing C. elegans epidermis*. Genetics. iyae005. doi: 10.1093/genetics/iyae005

The Doctoral thesis here presented is a compilation of data, part of which were already published or are in the process of preparation to submission for publication in international peer-reviewed journals. The author declares that he had an active role in the conception and execution of the experiments that originated the referred publications, as well as in their analysis, interpretation, discussion, and writing.

The following already published article has been included in this thesis:

Cátia Carvalho, Daniel J Barbosa, Ricardo Celestino, Esther Zanin, Ana Xavier Carvalho, Reto Gassmann (2024). *Dynein directs prophase centrosome migration to control the stem cell division axis in the developing C. elegans epidermis*. Genetics. iyae005. doi: 10.1093/genetics/iyae005

Resumo

A dineína citoplasmática 1 (dineína), o principal complexo motor que se move na direção da extremidade negativa dos microtúbulos em animais, é responsável pelo transporte de diversas cargas. A dineína está envolvida numa vasta gama de funções celulares, incluindo atividades cruciais na divisão celular e transporte de endossomas. Um aspeto consistente das suas diversas funções envolve a capacidade da dineína de se ancorar, utilizando distintas proteínas adaptadoras, em membranas. Uma vez ancorada, a dineína gera a força necessária para facilitar o posicionamento e a mobilidade de organelos e estruturas celulares complexas, como o fuso mitótico. Este papel central torna a dineína virtualmente essencial para todos os processos celulares que envolvem transporte em microtúbulos.

Na divisão celular, a dineína é fundamental para a separação dos centrossomas na prófase e para o subsequente posicionamento e orientação do fuso mitótico. Embora extensivamente estudada em embriões de *C. elegans*, o papel da dineína noutras fases do desenvolvimento permanece pouco claro. Neste trabalho, utilizei um mutante hipomórfico da dineína para explorar o seu papel no desenvolvimento pós-embrionário da epiderme. Este processo envolve várias rondas de divisões celulares semelhantes às das células estaminais, com distribuição assimétrica de determinantes de destino celular. Esta assimetria resulta na diferenciação e fusão das células-filhas anteriores das células *seam* com o sincício hyp7, enquanto as células-filhas posteriores mantêm a identidade das células *seam*. O desenvolvimento da epiderme termina durante o estadio L4, quando as células *seam* formam um sincício. Microscopia em tempo-real da última ronda de divisões das células *seam* mostra que as células mutantes separam os centrossomas, mas frequentemente falham em os alinhar corretamente com o eixo da fila de células, causando defeitos na posição das células-filhas, citocinese anormal e distribuição anormal dos determinantes de destino celular. Os animais mutantes apresentam interrupções no sincício, uma cutícula permeável e um tempo de vida mais curto devido à sua rutura espontânea após atingirem a idade adulta. Durante estas divisões, a dineína guia a orientação do fuso mitótico através da via GOA-1$^{G\alpha i}$-LIN-5^{NuMA}, influenciando o movimento dos centrossomas ao longo do eixo anterior-posterior da célula. Alongar as células resultou numa correção parcial do desalinhamento do fuso mitótico, o que indica que a dineína e a forma da célula, em conjunto, conduzem à divisão correta destas células estaminais. De um modo geral, o papel da dineína na orientação dos centrossomas assegura o comprometimento das células com o seu destino celular e a integridade da epiderme durante as divisões assimétricas.

A dineína também é fundamental para o transporte de diversas cargas, incluindo vários compartimentos endomembranares, e depende de proteínas adaptadoras para o fazer. Os adaptadores da família Hook desempenham um papel crucial no recrutamento da dineína para os endossomas iniciais, tanto nos fungos como nas células humanas. Para tal, formam um complexo com as proteínas FTS e FHIP, referido como complexo FHF. Este complexo, por sua vez, liga-se a proteínas de Rab5 ligadas à membrana dos endossomas. No entanto, em *C. elegans*, a proteína ZYG-12, com os domínios Hook e KASH, foi previamente compreendida como recrutando apenas a dineína para o envelope nuclear, particularmente em células germinativas e no embrião. Este recrutamento depende de uma interação entre o domínio KASH na proteína ZYG-12 e de uma proteína da membrana nuclear interna SUN-1. Neste trabalho, eu revelo um novo papel para a ZYG-12, distinto da sua função anteriormente conhecida no envelope nuclear. Especificamente nas células epiteliais, a ZYG-12 faz parte do complexo FHF. A deleção de uma região C-terminal conservada antes do domínio KASH não afeta o papel da ZYG-12 no envelope nuclear, mas impede completamente o seu recrutamento para os endossomas iniciais. Além disso, mutações em motivos conservados revelam a importância da interação da ZYG-12 com FTS e FHIP. Este estudo identifica elementos moleculares cruciais responsáveis pelo recrutamento da dineína para os endossomas iniciais.

Em resumo, o trabalho desta tese resultou em dois resultados principais: primeiro, a construção de um mutante hipomórfico da dineína permitiu um estudo abrangente sobre o impacto da orientação do fuso mitótico durante as divisões de células estaminais no contexto da morfogénese de tecidos. Em segundo lugar, a caraterização de um novo papel para a ZYG-12 em células epiteliais, nomeadamente no recrutamento dos endossomas iniciais através do complexo FHF.

Palavras-Chave: Dineína; Divisão Celular Assimétrica; Orientação Fuso Mitótico; Transporte nos Microtubulos; Endosomas; ZYG-12; Proteínas Hook

Abstract

Cytoplasmic dynein 1 (dynein), the main microtubule minus-end directed motor in animals, transports diverse cargo. Dynein is involved in a wide range of cellular functions, including crucial activities in cell division and endosome transport. A consistent aspect of its diverse functions involves dynein's capacity to anchor itself, utilizing numerous adaptor proteins, onto membranes. Once anchored, dynein generates the necessary force facilitating the positioning and mobility of endosomes and intricate cellular structures like the mitotic spindle. This central role renders dynein virtually essential for all cellular processes involving microtubule-based transport.

In cell division, dynein is critical for centrosome separation in prophase and subsequent positioning and orientation of the mitotic spindle. While extensively studied in *C. elegans* embryos, dynein's role at other developmental stages remains unclear. I used a hypomorphic dynein mutant to explore its role in postembryonic epidermal development. This process involves several rounds of stem cell-like divisions, in which the uneven distribution of cell fate determinants results in the differentiation and fusion of anterior seam cell daughters with the hyp7 syncytium, while posterior daughters retain seam cell identity. Epidermal development concludes at the L4 stage, when the seam cells form a syncytium. Live imaging of the last round of seam cell divisions showed that the mutant cells separate centrosomes but frequently fail to align them properly with the seam cell row axis, resulting in mis-oriented division. This caused misplacement of daughter cells, abnormal cytokinesis, and abnormal distribution of cell fate determinants. Mutant animals exhibited gaps in the syncytium, a permeable cuticle, and a shorter lifespan due to spontaneous rupture shortly after reaching adulthood. I showed that dynein guides spindle orientation via the cortical GOA-1$^{G\alpha i}$–LIN-5^{NuMA} pathway, influencing centrosome movement along the cell anterior-posterior axis. Elongating cells partly corrected spindle misalignment, indicating that dynein and cell shape together drive correct division of stem cells. Overall, dynein's role in orienting centrosomes ensures proper cell fate and epidermal tissue integrity during asymmetric divisions.

Dynein is also critical to transport diverse cargo, including various endomembrane compartments, and relies on adaptor proteins to do it. The Hook family adaptors play a crucial role in recruiting dynein to early endosomes in both fungi and human cells. They accomplish this by forming a complex with FTS and FHIP, referred to as the FHF complex. This complex, in turn, binds to membrane-bound Rab5. However, in *C. elegans*, the Hook and KASH domain protein ZYG-12 was previously understood to solely recruit dynein to the nuclear envelope in the germline and early embryo. This recruitment relies on the interaction

between the KASH domain and the inner nuclear membrane protein SUN-1. In this thesis I describe a new role for ZYG-12, distinct from its function at the nuclear envelope. Specifically, I show that in epithelial cells, ZYG-12 is part of the FHF complex. Deleting a conserved C-terminal region before the KASH domain doesn't impact ZYG-12's role at the nuclear envelope but completely impedes its recruitment to early endosomes. Moreover, mutation of conserved motifs reveals the importance of ZYG-12's interaction with FTS and FHIP. This study identifies crucial molecular elements responsible for recruiting dynein to early endosomes.

In summary, the work in this thesis resulted in two main achievements: first, the construction of a hypomorphic dynein mutant facilitated a comprehensive study on the importance of spindle orientation for stem-like cell divisions in the context of tissue morphogenesis. Second, the characterization of a novel role for ZYG-12 in epithelia, namely in dynein recruitment to early endosomes via the FHF complex.

Keywords: Dynein; Asymmetric Cell Division; Spindle Orientation; Microtubule Transport; Early Endosomes; ZYG-12

Table of Contents

List of Figures

List of Supplementary Figures

List of Tables

List of Abbreviations

AB	Anterior Blastomere
ACD	Asymmetric Cell Divison
APC	Adenomatous Polyposis Coli Protein
aPKC	Atipical Protein Kinase C
ATP	Adenosine Triphosphate
BICD	Bicaudal D
CC	Coiled-Coil
CGC	Caenorhabditis Genetics Center
CRISPR	Clustered Regularly Interspaced Short Palindromic Repeats
cryo-EM	Cryogenic Electron Microscopy
DHC	Dynein Heavy Chain
DIC	Dynein Intermediate Chain
DLC	Dynein Light Chain
Dlg	Discs Large
DLIC	Dynein Light Intermediate Chain
DNA	Deoxyribonucleic Acid
DTT	Dithiothreitol
EEA-1	Early Endosome Antigen-1
FHF	FTS/Hook/FHIP Complex
FHIP	FHF Complex Subunit HOOK-Interacting Protein
FRAP	Fluorescence Recovery After Photo Bleaching
FTS	Fused Toes
GAP	GPTase-Activating Proteins
GDP	Hydrolyzing Guanosine Diphosphate
GEF	Guanine Nucleotide Exchange Factors
GFP	Green Fluorescent Protein
GPR-1/2	G-Protein Regulators 1 And 2
GSC	Germline Stem Cells
GTP	Hydrolyzing Guanosine Triphosphate
HEPES	N-2-Hydroxyethylpiperazine-N-2-Ethane Sulfonic Acid
ICD	Intercoiled Domain
INM	Inner Nuclear Membrane

IPTG	Isopropyl B- D-1-Thiogalactopyranoside
IRB	Isothermal Reaction Buffer
JIP	JNK-Interacting Protein
LB	Luria Broth
LGN	Leucine Glycine Asparagine
LIN-5	Abnormal Cell Lineage 5
LINC	Linker of Nucleoskeleton and Cytoskeleton
MAP	Microtubule Associated Protein
mCh	mCherry
mNG	mNeonGreen
MosSCI	Mos1-Mediated Single Copy Insertion
mRNA	Messenger Ribonucleic Acid
MT	Microtubules
MTBD	Microtubule-Binding Domain
MTOC	Microtubule Organizing Centers
Mud	Mushroom Body Defective
NAD	Nicotinamide Adenine Dinucleotide
NAD	Nicotinamide Adenine Dinucleotide
NE	Nuclear Envelope
NEB	Nuclear Envelope Breakdown
NGM	Nematode Growth Medium
NIN/L	Ninein/Ninein-Like
NUDE/L	Nuclear Distribution Protein E/ Like
NuMA	Nuclear Mitotic Apparatus Protein
ONM	Outer Nuclear Membrane
PAR	Partitioning-Defective Proteins
PCR	Polymerase Chain Reaction
PEG	Polyetylenoglycol
PH	Pleckstrin Homology
Rab	Ras-Related Protein in Brain
RFIP3	Rab11 Family-Interacting Protein 3
RILP	Rab-Interacting Lysosomal Protein
RNAi	RNA Interference
RNP	Ribonucleiproteins
ROI	Region Of Interest
rpm	Revolutions Per Minute

SDS-PAGE	Sodium Dodecyl Sulfate – Polyacrylamide Gel Electrophoresis
SEM	Standard Error of the Mean
sgRNA	Single Guide RNA
SMN1	Survival Motor Neuron Gene 1
SMN1	Survival Motor Neuron Gene 1
SOC	Super Optimal Broth with Catabolite Repression
TagRFP	Tag Red Fluorescent Protein
TIRF	Time-Lapse Total Internal Reflection Fluorescence
TRAK	Trafficking Kinesin-Binding Protein
UTR	Untranslated Region
UV	Ultraviolet
v	Volume
w	Weight
WT	Wild-Type
γ-TuRC	Γ-Tubulin Ring Complex

Thesis Outline

Dynein's multifaceted functions requires regulation by numerous cofactors and cargo adaptors. This thesis delves into the roles and regulation of dynein across five chapters, examining its functions in an epithelial tissue within two distinct contexts: asymmetrical cell division and endosome transport.

Chapter I introduces the significance of the microtubule motor dynein, providing an overview of dynein functions. In particular, the mechanisms that underly dynein regulation during asymmetrical cell division and endosome trafficking are discussed.

Chapter II defines the aims of the thesis.

Chapter III includes a peer-reviewed published study, where the relevance of dynein for asymmetrical stem cell-like divisions was explored in *C. elegans* seam cells. In this study, I showed that cortical dynein orients the mitotic spindle by directing the migration of prophase centrosomes along the anterior–posterior axis and demonstrate the importance of oriented division for epidermal morphogenesis, including cell fate decisions.

Chapter IV contains unpublished results pertaining to the molecular mechanisms governing dynein recruitment to early endosomes in the *C. elegans* epidermis, which requires a conserved C-terminal domain in the Hook protein ZYG-12.

Chaper V concludes this thesis by providing an overview of its scientific contributions and discussing future directions.

Chapter I. General Introduction

The Microtubule Cytoskeleton and Dynein

Microtubules and associated proteins

Microtubules (MTs) are one of the three classes of cytoskeletal filaments present in eukaryotic cells, together with actin filaments and intermediate filaments (Pollard & Goldman, 2018). Microtubules play a crucial role in numerous cellular activities: they provide structural support, form the mitotic spindle that segregates chromosomes during cell division (Valdez *et al.*, 2023), act as pathways for the movement and positioning of various cellular organelles (Barlan & Gelfand, 2017), and contribute to the regulation of cell polarity and morphogenesis by facilitating the intracellular distribution of proteins and mRNA. Mutations associated with the microtubule cytoskeleton are associated with neurodevelopmental and neurodegenerative diseases such as lissencephaly, epilepsy and polymicrogyria (Maday *et al.*, 2014).

Structurally, microtubules are cylindrical long hollow tubulin polymers of approximately 25 nanometres in outer diameter. Tubulin is a heterodimer of two closely related polypeptides, α- and β-tubulin (Goodson & Jonasson, 2018). The hollow tubes are formed by approximately 13 linear protofilaments, associated laterally and closed into a hollow core. These protofilaments are composed of arrays of tubulin dimers and, consequently, microtubules are polarized structures with two distinct ends: slowly dynamic minus-ends with exposed α-tubulin, and highly dynamic plus-ends with exposed β-tubulin, that grow and shrink through a process called dynamic instability (Goodson & Jonasson, 2018).

Dynamic instability is a process in which microtubules undergo rapid cycles of assembly and disassembly. At the plus-end, once a new heterodimer is added, free β-tubulin acts as a GTPase, binding and hydrolysing guanosine triphosphate (GTP) into guanosine diphosphate (GDP) after being incorporated into the microtubule lattice (Goodson & Jonasson, 2018). However, the hydrolysis of GTP weakens the binding affinity between neighbouring tubulins, promoting depolymerization and leading to the dynamic behaviour observed in microtubules (Goodson & Jonasson, 2018). Rapid disassembly of the microtubule is termed catastrophe, which can be followed by a transition to a growing state, termed rescue (Goodson & Jonasson, 2018). The persistent growth of microtubules is thought to depend on a stabilizing cap of GTP tubulin at the microtubule plus-end (Goodson & Jonasson, 2018). Generation of new microtubules relies on specialized nucleation machinery associated with γ-tubulin, called the γ-tubulin ring complex (γ-TuRC) (Goodson & Jonasson, 2018). This complex is typically enriched at specialized sites known as microtubule organizing centres (MTOCs) (Thawani & Petry, 2021). In animal cells, the

most relevant MTOC is the centrosome, which is usually located adjacent to the nucleus. In non-dividing epithelial cells, the γ-TuRC relocates to the apical surface, resulting in a polarized network in which the plus-ends face the basolateral surface and most of the minus-ends are in the apical region. In different cell types, organelles such as the Golgi can also serve as sites of nucleation. Additionally, microtubules also can facilitate the nucleation of new microtubules in a specific orientation by recruiting and aligning the γ-TuRC via microtubule-associated proteins, such as augmin (Almeida *et al.*, 2022; Sanchez-Huertas *et al.*, 2016).

Microtubule-associated proteins (MAPs) play various essential roles in regulating microtubule dynamics and functions and can be categorized into non-motor and motor proteins. Non-motor MAPs are involved in stabilizing microtubules, regulating their assembly and disassembly, and organizing the microtubule network within the cell. Examples of non-motor MAPs include tau, MAP2, and MAP4, which provide structural support to microtubules and modulate their interactions with other cellular components (Dehmelt & Halpain, 2004).

The two types of motor MAPs are kinesins and dyneins (Sweeney & Holzbaur, 2018). The kinesin superfamily is a large and diverse group, with over 40 members in humans (Kim & Endow, 2000). Plus end-directed transport of vesicles, organelles, proteins, and RNA particles is driven by kinesins, including the conventional kinesin-1, kinesin-2, and kinesin-3 (Endow *et al.*, 2010). Kinesins also help organize microtubule arrays (kinesin-1, kinesin-5, kinesin-6, and kinesin-14) and alter microtubule dynamics (kinesin-4, kinesin-8, and kinesin-13) (Endow *et al.*, 2010; Walczak *et al.*, 2013). Although the kinesin family 14 plays a minor role in minus end-directed transport, this function is primarily perfomed by cytoplasmic dyneins 1 and 2 (Reck-Peterson *et al.*, 2018).

The cytoplasmic dynein-1 motor complex

The human genome has 16 distinct dynein heavy chain genes that comprise the dynein family (Roberts, 2018). Most of these genes encode axonemal dyneins that enable the motion of motile cilia and flagella. Two types of dynein function as motors for cargo transport: cytoplasmic dynein-1 and -2 (Roberts, 2018). Cytoplasmic dynein-1 was first identified in 1987, when Paschal and colleagues identified MAP1C as a microtubule-activated ATPase capable of translocating microtubules *in vitro* (Paschal *et al.*, 1987). This work represented the discovery of the "*long sought cytoplasmic analog of axonemal dynein*", cytoplasmic dynein-1 (hereafter dynein).

A great variety of key cellular functions are performed by dynein (Roberts *et al.*, 2013). A common feature of its functional diversity is the ability of dynein to anchor itself, through adaptor proteins, to membranes (**Figure 1**). When anchored, dynein produces force that allows the positioning and movement of organelles, mRNAs and other complex cellular structures such as the mitotic spindle.

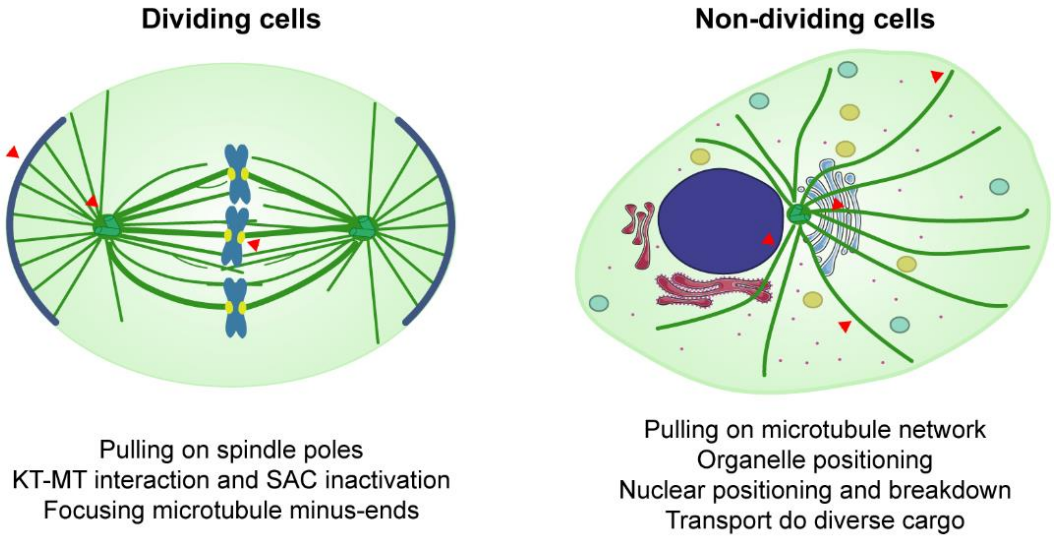

Figure 1 - Dynein functions in dividing and non-dividing cells.
By mediating cargo transport along microtubules, dynein regulates diverse processes from cell division to organelle positioning. Red arrows indicate the dynein typical subcellular localization at the cell cortex, spindle poles, kinetochores, microtubule lattice, and nuclear envelope. Created by the author with inspiration from (Roberts *et al.*, 2013).

Dynein composition and structure

Dynein is a 1.4 MDalton complex of six different subunits. At its core is a dimer of dynein heavy chain (DHC), which contains the motor domains and is encoded by the single human gene, DYNC1H1 (Reck-Peterson *et al.*, 2018). Additionally, other subunits bind to each monomer of DHC: the intermediate chain (DIC; encoded by DYNC1IC1 and DYNC1IC2), and the light intermediate chain (DLIC; encoded by DYNC1LI1 and DYNC1LI2). The three light chain families (DLC): Roadblock (Robl; encoded by DYNLRB1 and DYNLRB2), LC8 (encoded by DYNLL1 and DYNLL2), and Tctex (encoded by DYNLT1 and DYNLT3), form dimers and bind to the DIC N-terminal region (Figure 1.2). The most N-terminal domain of DHC (the "tail") contains the dimerization domain followed by a long region comprising nine helical bundles. Both DIC and DLIC bind to this DHC stretch of helical bundles. The most C-terminal domain includes the motor domain, which consists of the linker (made of helical bundles), a ring of AAA+ domains, and a microtubule-binding domain (MTBD). The AAA+ ring is formed by 6 ATPase domains that allow dynein to convert

chemical energy, ATP, into mechanical work by changing the position of a helical bundle on the surface of the ring, referred to as linker. The movement of this mechanical element, together with nucleotide-dependent changes in the affinity of the MTBD for microtubules, allows dynein motor to step along the microtubule track.

The DLIC subunit is responsible for mediating the binding to many intracellular cargos (Celestino *et al.*, 2019; Lee *et al.*, 2018). DLIC can be structurally divided into two regions: a conserved Ras-like domain that contacts DHC (Pfister & Lo, 2012; Schroeder *et al.*, 2014) and a C-terminal region featuring a conserved helix that binds all known dynein adaptors (Celestino *et al.*, 2019; Lee *et al.*, 2018).

DIC is an essential subunit whose C-terminal region contains seven WD repeats forming a globular β-propeller domain that interacts with DHC. Just upstream of the first WD-repeat domain starts the binding region for Roadblock, Tctex1, and LC8 (Pfister & Lo, 2012). The most N-terminal region of DIC contains a helix that binds, in a mutually exclusive way, to the dynein regulators dynactin p150 and NudE (Karki & Holzbaur, 1995; R. J. McKenney *et al.*, 2011; Okada *et al.*, 2023).

The accessory subunits are part of the mechanism that controls the localization, timing, and activity of the dynein motor, either directly or through regulatory factors.

Autoinhibition and activation of dynein by dynactin and LIS1

In cells, dynein achieves speeds typically ranging from 0.5 to 2 μm/s (Roberts, 2018). However, purified mammalian dynein is a weak processive motor on its own (M. Trokter *et al.*, 2012). To become processive, dynein needs to be in a complex with dynactin and an activating adaptor (**Figure 2**) (Schlager, Hoang*, et al.*, 2014).

Four years after the discovery of dynein, dynactin was characterized as its major co-factor (Schroer & Sheetz, 1991). Dynactin is a 1.0 MDalton complex composed of a short actin-like filament (eight copies of ARP1 and a single β-actin subunit) (Reck-Peterson, 2015). The barbed end is composed of the F-actin capping protein heterodimer CAPZαβ and the pointed end includes the actin-related protein ARP11. The pointed end is completed by three other proteins, p62, p27, and p25, that bind ARP11. On top of the ARP1 filament sits a shoulder domain composed by four copies of p50 (also known as dynamitin), two copies of p24, and two copies of the largest subunit $p150^{glued}$, whose N-terminal region forms a long projection, (Schroer, 2004). Located at the very N-terminus of p150 are two microtubule binding domains: the basic domain and the CAP-Gly domain. The elongated and flexible structure of the p150 N-terminus features two distinct coiled-coil stretches termed CC1 and CC2, with the globular intercoiled domain (ICD) betwen them. Within CC1,

there are two subdomains, CC1a and CC1b, that adopt a hairpin-like structure (Reck-Peterson, 2015).

Dynein alone adopts an autoinhibited conformation in which the motor domains self-dimerize (Torisawa *et al.*, 2014), referred to as the phi-particle because it resembles the Greek letter *phi* (Amos, 1989). Dynactin also adopts an autoinhibited conformation in which the CC1 of the p150 arm interacts with the dynactin pointed end (Lau *et al.*, 2021; Urnavicius *et al.*, 2015). This folded-back conformation implies that, with the p150 arm bound to the pointed end, adaptors will be physically hindered from interacting with dynactin (Lau *et al.*, 2021). In 2023, the latest advances in cryo-EM allowed the observation of the complete dynein complex sitting on microtubules together with its major regulators (Chaaban & Carter, 2022; Singh *et al.*, 2023).

Dynein and dynactin establish several contacts between different subunits (**Figure 2**). Pioneering cryo-EM studies showed that the N-terminal tail domain of DHC docks onto dynactin's actin filament (Lau *et al.*, 2021; Urnavicius *et al.*, 2015). In 1995, immunoprecipitation experiments showed that an interaction exists between the N-terminus of DIC and CC1b region of dynactin p150 (Karki & Holzbaur, 1995; Vaughan & Vallee, 1995), and the overexpression of CC1b fragments was used as a way of inhibiting dynein (King *et al.*, 2003). However, this interaction was not present in the early cryo-EM structures available, likely due to the flexibility of the regions (Lau *et al.*, 2021; Morgan *et al.*, 2021; Tripathy *et al.*, 2014). Recently, it became clear that the CC1b coiled-coil interacts simultaneously with the DHC motor region (specifically, AAA2 and AAA3), with the DIC N-terminal region (as previously described), and with LIS1 (Singh *et al.*, 2023).

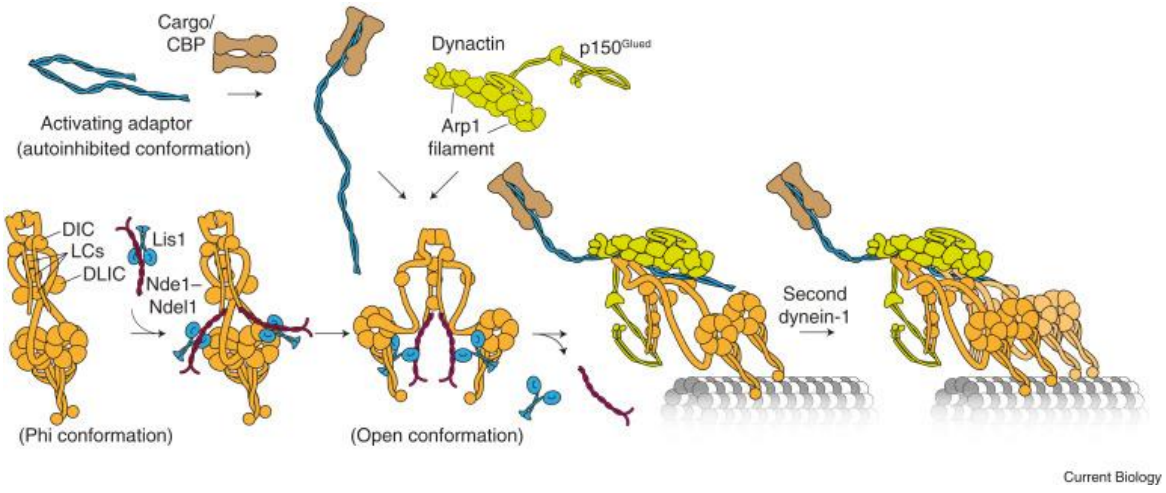

Figure 2 - Dynein motor complex assembled in a stepwise manner with dynactin, an adaptor protein, and its regulator LIS1.
Reproduced from (Yildiz & Zhao, 2023).

LIS1 (PAFAH1B1), which consists of a *C*-terminal β-propeller and an N-terminal dimerization domain, is important for dynein recruitment to various cellular structures such as the nuclear envelope, microtubule plus-ends, vesicles, kinetochores, the cell cortex, and ribonucleoprotein complexes (Markus *et al.*, 2020). *In vitro* studies have shown that dynein depends on Lis1 to acquire its uninhibited conformation (Markus *et al.*, 2020), as LIS1 directly binds to AAA3 of the DHC motor domain (Huang *et al.*, 2012; Toropova *et al.*, 2014). Recent work show that the same LIS1 dimer that binds through its β-propeller to DHC AAA3 also binds the CC1b region of dynactin p150 (**Figure 2**) (Singh *et al.*, 2023).

This groundbreaking work provides insight into how motile dynein-dynactin-adaptor complexes are formed. Following the model proposed by Singh and colleagues, the folded-back conformation of the p150 CC1a/b is incompatible with the LIS1 binding to CC1b (Singh *et al.*, 2023). However, the DIC binding region is still accessible in this p150 conformation. These results strongly suggest that a key reason why DIC binds CC1b is to open up p150 to allow the subsequent interactions with LIS1. LIS1 binding appears to be important for orienting dynein for optimal dynactin and adaptor protein binding since the ability of LIS1 to contact both the CC1b and dynein allows p150 to dock along the heavy chain by binding the dynein tail and motor domains. Additionally, LIS1 binding reinforces the tethering of dynein to p150, avoiding the transition of the p150 arm to a folded-back conformation.

Several studies report that LIS1 recruitment to DHC is facilitated by DIC-bound NudE/L (Huang *et al.*, 2012; McKenney *et al.*, 2010; Wang *et al.*, 2013). NudE/L proteins are coiled-coil-containing proteins that interact with the DIC and LC8, as well as with LIS1. Recent evidence showed that LIS1 cannot bind simultaneously to NudE and dynein, indicating that NudE may tether LIS1 to dynein (Okada *et al.*, 2023). Intriguingly, NudE binding to CC1b and the DIC N-terminus is mutually exclusive [108]. Considering this, it seems unlikely that NudE recruits LIS1 to CC1b and DHC while bound to DIC N-terminal region since, according to the new structural data (Singh *et al.*, 2023), DIC N-terminus binding to CC1b is the first step in the formation of dynein-dynactin-adaptor complexes. Studies in cells and *in vitro* show that NudE/L contribute to dynein recruitment to cargo and help dynein withstand high loads during transport (McKenney *et al.*, 2010).

In summary, turning dynein into an ultra-processive motor capable of travelling along microtubules for many micrometers before detaching (Fellows *et al.*, 2023) requires several layers of regulation. Dynein must undergo both a release from its autoinhibited form and a stable interaction with dynactin, which requires an activating adaptor (McKenney *et al.*, 2014; Urnavicius *et al.*, 2015).

Activating adaptors

In 2012, single-molecule imaging experiments failed to detect effects on dynein processivity by the sole addition of the purified dynactin complex, suggesting the need for additional regulators (Martina Trokter *et al.*, 2012). Later, a group of proteins, collectively called activating adaptors, were shown to be required to stabilize the dynein-dynactin interaction, making the complex highly processive (**Figure 2**) (McKenney *et al.*, 2014).

Currently, approximately 25 known or putative activating cargo adaptors (Reck-Peterson *et al.*, 2018) are described, of which 16 have been shown to bind DLIC (**Table 1**). All these adaptors share a common feature: a C-terminal region with binding sites for other proteins that mediate cargo interactions, the presence of a long coiled-coil region allowing dimerization, and a N-terminal binding site for the DLIC C-terminal region (Reck-Peterson *et al.*, 2018). Four different types of DLIC binding motifs have been described so far: the Hook domain, the CC1-box, the EF-hand, and the RH1 domain. The CC1-box refers to a conserved coiled-coil motif conforming to the sequence A-A-xx-G that is utilized by BICD2, BICDL1, TRAK1, TRAK2, and Spindly for DLIC binding (Canty *et al.*, 2023; Gama *et al.*, 2017; Hoogenraad *et al.*, 2003; McKenney *et al.*, 2014; Schlager, Serra-Marques*, et al.*, 2014; Spronsen *et al.*, 2013; Urnavicius *et al.*, 2018). The Hook domain has been shown to bind the DLIC C-terminal region in Hook1 and Hook3 (Lee *et al.*, 2018; McKenney *et al.*, 2014; Schroeder & Vale, 2016). The EF-hand domain is present in RFIP3, CRACR2a, KASH5, Ninein, and Ninein-like (Agrawal *et al.*, 2022; Garner *et al.*, 2023; Horgan *et al.*, 2010; McKenney *et al.*, 2014; Redwine *et al.*, 2017; Wang *et al.*, 2018). Recently, the RH1 domain was shown to mediate the binding between DLIC and the adaptors JIP3, JIP4 and RILP (Arimoto *et al.*, 2011; Cantalupo *et al.*, 2001; Celestino *et al.*, 2022). The description of adaptor domains that link them to DLIC has led to an increase in the number of candidate activating adaptors. An example of this is the adaptor NuMA, which appears to have two variant versions of the CC1-box, as well as a Hook domain (Renna *et al.*, 2020).

Interestingly, certain adaptors have the ability to recruit two dyneins to a single dynactin. This results in a motor complex with enhanced speed and force generation (Grotjahn *et al.*, 2018; Sladewski *et al.*, 2018; Urnavicius *et al.*, 2018). Additionally, studies indicate that dynactin can accommodate a second copy of the adaptor (Chaaban & Carter, 2022), which is predicted to strengthen the stability of the transport machinery. While dynactin and LIS1 appear to be obligatory dynein regulators in virtually every context, most adaptors have cargo-specific functions.

Many of the described adaptors function in the transport of membrane-bound organelles and vesicles. Mutating the DLIC C-terminal region responsible for adaptor binding has been shown to affect vesicular transport (Celestino *et al.*, 2022; Celestino *et*

al., 2019; Koushika *et al.*, 2004; Lee *et al.*, 2020; Renna *et al.*, 2020). The Hook family is involved in early endosome transport (Bielska *et al.*, 2014), while TRAK proteins show specificity for mitochondria trafficking (Canty *et al.*, 2023). During mitosis and meiosis, dynein is recruited by Spindly to kinetochores to help the attachment of chromosomes to microtubules (Gama *et al.*, 2017), and the meiosis-specific KASH5 acts as an nuclear envelope adaptor for dynein, which facilitates movement for homolog pairing (Agrawal *et al.*, 2022; Garner *et al.*, 2023).

Table 1 - Dynein complex activating adaptors with the correspondent cargo and domains of DLIC binding.

ADAPTOR	CARGO	DLIC BINDING	REFERENCES
Hook1 Hook3	RAB5 early endosomes	Hook domain	(Guo *et al.*, 2016; Lee *et al.*, 2018; McKenney *et al.*, 2014; Schroeder & Vale, 2016)
BICD2 BICDL1	Golgi vesicles, nuclear pore complexes, RAB6 vesicles	CC1-box domain	(Hoogenraad *et al.*, 2003; McKenney *et al.*, 2014; Schlager, Serra-Marques, *et al.*, 2014; Urnavicius *et al.*, 2018)
TRAK1 TRAK2	Mitochondria	CC1-box domain	(Canty *et al.*, 2023; Spronsen *et al.*, 2013)
Spindly	Kinetochores	CC1-box domain	(Gama *et al.*, 2017)
HAP1	Many membrane cargos (autophagosomes)	CC1-box domain	(Cason *et al.*, 2021)
NuMA	Minus-ends of MT in the spindle, cortical anchor	CC1-box-like / Hook domain	(Hueschen *et al.*, 2017; Renna *et al.*, 2020)
NIN NINL	Unknown	EF-hand pair	(Redwine *et al.*, 2017)
RFIP3	RAB11 recycling vesicles	EF-hand pair	(Horgan *et al.*, 2010; McKenney *et al.*, 2014)
CRACR2a	Distinct endosomal populations	EF-hand pair	(Wang *et al.*, 2018)
Rab45	Unknown	EF-hand pair	(Wang *et al.*, 2018)
KASH5	Meiotic chromosomes	EF-hand pair	(Agrawal *et al.*, 2022; Garner *et al.*, 2023)
JIP3	Activated JNK and lysosomes	RH1 domain	(Arimoto *et al.*, 2011; Celestino *et al.*, 2022; Singh *et al.*, 2023)

JIP4	Mature autophagic vacuoles	RH1 domain	(Celestino *et al.*, 2022)
RILP	RAB7 late endosomes and lysosomes	RH1 domain	(Celestino *et al.*, 2022)

Cell Division

Cell division is a fundamental process in all living organisms. In eukaryotes, there are two main types of cell division: meiosis and mitosis. While meiosis occurs in germ cells and results in the formation of gametes (sperm and eggs) (Ohkura, 2015), mitosis is needed to form, repair and maintain tissues (McIntosh, 2016). Most cells divide symmetrically, meaning that daughter cells have identical fates. In contrast, asymmetric cell division refers to any division in which daughter cells acquire distinct fates, which is an important mechanism to promote cellular diversity during development (Sunchu & Cabernard, 2020).

Mitosis: an overview

In 1882, Walther Flemming provided the initial description of mitosis, documenting the chronological progression and cellular changes that take place throughout the process of cell division [translated in (Flemming, 1965)]. Mitosis can be divided into five phases (**Figure 3**): prophase, prometaphase, metaphase, anaphase, and telophase, followed by the physical separation of cells, called cytokinesis (McIntosh, 2016; McIntosh & Hays, 2016).

The beginning of prophase is defined by the visible condensation of the chromosomes. Each chromosome is composed of two sister chromatids, in which, one of the two strands of DNA is the result of the semi-conservative DNA replication process that took place during the previous S-phase (McIntosh, 2016). As this occurs, the nucleolus disperses, and the nuclear envelope disassembles. The nuclear envelope (NE) is a double-layered membrane that encloses the genetic material in eukaryotic cells, and its breakdown (NEB) corresponds to the end of prophase (McIntosh, 2016). During prophase, centrosomes separate from each other, by migrating along the NE to opposite sides of the nucleus (Meraldi, 2016; Tanenbaum & Medema, 2010). This movement is driven by motor proteins, including dynein located at the cell cortex and/or at the NE (De Simone *et al.*, 2016; Gönczy *et al.*, 1999).

The beginning of prometaphase is marked by the presence of highly dynamic microtubules emanating from the centrosomes that probe the nuclear space in search of chromosomes. During prometaphase, microtubules radiating from the centrosomes engage with the chromosomes. The interaction between microtubules and chromosomes, mediated by supramolecular protein structures called kinetochores (Gassmann, 2023), leads to the formation of the bipolar mitotic spindle. Subsequently, the chromosomes undergo congression and alignment at the equator of the cell, giving rise to a metaphase plate (McIntosh, 2016). Once all sister chromatid pairs are properly attached to microtubules, they undergo synchronous separation and segregate towards opposite poles. During the

initial stages of anaphase, kinetochore microtubules undergo a shortening process (referred to as anaphase A) (McIntosh, 2016). This pulls the sister chromatids towards opposite poles. The spindle apparatus then elongates, causing the two poles to move apart, thereby carrying the chromosomes with them (referred to as anaphase B) (McIntosh, 2016). The two sets of chromatids begin to decondense, and the nuclear envelope reforms (telophase).

Cytokinesis starts when a contractile ring composed of actin and myosin II filaments forms in mid-anaphase (Green *et al.*, 2012). The contractile ring constricts and pinches the cell membrane inward, leading to the separation of the two daughter cells (Green *et al.*, 2012). This final process ensures the proper allocation of genetic material to the newly formed cells and the distribution of cellular organelles and cytoplasmic components.

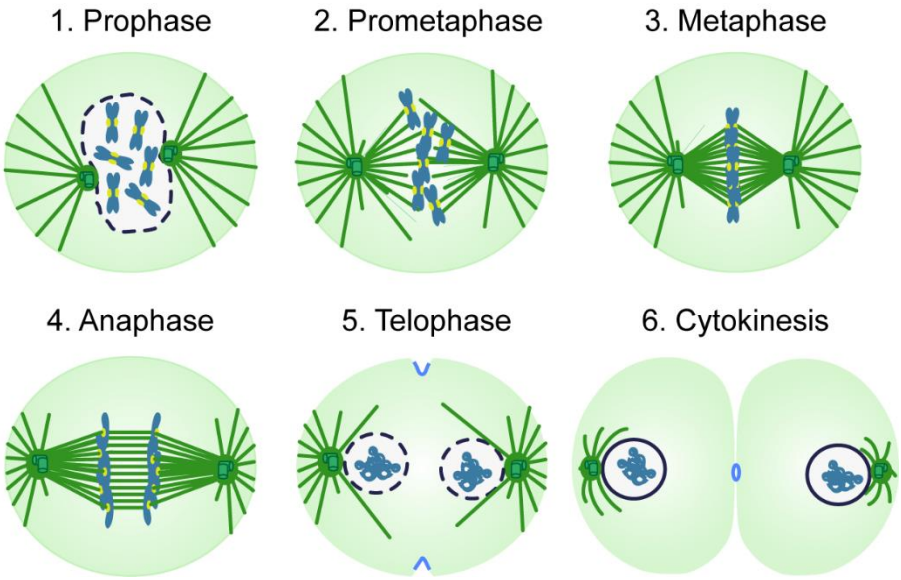

Figure 3 - Schematic representation of the mitotic phases highlighting the significant cellular changes that occur during this process.
Created by the author based on (Rocha, 2019).

The role of dynein in spindle orientation

Mitotic spindle orientation has been a subject of study since the 19th century. The first important parameter influencing spindle orientation to be discovered was cell shape (Hertwig, 1884). Deformation of sea urchin embryos, by application of mechanical forces, showed that cells tend to divide along their long axis (Hertwig, 1884). While Hertwig's rule continues to be relevant (Box *et al.*, 2019; Middelkoop *et al.*, 2023; Strauss *et al.*, 2006), spindle severing experiments in the *C. elegans* zygote, using ultraviolet laser microbeam microsurgery, revealed direct evidence for cortical pulling forces exerted on the spindle (Grill *et al.*, 2001). In agreement with this, perturbation of the actomyosin cortex of the *C. elegans*

embryo, results in membrane invaginations are observed that correspond to cortical sites of pulling from force generators (Redemann *et al.*, 2010). The amount of membrane invaginations observed when dynein or its regulators are perturbed is significantly decreased, indicating that dynein plays a central role in cortical pulling force generation (Redemann *et al.*, 2010).

In 2007, Nguyen-Ngoc and colleagues made use of a DHC temperature-sensitive *C. elegans* mutant that, upon temperature upshift, showed significantly reduced spindle oscillations and short spindles (Nguyen-Ngoc *et al.*, 2007). Work in the *C. elegans* zygote, *D. melanogaster*, and human cells (Kiyomitsu, 2019; Kotak, 2019; Kotak *et al.*, 2012; Kotak & Gonczy, 2013) showed that these forces were powered by the G protein subunit Gαi, which is anchored in the plasma membrane and, in its GDP–bound form, interacts with C-terminal GoLoco motifs in LGN (leucine glycine asparagine). N-terminal tetricopeptide repeats in LGN then recruit NuMA (nuclear mitotic apparatus), the coiled-coil adaptor for dynein–dynactin.

Gαi is part of the heterotrimeric G protein family and serves as an anchor for the ternary LGN-NuMA-dynein complex, since it localizes to the plasma membrane through myristylation (Kiyomitsu & Cheeseman, 2013; Polit *et al.*, 2021). G proteins act as molecular switches inside cells and their activity is regulated by factors that control their ability to bind to and hydrolyze GTP to GDP. Upon depletion of the *C. elegans* Gαi homologues GOA-1 and GPA-16, spindle severing experiments showed that spindle poles no longer move towards the cortex, indicating that the pulling forces are dependent on cortical Gαi proteins (Afshar *et al.*, 2005; Grill *et al.*, 2001). In *C. elegans,* RNAi-mediated depletion of either NuMA or LGN orthologues also leads to the total absence of pulling forces, resulting in an equal partitioning of the single-cell embryo (Jankele *et al.*, 2021). In fly neuroblasts, a presumptive *null* allele of the NuMA orthologue resulted in spindle misorientation that led to overgrowth and malformation of the adult fly brain (Bowman *et al.*, 2006).

In 2018, an optogenetic system that could link specific proteins to the membrane by fusing them to an artificial anchor showed that merely anchoring dynein at the cell cortex is not sufficient for it to pull on microtubules and generate force (Fielmich *et al.*, 2018). Interestingly, this study showed that optogenetically anchored NuMA at the cell cortex recruits dynein and forms the minimal complex necessary to generate cortical pulling forces. In 2020, NuMA was described as an dynein adaptor that interacts with DLIC through a variant of the Hook domain, recruiting and activating the dynein-dynactin complex (Renna *et al.*, 2020).

The canonical cortical force generation pathway (**Figure 4**) depicts Gαi proteins as the cortical anchor. However, additional proteins have been described as important

contributors to cortically anchor LGN-NuMA-dynein (**Table 2**; **Figure 4**). In fly neuroblasts, the LGN homolog Pins is described to interact with an apical protein, Inscuteable (Insc), known to bind the partitioning-defective (PAR) protein Par-3 from the apical polarity complex [Par-3, Par-6 and atypical protein kinase C (aPKC)], suggesting that the control of apical-basal (A-B) orientation of the spindle is mediated by the apical recruitment of the force generator dynein (Mauser & Prehoda, 2012). In other systems, such as the *Drosophila* follicular epithelium and chick neuroepithelium, polarization is not dependent on aPKC but on Discs large (Dlg) (Su *et al.*, 2013). Dlg is extensively studied in *Drosophila* and appears to have distinct roles depending on the cellular context. Briefly, Dlg binds directly to $Pins^{LGN}$ but localizes independently of it, suggesting that its localization determines the orientation of the spindle (Saadaoui *et al.*, 2014).

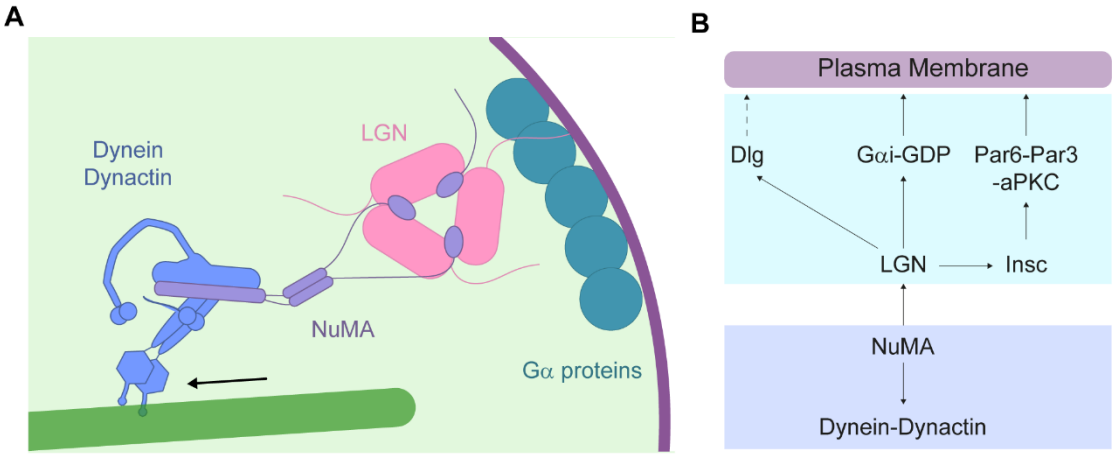

Figure 4 - Schematic of the cortical pulling machinery responsible for the force generation on the mitotic spindle (**A**) and molecular pathways associated (**B**).
Dynein motor complex (dark blue shade) is recruited by LGN bound to Gαi-GDP proteins anchored (light blue shade) at the plasma membrane. Additional mechanisms involving junctional proteins and/or the apical polarity complex exist that reinforce and regulate dynein recruitment. Created by the author based on (Lechler & Mapelli, 2021).

Studies in fly neuroblasts, zebrafish embryos and *C. elegans* blastomeres show that the centrosome-centrosome axis undergoes significant rotation during or after centrosome separation, and that the spindle achieves its final orientation in metaphase (Middelkoop *et al.*, 2023; Strauss *et al.*, 2006). In contrast, mitotic spindle orientation in Xenopus blastomeres is already defined during prophase (Strauss *et al.*, 2006). In mammalian cell lines, the mitotic spindle is generally positioned parallel to the substrate, close to the center of the cell. Cortical levels of NuMA and dynein are significantly enriched during the metaphase to anaphase transition, reflecting their role in spindle elongation (Kiyomitsu & Cheeseman, 2013). Interestingly, a study from 2012 showed that if the spindle is centrally

positioned in early mitosis (i.e. prometaphase to metaphase transition) cortical dynein and dynactin are either absent or at both poles with a crescent-shaped distribution (Collins *et al.*, 2012). However, if the mitotic spindle is wrongly positioned, cortical dynein and dynactin appear in bright patches on the cortical region that is more distant from the spindle, strongly suggesting a role in re-positioning the mitotic spindle. Kiyomitsu and Cheeseman also showed that mitotic spindle movements are dependent on cortical dynein distribution: if dynein is enriched on one side of the cell, the spindle moves towards it; if cortical dynein is redistributed, the spindle oscillates (Kiyomitsu & Cheeseman, 2012).

Table 2 - Summary of the proteins that form the cortical anchoring machinery in the different models discussed.

MAMMALS	***C. elegans*** **HOMOLOGUE**	***D. melanogaster*** **HOMOLOGUE**
NuMA	LIN-5	Mud
LGN	GPR-1 / GPR-2	Pins
Gαi	GOA-1 / GPA-16	Gαi
Dlg	DLG-1	Dlg
mInsc	-	Insc
Par-3	PAR-3	Bazooka
Par-6	PAR-6	DmPar6
aPKC	PKC-3	DaPKC

In addition to force generation by dynein, microtubule dynamics makes an important contribution to spindle orientation. Nguyen-Ngoc and colleagues established an elegant set of experiments using time-controlled dosage of the microtubule-stabilizing drug Taxol to show that compromising microtubule depolymerization diminishes pulling forces to a similar extend as Gαi protein depletions (Nguyen-Ngoc *et al.*, 2007). In *Drosophila* S2 cells, depletion of GCP4, a γ-tubulin complex component, resulted in spindle misorientation (Bouissou *et al.*, 2014). Curiously, this phenotype did not arise from defects in microtubule nucleation but from an increase in astral microtubule length and dynamics (Bouissou *et al.*, 2014).

In summary, mitotic spindle positioning and orientation is regulated by the interaction of astral microtubules with cortical force generators, in both symmetric and asymmetric divisions. The spindle's position dictates the site of the cleavage furrow (Oliferenko *et al.*, 2009), thus determining the axis along which the cell will divide. This in turn has an impact on the architecture of the tissues and the shape of organs (Lechler & Mapelli, 2021).

Asymmetric Cell Division

Asymmetric cell division was first described in 1905 by Ed Conklin (Conklin, 1905). Conklin found that in early ascidian embryos an area of yellow cytoplasm always co-segregates with cells that will become muscle cells (Conklin, 1905).

Stem cells, with their remarkable capability to differentiate into a wide range of cell types, serve as the prime example of cells capable of dividing asymmetrically. Each stem cell division results in a daughter cell that retains the original stem cell properties and mitotic potential, while the other daughter is re-programmed to follow a specific non-stem cell fate (i.e., the cell differentiates). Since Conklin's first observation, work in *D. melanogaster* and *C. elegans* have played a key role in deciphering the molecular mechanisms that underlie asymmetric divisions.

Modes of asymmetric cell division

Cell fate determination is the process by which a cell acquires a specific identity and commits to a particular developmental pathway, ultimately leading to the expression of specific genes and the adoption of a distinct function (Wagers *et al.*, 2002). Asymmetric cell fate can arise from external signals or through the unequal inheritance of intrinsic determinants like proteins or mRNA (**Figure 5**).

When asymmetry is defined extrinsically, the cell fate is induced through signaling from surrounding cells (Petzold & Gentleman, 2021). The stem cell niche for germline stem cells (GSCs) in the *C. elegans* gonad is an example of asymmetric cell division via extrinsic cues (Byrd & Kimble, 2009). While GSCs produce daughters with similar developmental potential, the fate of these daughters is determined by their proximity to the distal tip cell niche (Byrd & Kimble, 2009). Daughters located near the niche remain in the mitotic cell cycle and continue to generate new germ cells. In contrast, daughters situated further away from this niche enter the meiotic cell cycle and eventually differentiate into either sperm or oocytes (Byrd & Kimble, 2009).

Fate asymmetry of daughter cells can also be defined intrinsically and requires two coupled events: the establishment of a cell polarity axis, achieved by pre-mitotic unequal distribution of cell fate determinants, and the alignment of the mitotic spindle with the cell polarity axis, resulting in unequal distribution of fate determinants when the cell divides. This relationship between the establishment of the polarity axis and spindle orientation has been explored in multiple studies in *Drosophila* neuronal progenitors, called neuroblasts (Loyer & Januschke, 2020). The mitotic spindle of neuroblasts is aligned in an apical-basal (A-B) fashion and the cell divides asymmetrically both in content and size (Loyer & Januschke, 2020). Cell polarization is achieved intrinsically by the unequal distribution of two

complexes: the basal differentiation complex and cell fate markers, and the apical polarity complex (Par-3, Par-6 and aPKC) (Deng & Wang, 2022). Upon A-B division, the basal daughter cell will differentiate due to the presence of a differentiation protein complex, and the apical daughter will retain its proliferative potential.

Par proteins have also been shown to be essential in the polarization of the fertilized *C. elegans* zygote. The first mitotic division produces two daughter cells that are asymmetric in size and fate. Size asymmetry arises from the movement of the centered spindle towards the posterior during metaphase, resulting in a larger anterior blastomere (AB) and a smaller posterior blastomere (P1) (Jankele *et al.*, 2021). The pulling forces acting on the spindle are controlled by the previously established Par polarity axis (Grill *et al.*, 2001). The polarity axis is established by the redistribution of the Par proteins upon sperm entry, and perturbation of Par proteins results in symmetric positioning of the mitotic spindle. A recent study showed that zygotes that divide symmetrically generate non-viable animals (Lim *et al.*, 2021).

Examples of intrinsic asymmetrical polarization also include unequal distribution of mRNAs, as it has been shown during spiralian development (Kingsley *et al.*, 2007), and of protein aggregates, as it happens in dividing budding yeast in which protein aggregates are segregated to the mother cell in order to produce rejuvenated daughters (Zhou *et al.*, 2011).

In summary, in both extrinsic and intrinsic asymmetric cell divisions, several factors play a role in making the two resulting cells have different fates. These factors, and how they work with the spindle orientation machinery, are crucial in shaping various biological processes and developmental outcomes, highlighting the remarkable complexity of cell division and cell fate determination.

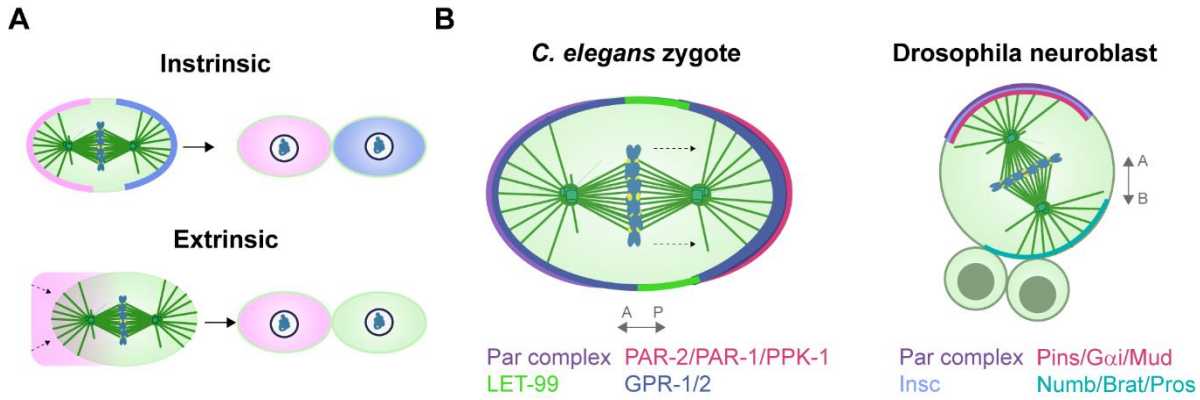

Figure 5 - Modes of asymmetrical cell division (**A**) and extensively studied worm and fly models (**B**). Intrinsic and extrinsic asymmetric cell division result in the generation of daughter cells with differing identities or functions. The most extensively studied models for understanding asymmetry in cell division, are the *C. elegans* zygote and Drosophila's neuroblasts. Created by the author.

The role of spindle orientation in asymmetric cell division

In 2006, studies in fly neuroblasts with misoriented mitotic spindles showed that when these cells divided perpendicularly to the A-P axis, cell fate determinants were segretated equally, which led to the production of two self-renewing daughter cells that went on to produce excess neurons. As a consequence, these flies showed defective formation of the mushroom body, an adult brain structure required for olfactory learning and memory (Bowman *et al.*, 2006). More recently, in vertebrates, kinesin KIF18B was shown to be specifically required for spindle orientation and cell fate specification in mice hair placodes but dispensable in the interfollicular epidermis (Moreci & Lechler, 2021), emphasizing not only the relevance of spindle orientation for cell fate determination in vertebrates, but also the distinct requirements for spindle orientation in different tissue contexts.

There are several ways to achieve a correctly oriented cell division (Siegrist & Doe, 2006), including correction mechanisms during telophase (Lough *et al.*, 2019). These regulatory mechanisms underscore the importance of correct spindle orientation during asymmetric divisions: spindle orientation defects have been linked to tumorigenesis (Knoblich, 2010) and brain pathologies in humans (Lancaster & Knoblich, 2012).

Tumorigenesis, also known carcinogenesis, refers to the process by which normal cells undergo a series of genetic and epigenetic changes that lead to uncontrolled proliferation of cells, ultimately forming a tumor (Tabassum & Polyak, 2015). One hypothesis suggests that spindle misorientation promotes tumorigenesis by increasing the number of cells that fail to divide asymmetrically, thereby retaining their proliferative potential. Work in flies shows that loss of asymmetrical stem cell division results in invasive cell proliferation (Caussinus & Gonzalez, 2005). Neverthless, the extent to which spindle misorientation

contributes to tumorigensis remains unclear, since the mutations associated with spindle misorientation in mammals also showed numerous others defects such as chromosome missegregation and alterations in intracellular transport (Noatynska *et al.*, 2012).

The same caveats apply when discussing spindle misorientation and its correlation with neuronal pathologies. Several human brain diseases, such as microcephaly, have been proposed to arise from defects in spindle orientation and asymmetrical cell division. In the case of microcephaly, for example, most of the genes linked to it encode proteins related to centrosomes, and some of these genes have been shown to be necessary for oriented divison in the mouse neocortex (Lancaster & Knoblich, 2012). Konno and colleagues (Konno *et al.*, 2008) found that the decision of a cell to opt for an asymmetric or symmetric cell division is not solely dependent on the orientation of the spindle axis. Randomizing the division plane by interfering with LGN did not affect cell fate directly (Morin *et al.*, 2007). Intriguingly, the relevance of proper spindle orientation of neuronal progenitors appears to vary along development. In the mammalian neocortex, precise orientation of mitotic spindles in the early stages is crucial for symmetric proliferative divisions (Lancaster & Knoblich, 2012). Conversely, in later stages, mitotic spindles can be angled or vertical, but the significance of this reorientation is somewhat less clear as cells can adopt different fates regardless of spindle orientation (Lancaster & Knoblich, 2012).

In summary, the orientation of the mitotic spindle during asymmetric cell divisions has an undoubtledy important role in cell fate decisions and tissue homeostasis, but further studies are needed to clarify the precise contribution of spindle misorientation to the development of neuronal pathologies and cancer.

Microtubule-based transport of endosomal organelles

Microtubule-based transport is required for efficient and accurate distribution of various organelles. Microtubules serve as transportation highways, enabling the movement of cargos such as endosomes, lysosomes, mitochondria, and nuclei (Barlan & Gelfand, 2017). This movement is mediated by kinesins and dynein, the central players of cargo transport.

The endocytic pathway and microtubule cytoskeleton contributions

Endosomes can be divided into early endosomes, recycling endosomes, and late endosomes (Wandinger-Ness & Zerial, 2014). After internalization of extracellular material (e.g., proteins, lipids, and signaling molecules) in a process called endocytosis (Redpath & Ananthanarayanan, 2023), early endosome (also termed sorting endosomes) are formed. Their function is to sort endocytosed material according to whether it needs to be recycled or degraded (**Figure 6**) (Jovic *et al.*, 2010; Redpath *et al.*, 2020). The degradation pathway will result in the transformation of the early endosome into a late endosome, while more content is added to it. Ultimately, accompanied by an acidification of their content, late endosomes will fuse with lysosomes, acidic compartments that degrade extracellular and intracellular material (Huotari & Helenius, 2011). In contrast, recycling ensures the return of endosomal cargo to the plasma membrane. Recycling is used to regulate cell surface receptors, cell junction components, and apical/basolateral specializations in polarized cells (Lock & Stow, 2005; Van Ijzendoorn, 2006). Early endosomes can be reintegrated into the plasma membrane at the location where the endocytosis occurred (Huotari & Helenius, 2011). In most instances, however, recycling and degradation involves long range movement of endosomes along microtubules (Wandinger-Ness & Zerial, 2014).

Experiments in the early 2000's showed that upon microtubule depolymerization using nocodazole, the transport of early endosomes to the recycling perinuclear compartment was blocked (Baravalle *et al.*, 2005), indicating an important role for the microtubule cytoskeleton in the endocytic pathway. It is well established now that all types of endosomes move along microtubules with extensive evidence coming from work in neurons.

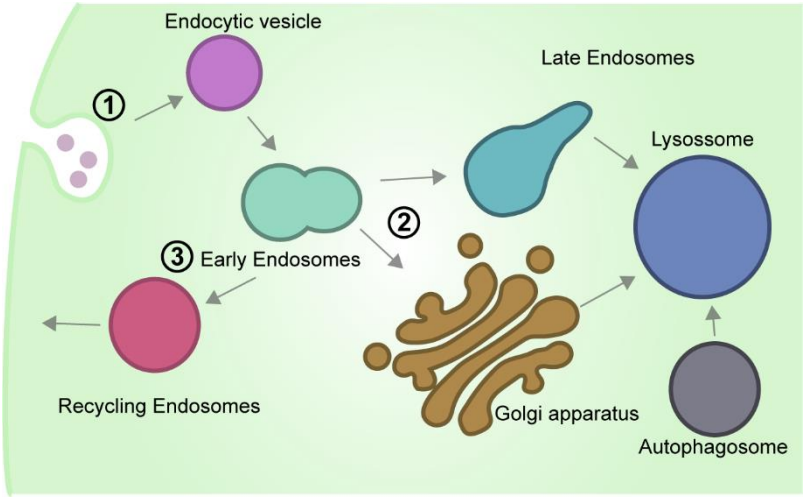

Figure 6 - Illustration describing the sequential stages of the endocytic pathway within a cell. The schematic outlines the path of endocytosed material, via early endosomes (*1*), to the degradation pathway upon processing in lysosomes (*2*), or potential recycling and release back into the extracellular space (*3*). Created by the author.

Rab GTPases as microtubule motor regulators

Microtubule-based endosomal transport occurs in a stepwise manner: 1) the endosome presents small proteins at its surface that can interact with specific adaptors; 2) those adaptors bound to endosomes are now able to interact with motor proteins; 3) the motor proteins adopt their uninhibited conformation upon interaction with adaptors and bind to microtubules, initiating processive movement.

Rab (Ras-related proteins in brain) GTPases play a central role in cargo-specific recognition by dynein and kinesin adaptors. Rabs are a family of monomeric G proteins, composed of 70 members in humans that are divided into 44 subfamilies. Of these, five Rabs (Rab1, Rab5, Rab6, Rab7, and Rab11) are found in all eukaryotic genomes (Pylypenko *et al.*, 2018). Rab proteins are small, contisting of approximately 200 residues (Yuan & Song, 2020). Rabs cycle between a GDP-bound and a GTP-bound state. In their GDP-bound state, Rabs are kept inactive in the cytosol. By contratst, GTP-bound Rabs bind to membranes through a lipid modification at their C-terminus and recruit effector proteins (Goody *et al.*, 2017). Rab-specific Guanine Nucleotide Exchange Factors (GEF) and GTPase-Activating Proteins (GAP) regulate the GDP- to GTP-bound cycle and are thus central for regulating Rab interaction with effectors.

Endosome compartments differ in Rab composition, which commonly leads to them to be identified using specific Rabs as markers. However, it is important to bear in mind that since endosomes are continuously formed and converted into each other, the same Rab may associate with multiple endosome types (Shearer & Petersen, 2019). Nevertheless,

Rab4 and Rab5 are generally associated with early endosomes, Rab11 with recycling endosomes, and Rab7 with late endosomes and lysosomes (Horgan & McCaffrey, 2011).

Rabs are recognized for their role in controlling organelle transport by by stablishing the link between membranes and motor proteins (Horgan & McCaffrey, 2011; Wandinger-Ness & Zerial, 2014). Some Rabs bind directly to kinesins and dynein. For example, the kinesin-6 KIF20A and the kinesin-3 KIF16B bind directly to Rab6 (Echard *et al.*, 1998) and Rab14 (Ueno *et al.*, 2011), respectively, and dynein interacts with Rab4 and Rab6. A yeast-to-hybrid screen revealed that the dynein accessory subunit DLIC interacts with Rab4-GTP (Bielli *et al.*, 2001). Both the dynein light chain Roadblock and the dynactin p150 subunit were shown to interact directly with Rab6 (Short *et al.*, 2002; Wanschers *et al.*, 2008). A more frequently employed pathway for motor recruitment by Rabs, however, involves adaptor proteins (Horgan & McCaffrey, 2011). In case of dynein, adaptors contain a Rab binding site at their C-terminus, leaving the N-terminus free to bind the motor. Swiching Rabs on endosomes, for example upon transition from early endosomes to late endosomes, or from early endosomes to recycling endosomes, also changes the identity of the adaptors present on the membrane. Rabs undoubtfully play a central role in specifying motor recruitment to endosomes. However, the current array of Rabs and cargo adaptors remains insufficient to fully explain microtubule-based endosomal transport, particularly in the context of minus end-directed transport powered by dynein.

Early endosome transport powered by dynein

Early endosomes are membranous organelles transported by dynein (Aniento *et al.*, 1993). These organelles emerge from endocytosis events and their function is to sort their content into recycling and degradative compartments of the cell. In 2008, Loubéry and colleagues (Loubery *et al.*, 2008) isolated early endosomal compartments from HeLa cells, aiming to reconstruct *in vitro* the movements of these compartments along microtubules. They found that both kinesin-1 and kinesin-2, and dynein are present on moving early endosomes. Retrograde transport has been shown to be mostly mediated by dynein (Driskell *et al.*, 2007; Hernandez-Perez *et al.*, 2023; Xiang *et al.*, 2015; Yap *et al.*, 2022), with some evidence suggesting a contribution of kinesin-14 KIFC1 to retrograde movement (Villari *et al.*, 2020).

Rab5 GTPases, which in humans include Rab5a, Rab5b and Rab5c, regulate early endosome' movement and fusion of early endosomes with each other (Yuan & Song, 2020). Rab5 interacts with more than 25 different effectors, which include early endosome antigen-1 (EEA1) and rabaptin-5 (Yuan & Song, 2020). Both dynein and several kinesins, particularly from the kinesin-3 family, were shown to colocalize with Rab5 on endosomes

(Driskell *et al.*, 2007; Hoepfner *et al.*, 2005; Pupo *et al.*, 2018). At the same time, perturbation of anterograde or retrograde transport, either by disrupting motor function (Schuster *et al.*, 2011) or the microtubule network (Baravalle *et al.*, 2005), blocked early endosome trafficking.

Most of the evidence implicating dynein in early endosome transport comes from studies in filamentous fungi (Xiang *et al.*, 2015). Studies in fungi show that dynein-driven transport of early endosomes is associated with adaptors belonging to the Hook family (Bielska *et al.*, 2014; Christensen *et al.*, 2021; Guo *et al.*, 2016; Kendrick *et al.*, 2018; Olenick *et al.*, 2016). Hook was first described in flies, where mutations were found to result in abnormalities in endocytic trafficking (Krämer & Phistry, 1998). Mammals have three Hook proteins: Hook1, Hook2, and Hook3. While Hook2 is described as having functions related to mitosis (Dwivedi *et al.*, 2019), Hook1 and Hook3 are implicated in a variety of endosomal trafficking pathways, in particular Rab5-associated endosomes (Guo *et al.*, 2016; Luiro *et al.*, 2004; Maldonado-Baez *et al.*, 2013; Xu *et al.*, 2008).

In 2008, Xu and colleagues (Xu *et al.*, 2008) described that Hooks form a stable complex, the FHF complex, with other two proteins: Fused Toes (FTS) and FHF Complex Subunit Hook-Interacting Protein (FHIP) (**Figure 7**). Besides having three Hook proteins, mammals have four FHIP proteins and one FTS protein. This diversity means that the FHF complex may be composed of different combinations of Hook and FHIP proteins, resulting in the recruitment of dynein to different membrane compartments (Christensen *et al.*, 2021). Christensen and colleagues (Christensen *et al.*, 2021) identified the FHF complex composed of Hook3, FHIP1B and FTS, as the one responsible for linking early endosomes to dynein.

In the fungus *Aspergillus nidulans*, FHF consists of FtsA, HookA, and FhipA, and pertubation of any of these subunits results in defects in RabA/Rab5-associated early endosome motility (Yao *et al.*, 2014). Interestingly, the Hook protein in the fungus *Ustilago maydis*, Hok1, mediates both dynein and kinesin-3 recruitment to early endosomes and thus regulates their bidirectional motility (Bielska *et al.*, 2014). How Hook controls the directionallity of endosome movement is still under exploration. In the case of fungal hyphae, microtubule plus-ends are oriented towards the tip, meaning that Rab5-endosomes will be transported towards the base of the hyphae by dynein and to the tip by kinesin. However, in situations where microtubule arrays have mixed polarity, for example the dendrites of vertebrate neurons, additional regulatory mechanisms must exist to confer directionality to endosome transport.

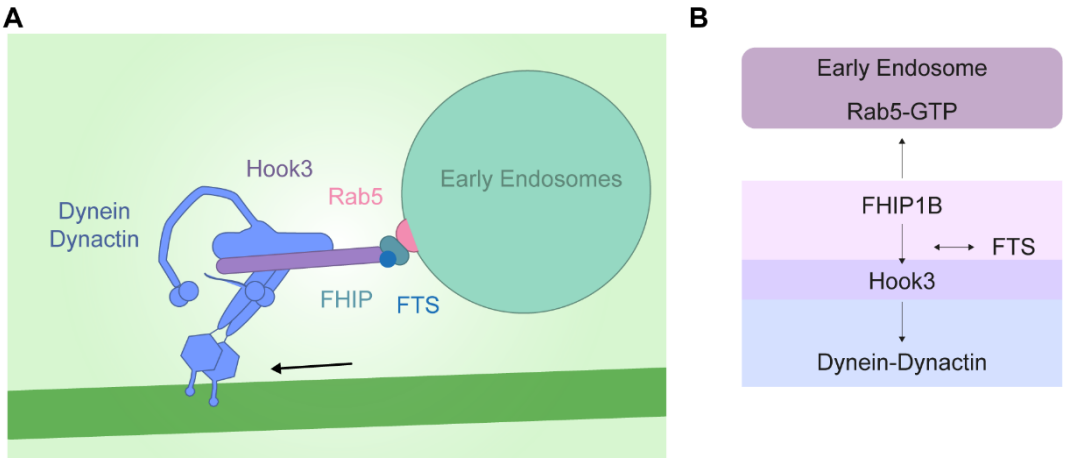

Figure 7 - The retrograde transport of early endosomes depends on a tight interaction between the motor complex and early endosomes through the FHF complex.
Simplified schematics of the FHF complex bridge between dynein motor complex and early endosomes (**A**) and pathway of recruitment described in mammals (**B**). Created by the author.

Functional significance of the transport

Microtubule-based transport of endosomal organelles is a critical process that contributes to the maintenance of cellular homeostasis, intracellular communication, and the overall functionality of cells (Barlan & Gelfand, 2017).

Motor-driven transport plays a particularly crucial role in highly polarized cells such as neurons, In some species, neurons can extend over several meters in length, making cytoplasmic diffusion an ineffective mechanism for the timely delivery of cargoes to their required destinations (Zhang *et al.*, 2021). Mutations in motor-related proteins are implicated in several neurodegenerative and neurodevelopmental diseases, such as spinal muscular atrophy, motor neuron disease, Perry syndrome, and Charcot-Marie-Tooth 2 disease (Maday *et al.*, 2014). Spinal muscular atrophy emerges due to mutations in SMN1 (survival motor neuron gene 1). When these mutations were examined in *C. elegans*, they were found to induce abnormalities in endosomal trafficking, resulting in a decline in synaptic function (Dimitriadi *et al.*, 2016). Charcot-Marie-Tooth 2 disease is a motor and sensory neuropathy, included in a diverse collection of disorders impacting the peripheral nervous system (Morena *et al.*, 2019). While the pathology encompasses multiple contributing factors, the involvement of intracellular transport is evident due to the disease-associated mutations in kinesins and dynein, as well as in Rab proteins like Rab7 (Zhang *et al.*, 2013). Notably, a majority of the mutations linked to the disorder have been found to display trafficking-related phenotypes (Morena *et al.*, 2019).

Endosomal transport is not only important in neurons. Several studies sugest a role for endosomal transport during cell division, particularly during cytokinesis and mitotic

spindle positioning and organization. During cytokinesis, temporally and spatially regulated membrane addition is needed at the cleavage furrow. Recycling endosomes accumulate at centrosomes before cytokinesis, from where they can be targeted to the cleeavage furrow by the activity of microtubule motors (Ai & Skop, 2009; Simon & Prekeris, 2008).

Moreover, endosome transport mediated by dynein has been associated with the centration of the nucleus-centrosome complex during the first *C. elegans* zygotic division (Barbosa *et al.*, 2017; Kimura & Kimura, 2011). Impairment of the minus-end directed movement resulted in delayed centration (Barbosa *et al.*, 2017; Kimura & Kimura, 2011), implying that the motion of small organelles generates sufficient force to move the nucleus-centrosomes complex. Recycling endosomes also have a role in spindle orientation (Hehnly & Doxsey, 2014; Zhang, Squirrell*, et al.*, 2008). Recycling endosomes associate with spindle poles in a Rab11-dependent manner, and impairment of Rab11 function generates spindle misorientation. Upon Rab11 depletion, spindle microtubule density, including the astral microtubule population, is decreased (Hehnly & Doxsey, 2014), suggesting that recycling Rab11-endosomes may be important for the transportation of microtubule nucleation components like γ-tubulin (Hehnly & Doxsey, 2014).

In summary, endosomal trafficking helps cells organize their cytoplasm under distinct temporal and spatial requirements. In differentiated cells as well as in proliferating cells, endosomal trafficking has been repeatedly shown to have functional relevance. It is therefore important to understand the regulatory mechanisms underlying endosome transport.

The *Caenorhabditis elegans* epidermis as a model epithelium

In 1974, Sydney Brenner introduced *C. elegans*, a soil nematode, as a model to study development and neurobiology (Brenner, 1974). This model offers a vast array of powerful genetic tools. *C. elegans* was the first multicellular organism with a fully sequenced genome (100 Mbp), which contains more than 20000 protein-coding genes [*C. elegans* Sequencing Consortium (1998)]. Thirty eight percent of *C. elegans* genes have a predicted orthologue in humans, and 40 % of the genes associated with human disease have a nematode orthologue (Culetto & Sattelle, 2000; Shaye & Greenwald, 2011).

Years after Brenner's foundational work, the complete *C. elegans* cell lineage was described thanks to herculean efforts from Sulston that tracked the fate of every cell between fertilization and adulthood in live animals (Kimble & Hirsh, 1979; Sulston & Horvitz, 1977). *C. elegans* has an invariant number of somatic cells. Exactly 959 somatic cell nuclei plus about 2000 germ cells are present in hermaphrodites, and exactly 1031 somatic cell nuclei plus about 1000 germ cells are present in males. Using electron microscopy, *C. elegans* anatomy has been fully reconstructed. The anatomy of the worm is bilaterally symmetrical, with an elongated body composed of the same type of tissues as in other animals: muscle, nerves, gut, gonad, and skin.

Skin anatomy, functions & morphogenesis

Animal development and survival depend on the integrity of the skin. This tissue constitutes an outer protective layer that acts as a permeability barrier and participates in innate immunity, secretion, mechanosensation, and wound healing (Chisholm & Hsiao, 2012). In *C. elegans*, the shape and growth of the animal is regulated by the epidermis (also referred to as hypodermis). Like flies, *C. elegans* grows via larval molts, a process in which the animal replaces the cuticle - a collagenous exoskeleton - with a new one (Lazetic & Fay, 2017; Page & Johnstone, 2007). Between hatching and adulthood, worms go through four molts, all of which require stereotypical morphogenetic events.

The epidermis is composed of a simple epithelium, largely syncytial, in which the internal basal surface is covered by a basal lamina and the apical surface faces the environment and secretes components that form the collagenous cuticle (**Figure 8**) (Chisholm & Hsiao, 2012). The epidermis derives from the ectoderm, more specifically from the AB blastomere, and a few cells come from the C blastomere. The major morphogenetic events such as ventral enclosure and elongation occur during embryogenesis (Chisholm & Hsiao, 2012).

In adult animals, the fully matured epidermis occupies approximately 0.1 mm^2 that include approximately 230 nuclei (Chisholm & Hsiao, 2012). Postmitotic syncytia, named hyp1 through hyp11, constitute most of the larval and adult epidermis, which is formed by the fusion of mononucleate precursors during embryogenesis. The single epidermal cell hyp7 covers most of the larvae body. At each larval stage, additional cells fuse with the hyp7 cell so that in adult animals this cell contains 80% of all epidermal nuclei (139 of the total 230 epidermal nuclei) (Chisholm & Hsiao, 2012). The remaining epidermal cells hyp1 to hyp5 and hyp8 to hyp11 form the head and the tail, respectively. These cells are generated during embryogenesis and do not acquire additional nuclei by fusion during post-embryonic development. Additionally, the *C. elegans* epidermis also includes stem-like seam cells that sustain hyp7 development and growth.

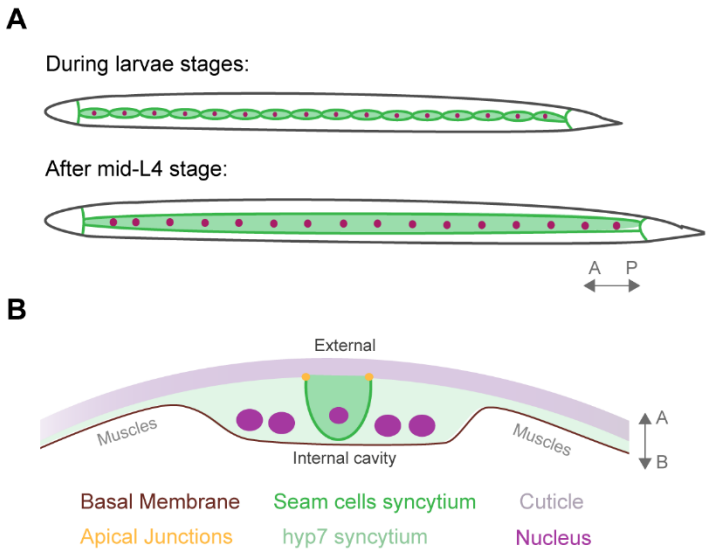

Figure 8 - Comprehensive representation of the epidermal structure of *Caenorhabditis elegans*. This figure provides both a top view (**A**) and a cross-sectional body view (**B**) to elucidate the intricate details of its epidermal layer. (**A**) Top body view shows how seam cells are organized throughout development, and (**B**) cross body view elucidates for the apical-basal details of this epithelium. Created by the author.

The Seam

The seam cells correspond to two rows of lateral epidermal cells that run the length of each side of the *C. elegans* body (H0–H2, V1–V6, and T; **Figure 8**). These cells emerge during embryogenesis and undergo stem cell-like divisions in post-embryonic development (**Figure 9**), except of H0. During the L1 larvae stage, each seam cell goes through an asymmetric cell division, in which the anterior daughter endoreduplicates its DNA and fuses with the surrounding hyp7 syncytium in a process mediated by the Wnt/β–catenin

asymmetry pathway; the posterior daughter retains its mitotic potential as a seam cell. In the second larvae stage, L2, seam cells undergo a symmetrical doubling division, prior to an asymmetric division. The anterior seam daughter V5.p does not fuse with hyp7 but instead becomes a neuroblast. During the L3 and L4 larvae stage, seam cells divide again asymmetrically as described for the L1 stage divisions (**Figure 9**). At the mid-L4 stage, the remaining seam cells terminally differentiate and fuse to form a syncytium that runs along the worm's body (**Figure 9**).

Cell fate determination is regulated by the Wnt/β–catenin asymmetry pathway, a variant of canonical Wnt signalling. Through dynamic control of β-catenin–TCF interactions, target genes are differentially expressed in the two daughter cells, which results in a coordinated balance between self-renewal and differentiation (Sawa, 2012).

During larval development, worms grow six-fold in length, several-fold in diameter, and show an overall 32-fold increase in volume (Chisholm & Hsiao, 2012). Seam cell homeostasis is essential for animal elongation beyond the larvae stages. In fact, during the first 4 days of adulthood, worms continue to grow and almost double their volume. Such post-L4 growth involves increased epidermal cell size, driven by polyploidization of epidermal nuclei in the hyp7 (Flemming *et al.*, 2000). Seam cells are responsible for the formation of the lateral alae, a protruding ridge that forms longitudinally in many nematodes. The function of the alae is not clear yet but is generally associated with cuticle strength and animal movement.

Morphogenesis of the epidermis involves changes in epidermal cell shape and position, but also interactions with internal tissues, including the developing nervous system and body wall muscles (Liang *et al.*, 2015). Components of the epidermal cytoskeleton, cellular junctions, cell signalling pathways, and the extracellular matrix are therefore required for epidermal morphogenesis (Pasti & Labouesse, 2014; Quintin *et al.*, 2016; Wang *et al.*, 2015). The diversity of cellular structures and processes that occur during epidermal morphogenesis, together with the fact that the outermost layer of the worm is readily accessible by microscopy, make the epidermis an excellent experimental system to examine how fundamental cellular processes such as cell division impact tissue development.

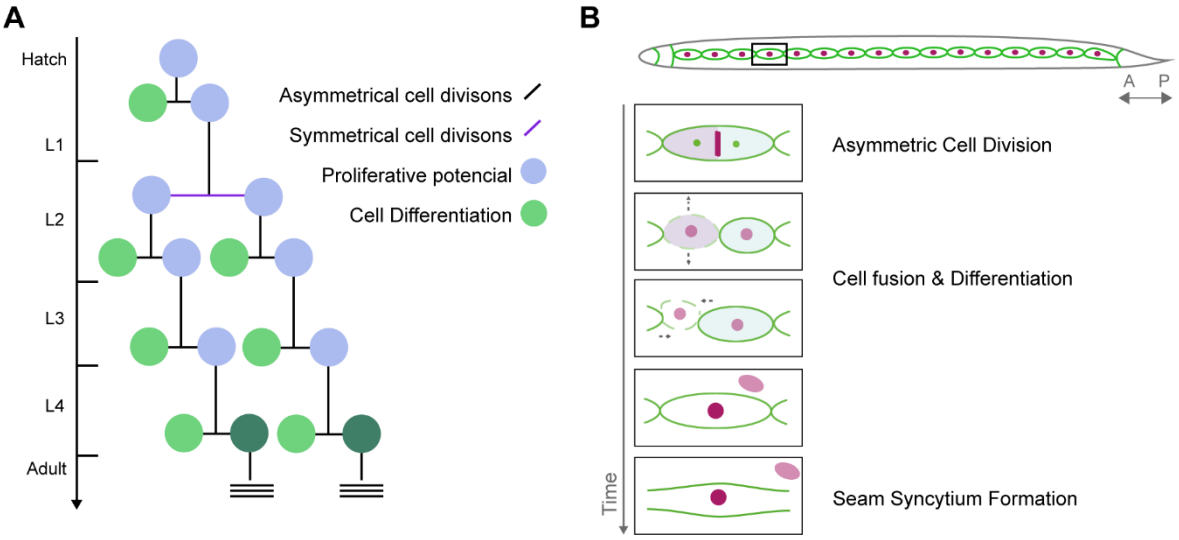

Figure 9 - Syncytial seam cell development.

Schematic of the seam cell lineage using ventral seam cells (V1-V4) as example (**A**) and representation of the major processes that occur during the seam cell postembryonic development (**B**). Epidermis development is only terminated upon formation of the seam cell syncytium that occurs after asymmetrical cell division during the L3-L4 molt. Created by the author.

Chapter II. Aims

Aims

Cytoplasmic dynein 1 plays a role in many cellular activities, including the transport and positioning of organelles, and the assembly and positioning of the mitotic spindle. Achieving this functional versatility requires regulation of dynein at multiple levels. In this thesis, the *C. elegans* epidermis was used to explore the mechanisms dynein regulation in two distinct functional contexts: asymmetric cell division and early endosome transport.

Aim I: Characterize dynein's role during asymmetric cell division in the developing epidermis

I took advantage of a hypomorphic dynein mutant to characterize dynein's role in the developing larval seam. Using live imaging at high spatio-temporal resolution, my aims were to:

- Define dynein's contribution to spindle orientation during the asymmetric stem cell-like division of seam cells;
- Determine how dynein is recruited to the seam cell cortex to generate pulling forces for spindle orientation;
- Study the impact of mis-oriented division caused by mutant dynein on epidermal tissue architecture and cell fate decisions.

Aim II: Reveal the molecular mechanism of dynein recruitment to early endosomes

Using an endogenous GFP fusion, I discovered that the Hook domain protein ZYG-12, previously characterized as a dynein adaptor for the nuclear envelope in the germline and early embryo, localizes to early endosomes in the epidermis. Using CRISPR/Cas9-mediated genome editing and live imaging, my aims were to:

- Establish whether ZYG-12 recruits dynein to early endosomes as part of the FHF complex, which has not been characterized in *C. elegans;*
- Identify the ZYG-12's domain(s) responsible for early endosome association and determine whether they are distinct from the domain that mediates nuclear envelope targeting.

Chapter III. Dynein directs prophase centrosome migration to control the division axis of stem cells in the developing *C. elegans* epidermis

Dynein directs prophase centrosome migration to control the division axis of stem cells in the developing C. elegans epidermis

This chapter was published as in **Cátia Carvalho**, Daniel J Barbosa, Ricardo Celestino, Esther Zanin, Ana Xavier Carvalho, Reto Gassmann, *Dynein directs prophase centrosome migration to control the stem cell division axis in the developing C. elegans epidermis*, Genetics, 2024;, iyae005, https://doi.org/10.1093/genetics/iyae005

Personal contribution: Cátia Carvalho participated in the study design, performed the experiments, analysed the data, prepared the figures, and wrote, review and edited the manuscript.

Abstract

The microtubule motor dynein is critical for the assembly and positioning of mitotic spindles. In *C. elegans*, these dynein functions have been extensively studied in the early embryo but remain poorly explored in other developmental contexts. Here we use a hypomorphic dynein mutant to investigate the motor's contribution to asymmetric stem cell-like divisions in the larval epidermis. Live imaging of seam cell divisions that precede formation of the seam syncytium shows that mutant cells properly assemble but frequently mis-orient their spindle. Mis-oriented divisions misplace daughter cells from the seam cell row, generate anucleate compartments due to aberrant cytokinesis, and disrupt asymmetric cell fate inheritance. Consequently, the seam becomes disorganized and populated with extra cells that have lost seam identity, leading to fatal epidermal rupture. We show that dynein orients the spindle through the cortical GOA-1$^{G\alpha i}$–LIN-5^{NuMA} pathway by directing the migration of prophase centrosomes along the anterior–posterior axis. Spindle mis-orientation in the dynein mutant can be partially rescued by elongating cells, implying that dynein–dependent force generation and cell shape jointly promote correct asymmetric division of epithelial stem cells.

Introduction

Animal mitosis requires the assembly of a microtubule-based chromosome segregation machine called the spindle, in which microtubules grow out from centrosome-containing spindle poles (Valdez *et al.*, 2023). Astral spindle microtubules, which in most

cells make contact with the cell cortex, are used to position the spindle (McNally, 2013; Pietro *et al.*, 2016), and this in turn determines the division axis and the relative size of daughter cells. In oriented divisions, which play a major role in the development and maintenance of tissues (Lechler & Mapelli, 2021), the spindle axis aligns with a pre-defined axis in the tissue. Regulated positioning of the spindle is particularly important for asymmetric cell division that generates daughter cells with distinct fates, such as the choice between self-renewal versus differentiation in stem cells (Bergstralh & St Johnston, 2014; Dewey *et al.*, 2015; Williams & Fuchs, 2013).

Among the mechanisms that control spindle positioning are cortical cues. These typically involve the microtubule minus-end-directed motor complex cytoplasmic dynein 1 (dynein), which contains two copies each of a motor heavy chain (HC), an intermediate chain (IC), a light intermediate chain, and three light chains. To be active, dynein needs to stably associate with the dynactin complex (Carter *et al.*, 2016). One of the interactions between the two complexes involves the dynactin p150 subunit and the N-terminus of dynein IC, which also binds the dynein co-factor paralogs Nde1 and Ndel1 (Richard J. McKenney *et al.*, 2011). Whether these interactions mediated by dynein IC play a role in spindle positioning remains to be determined.

When localized at the cell cortex together with dynactin, dynein can exert pulling forces on astral microtubules, and studies in *C. elegans*, *D. melanogaster*, and human cells have identified a set of core components required for this activity (Kiyomitsu, 2019; Kotak, 2019; Kotak & Gonczy, 2013): the G protein subunit Gαi, which has two *C. elegans* orthologues called GOA-1 and GPA-16, is anchored in the plasma membrane and in its GDP–bound form interacts with C-terminal GoLoco motifs in *D. melanogaster* Pins, *C. elegans* GPR1/2 (G-protein regulators 1 and 2) and vertebrate LGN (leucine glycine asparagine). N-terminal tetratricopeptide repeats in these proteins then recruit the coiled-coil adaptor for dynein–dynactin, called *D. melanogaster* Mud (Mushroom body defective), *C. elegans* LIN-5 (abnormal cell lineage 5) and vertebrate NuMA (nuclear mitotic apparatus).

In *C. elegans*, studies addressing dynein–dependent cortical force generation during asymmetric cell division have focused on the P-cell lineage in the early embryo (Colombo *et al.*, 2003; Couwenbergs *et al.*, 2007; Gotta & Ahringer, 2001; Grill *et al.*, 2001; Grill *et al.*, 2003; Gusnowski & Srayko, 2011; Miller *et al.*, 2000; Nguyen-Ngoc *et al.*, 2007; Portegijs *et al.*, 2016; Rodriguez-Garcia *et al.*, 2018; Srinivasan *et al.*, 2003; Tsou *et al.*, 2003). This has revealed instances in which the direction of dynein–dependent centrosome or spindle movement correlates with asymmetric distribution of the motor's cortical recruitment machinery. In the embryonic founder cell P0, sequential enrichment of GPR-1/2 at the

anterior cortex during prophase and the posterior cortex at metaphase/anaphase is thought be at least partly responsible for the asymmetry of pulling forces that center the nuclear–centrosome complex and displace the spindle toward the posterior, respectively (Colombo *et al.*, 2003; Gotta *et al.*, 2003; Park & Rose, 2008). In the P2 cell of the four–cell embryo, GPR-1/2 become enriched at the EMS/P2 boundary, which likely helps bring about the rotation of the nuclear–centrosome complex in late prophase such that one of the nascent spindle poles faces the GPR-1/2–enriched region (Heppert *et al.*, 2018; Werts *et al.*, 2011; Zhang, Skop*, et al.*, 2008). In addition to positioning the spindle, dynein plays essential roles in spindle assembly, including nuclear attachment of centrosomes and their separation to opposite sides of the nucleus in prophase (Raaijmakers & Medema, 2014). In the *C. elegans* early embryo, dynein inhibition prevents prophase centrosome separation and, consequently, formation of a bipolar spindle, resulting in chromosome segregation failure (Gönczy et al., 1999; Schmidt *et al.*, 2005). Dynein's essential role during embryonic cell division makes it challenging to examine how the motor contributes to asymmetric cell divisions in post-embryonic tissues. Furthermore, dynein's involvement in spindle assembly means that dynein *null* mutants are of limited use when trying to assess the motor's specific contribution to spindle orientation.

Seam cells in the *C. elegans* epidermis are a model for asymmetric division within a polarized epithelium (Chisholm & Hsiao, 2012). In larvae, seam cells form a linear row on each lateral side. Apical junctions connect seam cells with each other and with the surrounding hyp7 syncytium, which is generated in the embryo. Larval development of the seam involves a stereotypical series of proliferative (L2 stage) and self-renewing asymmetric divisions (L1, L2, and L3 stage) that expand the number of seam cells and generate daughters with distinct fates, respectively. Following an asymmetric division, the anterior daughter cell undergoes terminal differentiation either by fusing with hyp7 or adopting a neuronal identity. The posterior daughter retains seam identity and goes on to form an apical junction with its neighbor, thereby closing the gap in the seam left by the differentiated anterior daughter. Seam cells can therefore be regarded as stem cells with limited potential for self-renewal. At the L4 stage, the 16 lateral seam cells fuse with each other to generate the mature seam syncytium. The seam secretes components of the cuticle, the external structure that acts as a permeability barrier and is critical for the integrity of the animal (Chisholm & Xu, 2012).

The Wnt/β–catenin asymmetry pathway, a variant of canonical Wnt signaling, plays important roles during seam cell division. Its components, which include the APC homolog APR-1, are asymmetrically distributed along the anterior–posterior axis (Mizumoto & Sawa, 2007), and this is critical for the correct fate of daughter cells (Gleason & Eisenmann, 2010; Yamamoto *et al.*, 2011). Additionally, the Wnt/β–catenin asymmetry pathway controls the

division axis by providing cues for orienting the mitotic spindle along the anterior–posterior axis. This function is redundant with geometrical cues provided by cell shape (Wildwater *et al.*, 2011) (Wildwater *et al.*, 2011), which remains elongated in mitosis due to persistent attachment between seam cells through apical junctions. The role of dynein during seam development, including the motor's potential contribution to oriented division, has not been investigated.

Here, we describe an N-terminal deletion of *C. elegans* dynein IC that supports development until adulthood but results in a disorganized seam and premature death by epidermal rupture. Live imaging analysis shows that the mutant perturbs spindle orientation, but not spindle assembly, during the last round of asymmetric seam cell divisions. This hypomorphic phenotype allowed us to determine the importance of oriented divisions for seam development, including cell fate decisions. Characterization of the cortical dynein pathway in seam cells suggests that dynein ensures spindle orientation along the anterior–posterior axis by directing the path of prophase centrosome migration and reveals interplay between dynein and cell shape-based cues.

Materials and Methods

General Cloning

For plasmid construction, DNA extraction from bacterial cultures was done using the NucleoSpin® Plasmid Mini-Prep Kit (Macherey-Nagel, Düren, Germany) according to the manufacturer’s instructions. Both DNA extraction PCR and agarose-bands were performed with NucleoSpinGel and PCR Clean-up Kit, (Macherey-Nagel). The protocol was then followed according to the manufacturer’s instructions.

Gibson Assembly and Ligation reactions

Gibson assembly was used for plasmid engineering (**Table 3**), allowing the assembly of several DNA molecules in an isothermal single reaction (Gibson *et al.*, 2009). For the use of this method, every DNA molecule to be assembled had an overlap of 20-40 base pairs. This assembly uses three enzymes: a T5 exonuclease, a DNA polymerase, and a DNA ligase in an isothermal reaction buffer (IRB - 25% (w/v) PEG-8000, 500 mM Tris-HCl, pH 7.5, 50 mM MgCl2, 50 mM DTT, 1 mM of each nucleotide, and 5 mM of NAD). The T5 exonuclease (New England BioLabs) chews back the 5’ end, the Phusion polymerase (Thermo Scientific/Apex Bio) incorporates new nucleotides in the gap, and the DNA ligase

(New England BioLabs) joins the DNA and removes any nicks. The final Gibson assembly mix was always freshly prepared with nuclease-free water, 5x IRB, Taq ligase (40 U/μL), T5 exonuclease (1 U/μL), and Phusion polymerase (2 U/μL), and this reaction was incubated at 50 ºC for 1 h. An amount between 100-200ng of predicted assembled DNA was transformed into competent *Escherichia coli* DH5α bacteria.

L4440 carrying the *alg-1* sequence was built by cloning a *alg-1* cDNA fragment amplified with primers (5' TCCATGCTTCTGCAAGTACG 3' and 5' ACCTGCACAGCTCTAGCCAT 3') from N2 cDNA into the EcoRV restriction enzyme site (**Table 3**). L4440 plasmid and amplified DNA fragments were digested with EcoRV (Fermentas Fast Digest) for 1 hour at 37 °C and the digestion products were separated in agarose gels and the bands purified as described previously. Digested L4440 was incubated with calf intestinal phosphatase (Roche) for 30 minutes at 37 °C. The purified DNA fragment was incubated with T4 Polynucleotide Kinase (Thermo Scientific) for 20 minutes at 37 °C and for 10 minutes at 75 °C. Ligation reactions were carried out with T4 DNA ligase (New England Biolabs) with the supplied buffer, using a 5:1 insert to plasmid ratio and overnight incubation at 16 °C (total volume 10 μL).

Table 3 - Plasmids constructed and used during the work developed on this chapter.

Plasmid	Backbone	Strategy	Description
pRG371	pDD162	Ligation	Peft-3::Cas9-sgRNA#1 construct for dyci-1
pRG393	pDD162	Ligation	Peft-3::Cas9-sgRNA#2 construct for dyci-1
pRG1131	pCFJ151	Gibson Assembly	Pdpy-7::dyci-1(WT)::3xFLAG::tbb-2 3' UTR
pRG1132	pCFJ151	Gibson Assembly	Pdpy-7::dyci-1(∆4-36)::3xFLAG::tbb-2 3' UTR
pRG1202	pCFJ151	Gibson Assembly	Pwrt-2::GFP::his58::tbb-2 3'UTR::operon linker::GFP:PH::unc-54 3'UTR
pRG1284	pCFJ151	Gibson Assembly	Pwrt-2::mCherry::H2B::tbb2 3'UTR::operon linker::mCherry::PH::unc 54 3'UTR
pRG1337	pCFJ151	Gibson Assembly	scmp::NLS(egl-13)::GFP::NLS(SV40)::tbb-2 3'UTR::operon linker::GFP:PH::unc-54 3'UTR
pRG1403	pL4440	Ligation	alg-1 [1135 bp] for feeding RNAi

Competent cells transformation and colonies screening

To transform DH5α/HT1105 chemically competent *E. coli* cells (homemade), cells aliquots were removed from the -80°C freezer and thaw completely on ice (10-15 minutes). The DNA was gently added, and the mix was incubated on ice for 15 minutes. After the ice incubation, the cells were heat shocked at 42°C for precisely 1 minute and then, transferred to ice for 2 minutes. For recovery, 1 mL of super optimal broth with catabolite repression (SOC) medium (home-made; 2% tryptone, 0.5% yeast extract, 1% of 1M NaCl, and 0.25% of 1M KCl) was added to the cells followed by 1 hour incubation at 37ºC in a shaker incubator. After incubation, the cells were spined for 3 minutes at 850 G, most of the supernatant was discarded, and the pellet resuspended. The total volume of the resuspended pellet was spread on prewarmed selection plates using a sterilized spreader and the plates were incubated overnight at 37°C. After checking plates for colonies, some colonies (how many colonies to pick will depend on the complexity of the assembly) were selected to grew in a 5mL LB- selective antibiotic culture. After plasmid purification, the plasmids were diagnosed using restriction enzymes and then sequenced.

Caenorhabditis elegans

The Bristol wild-type N2 strain was acquired from the Caenorhabditis Genetics Center (CGC) which is supported by the National Institutes of Health - Office of Research Infrastructure Programs (http://biosci.umn.edu/CGC/CGChomepage.html). Strains (**Table 4**) were maintained at 20 ºC, except for *lin-5(ev571)* (16 ºC), on standard nematode growth media (NGM) plates seeded with OP50 bacteria. NGM was constituted by 3 g NaCl, 2.5 g Peptone, and 17 g of agar per liter; and after autoclave 1 mL of 5 mg/mL of cholesterol, 1 mL of 1 M CaCl2, 1 mL of 1 M MgSO4 and 25 mL of 1 M KH2PO4, pH 6 were added. These plates were seeded with *E. coli* strain OP50 as a food source obtained from the CGC (Brenner, 1974). Every strain was cryopreserved at -80 ºC, in S-Basal solution (50 mM KH2PO4, 100 mM NaCl, 5mg/L cholesterol in EtOH) with 15% (v/v) glycerol. In the case of bacterial and fungal contamination, a common issue in NGM plates, worm cultures were decontaminated by bleaching gravid adult hermaphrodites with a bleach solution (5% solution of sodium hypochlorite in 0.5 M NaOH). Embryos were able to survive the bleach treatment, allowing to obtain uncontaminated offspring (Stiernagle, 2006).

Insertion of new *locus* was done using CRISPR-Cas9 system or single copy insertion of transgenes (MoSCi) as described below. All subsequent modifications were added by mating. Mating was usually performed by placing males and hermaphrodites, in a proportion of 2:1, in a mating plate overnight at 25 ºC (unless with temperature sensitive strains). The next day the mated hermaphrodites were single-outed, and the mate was considered

successful if approximately 50% of their progeny were males. In these plates, analysis of the following generations allowed the isolation of animals with several modified alleles.

Table 4 - Strains used and constructed during the work developed on this chapter.

STRAIN	GENOTYPE
N2	*N2 Bristol wild isolate*
OD1741	*ltSi570[pOD1527/pSW232; Pdpy-7::GFP::tbb-2::mCHerry::his-11; cb-unc-119(+)] I; unc-119 (ed3)III*
OD961	*ltSi249[pOD1274/pSW098; Pdlg-1delta7::dlg-1::GFP::unc-54-3' UTR; cb-unc-119(+)] I*
LP585	*lin-5(cp288[lin-5::mNG-C1^3xFlag]) II*
GCP2	*dyci-1(tm4732) IV; unc-5(e53) IV/nT1[qls51] (IV/V); dpy-11(e224) V/nT1[qls51] (IV/V)*
GCP786	*dyci-1[prt152(Δaa4-36)] IV; IV/nT1[qls51];V/nT1[qls51](IV/V)*
GCP893	*dyci-1[prt152(Δaa4-36)]IV; IV/nT1[qls51];V/nT1[qls51](IV/V); ltSi249[pOD1274/pSW098; Pdlg-1delta7::dlg-1::GFP::unc-54-3' UTR; cb-unc-119(+)]I*
GCP902	*dyci-1[prt152(Δaa4-36)]IV; IV/nT1[qls51];V/nT1[qls51](IV/V); ltSi570[pOD1527/pSW232; Pdpy-7::GFP::tbb-2::mCHerry::his-11; cb-unc-119(+)]I; unc-119 (ed3)III*
GCP972	*prtSi193[pRG1131; Pdpy-7::dyci-1(WT)::3xFLAG::tbb-2 3' UTR ; cb-unc-119(+)] II; dyci-1[prt152(Δaa4-36)]IV; IV/nT1[qls51];V/nT1[qls51](IV/V); unc-119(ed3) III*
GCP984	*prtSi199[pRG1132; Pdpy-7::dyci-1(Δaa4-36)::3xFLAG::tbb-2 3' UTR ; cb-unc-119(+)] II; dyci-1[prt152(Δaa4-36)]IV; IV/nT1[qls51];V/nT1[qls51](IV/V); unc-119(ed3) III*
GCP1055	*prtSi222[pRG1202; Pwrt-2::GFP::his-58::tbb-2 3' UTR::operon linker::GFP::PH::unc-54 3' UTR; cb-unc-119(+)] II; unc-119(ed3) III*
GCP1062	*prtSi222[pRG1202; Pwrt-2::GFP::his-58::tbb-2 3' UTR::operon linker::GFP::PH::unc-54 3' UTR; cb-unc-119(+)] II; dyci-1[prt152(Δaa4-36)]IV; IV/nT1[qls51];V/nT1[qls51](IV/V); unc-119(ed3) III*
GCP1137	*prtSi239[pRG1284; Pwrt-2::mCherry::his-58::tbb-2 3' UTR::operon linker::mCherry::PH::unc-54 3' UTR; cb-unc-119(+)] II; dhc-1(he264[N-terminal egfp]) I; unc-119(ed3) III*
GCP1159	*prtSi239[pRG1284; Pwrt-2::mCherry::his-58::tbb-2 3' UTR::operon linker::mCherry::PH::unc-54 3' UTR; cb-unc-119(+)] I ; dhc-1(he264[N-terminal egfp]) I; dyci-1[prt152(Δaa4-36)] IV; IV/nT1[qls51];V/nT1[qls51] IV/V; unc-119(ed3) III*

GCP1171	*ltSi249[pOD1274/pSW098; Pdlg-1delta7::dlg-1::GFP::unc-54-3' UTR; cb-unc-119(+)] I; unc-119(ed3) III; prtSi239[pRG1284; Pwrt-2::mCherry::his-58::tbb-2 3' UTR::operon linker::mCherry::PH::unc-54 3' UTR; cb-unc-119(+)] II*
GCP1174	*prtSi222 [pRG1202; Pwrt-2::GFP::his-58::tbb-2 3' UTR::operon linker::GFP::PH::unc-54 3' UTR; cb-unc-119(+)] II; lon-1(e185), unc-119(ed3) III*
GCP1175	*prtSi222 [pRG1202; Pwrt-2::GFP::his-58::tbb-2 3' UTR::operon linker::GFP::PH::unc-54 3' UTR; cb-unc-119(+)] II; dpy-11 (e224) V; unc-119(ed3) III*
GCP1177	*ltSi249[pOD1274/pSW098; Pdlg-1delta7::dlg-1::GFP::unc-54-3' UTR; cb-unc-119(+)] I; prtSi239[pRG1284; Pwrt-2::mCherry::his-58::tbb-2 3' UTR::operon linker::mCherry::PH::unc-54 3' UTR; cb-unc-119(+)] II; dyci-1[prt152(Δaa4-36)] IV; IV/nT1[qls51];V/nT1[qls51] IV/V; unc-119(ed3) III*
GCP1188	*lon-1(e185), unc-119(ed3) III; prtSi222 [pRG1202; Pwrt-2::GFP::his-58::tbb-2 3' UTR::operon linker::GFP::PH::unc-54 3' UTR; cb-unc-119(+)] II; dyci-1[prt152(Δaa4-36)]IV; IV/nT1[qls51];V/nT1[qls51] IV/V*
GCP1205	*dhc-1(he250[mCherry::dhc-1]) I; lin-5(cp288[lin-5::mNG-C1^3xFlag]) II*
GCP1287	*prtSi222 [pRG1202; Pwrt-2::GFP::his-58::tbb-2 3' UTR::operon linker::GFP::PH::unc-54 3' UTR; cb-unc-119(+)] II; dyci-1[prt152(Δaa4-36)]IV; IV/nT1[qls51]; dpy-11 (e224) V; V/nT1[qls51] IV/V; unc-119(ed3) III*
GCP1325	*prtSi222[pRG1202; Pwrt-2::GFP::his-58::tbb-2 3' UTR::operon linker::GFP::PH::unc-54 3' UTR; cb-unc-119(+)] II; ani-1(syb4317 [TagRFP::ani-1]), unc-119(ed3) III*
GCP1341	*prtSi222[pRG1202; Pwrt-2::GFP::his-58::tbb-2 3' UTR::operon linker::GFP::PH::unc-54 3' UTR; cb-unc-119(+)] II; dyci-1[prt152(Δaa4-36)] IV; IV/nT1[qls51];V/nT1[qls51](IV/V); ani-1(syb4317 [TagRFP::ani-1]), unc-119(ed3) III*
GCP1430	*lin-5(ev571) II; ltSi570[pOD1527/pSW232; Pdpy-7::GFP::tbb-2::mCHerry::his-11; cb-unc-119(+)] I; unc-119 (ed3)III*
GCP1431	*prtSi239[pRG1284; Pwrt-2::mCherry::his-58::tbb-2 3' UTR::operon linker::mCherry::PH::unc-54 3' UTR; cb-unc-119(+)] II; vsSi32(goa-1::gfp), unc-119(ed3) III*
GCP1438	*prtSi239[pRG1284; Pwrt-2::mCherry::his-58::tbb-2 3' UTR::operon linker::mCherry::PH::unc-54 3' UTR; cb-unc-119(+)] II; apr-1(cp166[mNG-C1^3xFlag::apr-1]) I; unc-119(ed3) III*
GCP1463	*prtSi239[pRG1284; Pwrt-2::mCherry::his-58::tbb-2 3' UTR::operon linker::mCherry::PH::unc-54 3' UTR; cb-unc-119(+)] II; prtSi262 [pRG1337; scmp::NLS(egl-13)::GFP::NLS(SV40)::tbb-2 3'UTR::operon linker::GFP:PH::unc-54 3'UTR; cb-unc119(+)] V; unc-119(ed3) III*
GCP1464	*prtSi239[pRG1284; Pwrt-2::mCherry::his-58::tbb-2 3' UTR::operon linker::mCherry::PH::unc-54 3' UTR; cb-unc-119(+)] II; dyci-1[prt152(Δaa4-36)]IV; IV/nT1[qls51];V/nT1[qls51](IV/V); prtSi262 [pRG1337; scmp::NLS(egl-*

	13)::GFP::NLS(SV40)::tbb-2 3'UTR::operon linker::GFP:PH::unc-54 3'UTR; cb-unc119(+)] V; unc-119(ed3) III
GCP1468	*prtSi239[pRG1284; Pwrt-2::mCherry::his-58::tbb-2 3' UTR::operon linker::mCherry::PH::unc-54 3' UTR; cb-unc-119(+)] II; apr-1(cp166[mNG-C1^3xFlag::apr-1]) I; dyci-1[prt152(Δaa4-36)] IV; IV/nT1[qIs51];V/nT1[qIs51](IV/V); unc-119(ed3) III*

Genome engineering using the CRISPR-Cas9 system

The *dyci-1* N-terminal deletion mutant *prt152* was generated by CRISPR/Cas9-mediated genome editing as described (Arribere *et al.*, 2014; Paix *et al.*, 2014), using two crRNAs targeting the genomic regions 5' TTTCAGAATGTCAGAACTGAGG 3' and 5' CCGTTCCACAAATGAAAATGGA 3' and a single-stranded oligonucleotide repair template. The 99-bp deletion was confirmed by sequencing. To remove potential off-target mutations, *dyci-1(ΔN)* animals were outcrossed 6x with the wild-type N2 strain.

Single copy insertion of transgenes

A Mos1 transposon-based strategy (Frøkjær-Jensen *et al.*, 2008) was used to generate strains stably expressing transgenes under the control of the *dpy-7* and *wrt-2* promoter for expression in epidermal cells and under the control of an artificial sequence SCM for specific expression in the seam cells. This strategy was used to generate prtSi193 (*Pdpy-7::dyci-1[wt]::3xFLAG*), prtSi199 (*Pdpy-7::dyci-1[Δ4-36]::3xFLAG*), prtSi222 (*Pwrt-2::GFP::his-58::operon_linker::GFP::PH[PLC1δ1]*), prtSi239 (*Pwrt-2::mCherry::his-58::operon_linker::mCherry::PH[PLC1δ1]*), and prtSi262 (*Pscm::NLS[egl-13]::GFP::NLS[SV40]::operon_linker::GFP::PH[PLC1δ1]*). Transgenes were cloned into pCFJ151 for insertion on chromosome 2 (ttTi5605 locus) and chromosome 5 (oxTi365), and transgene integration was confirmed by PCR.

Outcrossing, balancing and maintenance of balanced strains

After endogenous genome editing by CRISPR-Cas9, modified strains were outcrossed at least 3x with N2 to remove other genetic modifications that might have occurred as result of off-target mutations. The process of outcrossing consisted in consecutive mattings of the modified worms with N2 males. In the case of strains carrying recessive lethal mutations that cannot be propagated as homozygotes, genetic balancers are used to allow the differentiation between progeny heterozygous for a lethal-bearing chromosome and those homozygous for the non-lethal homologue. Genetic balancers are genetic constructs or chromosomal rearrangements that allow lethal or sterile mutations to

be stably maintained as heterozygotes (Edgley *et al.*, 2006). In this work, the *dyci-1(⊿N)* mutant required the use of a balancer for chromosome IV. The genetic balancer used consisted of a translocation, in which parts of non-homologous chromosomes exchange genetic information (nT1, reciprocal translocation of the right arm of chromosome IV and left arm of chromosome V). This balancer labelled the pharynx with GFP and was not viable when homozygous. Therefore, after balancing the strain, only heterozygous worms survived, and were identifiable by their green pharynx, or worms homozygous for the deletion, that lacked the GFP fluorescence. For maintaining this strain, heterozygous animals for the deletion were identified by the GFP-labelled pharynx in a fluorescent-adapted stereoscope.

Immunoblotting

For each strain, 200 adults were collected into cold 0.7x Egg Salts buffer (1x Egg Salts buffer is 5 mM HEPES pH 7.4, 118 mM NaCl, 40 mM KCl, 3.4 mM MgCl2, 3.4 mM CaCl2), washed 3 times with cold 0.7x Egg Salts buffer, and washed once with 0.7x Egg Salts buffer containing 0.05 % Triton X-100. To 100 µL of worm suspension, 33 µL 4x SDS-PAGE sample buffer [250 mM Tris-HCl pH 6.8, 30 % (v/v) glycerol, 8 % (w/v) SDS, 200 mM DTT and 0.04 % (w/v) bromophenol blue] and 20 µL glass beads were added. Samples were incubated for 3 min at 95 ºC and vortexed for 2 x 5 min. Supernatants were collected after centrifugation at 20000 x g for 1 min at room temperature. Proteins were resolved by SDS-PAGE and transferred to 0.2 µm nitrocellulose membranes (Hybond ECL, Amersham Pharmacia Biotech). Membranes were rinsed 3 x with TBS (50 mM Tris-HCl pH 7.6, 145 mM NaCl), blocked with 5 % non-fat dry milk in TBST (TBS with 0.1 % Tween-20) and probed at 4 ºC overnight with the following primary antibodies: mouse monoclonal anti-FLAG M2 (Sigma-Aldrich F3165, 1:1000), mouse monoclonal anti-α-tubulin B512 (Sigma-Aldrich T5168, 1:5000), rabbit polyclonal anti-DYCI-1 GC1 [(Barbosa *et al.*, 2017), 1:2000], rabbit polyclonal anti-DHC-1 GC4 [(Simões *et al.*, 2018), 1:1000], rabbit polyclonal anti-DLI-1 GC11 [(Carvalho *et al.*, 2024), 1:2500]. Membranes were washed 3 x with TBST, incubated with goat polyclonal anti-mouse IgG (Jackson ImmunoResearch 115-035-044, 1:10000) or anti-rabbit IgG (Jackson ImmunoResearch 111-035-003, 1:10000), coupled to HRP, for 1 hour at room temperature, and washed again 3 x with TBST. Proteins were detected by chemiluminescence using Pierce ECL Western Blotting Substrate (Thermo Scientific) and X-ray film (Fuji).

Synchronization at the L1 stage

The selection of synchronized population (same age group) is needed in any model organism that has different developmental stages such as embryonic, larval, and adult. In *C. elegans*, several protocols are available however they tend to not allow a developmental resolution by hours. Bleaching of adult gravid hermaphrodites followed by overnight no-bacterial buffer incubation at room-temperature allows the synchronization of the embryo's population in L1 larvae. The development of this population is restarted (recovered) by the animals to a media with a food source.

Plates confluent with adult animals were washed with M9 buffer and worms were pelleted for 3 min at 600 x g. The pellet was washed once with 0.1 M NaCl, bleaching solution (67 % 0.1 M NaCl, 22 % house-hold bleach, 11 % 5 N NaOH) was added, and the worm suspension vortexed for 10 min. Embryos were pelleted, washed 4 x with M9 buffer, and allowed to develop and hatch in M9 buffer overnight at room temperature. For release from L1 arrest, animals were transferred to an NGM plate with bacteria.

Life span

In nematodes, life span is typically defined as the number of days an animal remains responsive to external stimuli. This assessment allows a good readout for the health status of the animals. To do it proficiently, the worm population was synchronized at the L1 stage. Synchronized animals were collected 24 h after release from L1 arrest and transferred every 2 days to a new NGM plate with bacteria. Animals were examined every day and scored as dead if they did not respond to touch and if there was no evidence of pharyngeal pumping. Animals that escaped or were found dead on the edge of the plate were excluded from the assay.

Permeability

Synchronized animals at the adulthood day 1 stage (72 h after release from L1 arrest) were incubated in a depression slide well with 1 µg/mL of Hoechst dye 33342 (Invitrogen) for 15 min in the dark. Animals were washed 2 times with 0.7x Egg Salts buffer, immobilized with 5 mM levamisole for 10 min, and mounted on a freshly prepared 2 % (w/v) agarose pad for imaging. Animals were scored as permeable if at least three epidermal nuclei were stained with the Hoechst dye.

Animal length

Synchronized animals 48 h after release from L1 arrest were transferred to a new NGM plate with a thin layer of bacteria. Images were taken at 20 ºC using an SMZ 745T stereoscope (Nikon) with a QIClic CCD camera (QImaging) and controlled by Micro-Manager software (Open Imaging). Animal length was determined by tracing a segmented line along the body using Fiji software (Image J).

RNA interference by feeding

RNAi was performed by feeding animals with HT115 E. coli bacteria expressing dsRNA. The L4440 plasmids targeting *goa-1* and *lin-5* were obtained from the Ahringer library [(Kamath *et al.*, 2003); distributed by Source BioScience] and L4440 targeting *alg-1* was generated as described. To prepare feeding plates, bacteria were grown in LB containing 12.5 µg/mL tetracycline and 100 µg/mL ampicillin until an OD600 of 1.6, then pelleted at 2500 x g for 10 min and resuspended in LB with 12.5 µg/ml tetracycline, 100 µg/mL ampicillin, and 1 mM IPTG. Resuspended bacteria were spread onto NGM agar plates (~75 µL/plate) previously soaked with 100 µL of a 1:1:1 mixture of 100 mg/mL ampicillin, 5 mg/mL tetracycline and 1 M IPTG. Plates were dried in the dark at room temperature for 1 – 3 days to induce RNA expression. L1 animals were placed on the plates and incubated at 20 °C until imaging.

Microscopy

Animals were immobilized with 5 mM levamisole for 10 min, mounted on a freshly prepared 2 % (w/v) agarose pad, and covered with an 18 mm × 18 mm coverslip (No. 1.5H, Marienfeld). For time-lapse imaging, the coverslip was sealed with VALAP (1:1:1 Vaseline: lanolin: paraffin) to prevent desiccation. Imaging was performed at 20 ºC using the following two microscopes: a Zeiss Axio Observer, equipped with an Orca Flash 4.0 camera (Hamamatsu) and a Colibri 2 light source (Zeiss), controlled by ZEN software (Zeiss); and a Nikon Eclipse Ti coupled to an Andor Revolution XD spinning disk confocal system, composed of an iXon Ultra 897 CCD camera (Andor Technology), a solid-state laser combiner (ALC-UVP 350i, Andor Technology), and a CSU-X1 confocal scanner (Yokogawa Electric Corporation), controlled by Andor IQ3 software (Andor Technology).

Seam morphology, seam cell fate markers, and epidermal microtubules

For DLG-1::GFP imaging, late-L4 stage animals were imaged on the Axio Observer microscope with a 40x NA 1.3 Plan-Neofluar objective. For imaging of

GFP::NLS/GFP::PH(PLC1δ1)/mCh::HIS-11/mCh::PH(PLC1δ1), 5-µm z-stacks (step size 0.1 – 0.5 µm) were acquired on the spinning disk confocal system using a 60x NA 1.4 Plan-Apochromat objective. For imaging of GFP::TBB-2, z-stacks (step size 0.1 µm) were acquired on the spinning disk confocal system using a 100x NA 1.45 Plan-Apochromat objective.

Live imaging of dividing seam cells

Developmentally synchronized animals were imaged 30 h after release from L1 arrest. Since feeding with HT115 bacteria slightly delays development, animals in RNAi experiments were imaged at the 36 h time point. Imaging was performed on the spinning disk confocal system using a 60x NA 1.4 Plan-Apochromat or 100x NA 1.45 Plan-Apochromat objective. A 3- to 5-µm z-stack was acquired every 30 s from the start of centrosome separation until cytokinesis.

Cherry-temp setup

Rapid temperature shifts were performed using the CherryTemp heater-cooler (Cherry Biotech) coupled to the spinning disk confocal system. Animals were kept at 16 ºC for 55 h after release from L1 arrest and mounted on a thin 2 % (w/v) agarose pad, which was inverted onto another pad and cropped to fit in the 20 µm spacer. This setup was transferred to the CherryTemp chip, engravements facing down, pad centred on the thermalising pattern. Temperature was initially set to 16 ºC (permissive temperature). After identification of dividing cells, temperature was upshifted to 26 ºC (restrictive temperature), focus was adjusted, and live imaging was performed with a 60x NA 1.4 Plan-Apochromat objective.

Imaging analysis

Image analysis was performed with Fiji (ImageJ) and Imaris (Oxford Instruments) software. Quantified images were acquired in at least 3 independent experiments, using the same laser power and exposure times within experiments.

Microtubule bundle density

After maximum intensity projection of the z-stack, the 'Plot Profile' function in Fiji was used on a free-hand line of approximately 40 µm drawn along the A–P axis in the dorsal or ventral region. Microtubule bundle density was calculated by dividing the number of distinct GFP::TBB-2 peaks by the length of the line.

Spindle orientation and length

In GFP::TBB-2/mCh::HIS-11 movies, the XYZ coordinates of centrosomes and spindle poles were determined automatically using Imaris software (Oxford Instruments), and the tracks were manually verified. In GFP::PH(PLC1δ1)/GFP::HIS-11 movies, the XY coordinates of the two outermost chromosomes of the metaphase plate were determined using the MTrackJ plugin in Fiji to define the metaphase plate axis. The A–P axis was defined by the coordinates of two points on the seam cell long axis.

Cell shape

The elongation factor was determined by dividing the length of the cell by its width. Measurements were performed in the frame before anaphase onset in an apical z-plane where the junctions that connect seam cells are visible.

Dynein intensity during seam cell asymmetrical division

To quantify GFP::DHC-1 intensity variation at the cell-cell contacts during division, the Poligon selection tool was used to draw the Region of Interest (ROI). The Raw Integrated Density was measured every frame using ROI, and a new box was draw on the seam cell cytoplasm to measure the background signal. Background signal was subtracted to the ROI measured levels. Whenever possible, both anterior and posterior seam cell contacts were measured. Examples where cell boundaries were not clearly distinguishable either were out of focus were excluded from the analysis. To each example, intensity levels normalized to the maximum value found within the time course of that example. Finally, the normalized kinetics curve for each cell contact was aligned relative to NEBD.

Cortical line profiles

For line profiles across the hyp7–seam cell border, a straight line was drawn perpendicularly to the border in unprojected z-stacks, starting in the hyp7 cell. The line was 4 µm long and 10 pixels wide, except for mCh::DHC-1/LIN-5::mNG (3 µm long and 4 pixels wide). The line was then centered on the border, and the fluorescence profile was recorded using the 'Plot Profile' function in Fiji. The average of the first 5 signal intensity values was designated as background and was subtracted from the line profile. GFP/mCherry profiles were aligned relative to peak mCherry signal, profiles of replicates were averaged, normalized to the maximum average, and plotted as mean ± SEM. GFP::DHC-1 values in *dyci-1(ΔN)* were normalized to the maximum average of the control profile to allow for

relative comparison of intensities. For line profiles along the hyp7–seam cell border, a segmented line was drawn along the lateral side of the cell in 2 - 3 successive z-planes for a total of 4 - 6 line profiles per cell. The line was 4 pixels and 5 pixels wide for LIN-5::mNG and GOA-1::GFP, respectively. Signal intensity values were normalized to line length and averaged over 1 % intervals. For LIN-5::mNG, the lowest value in the profile plot was considered background. For GOA-1::GFP, the mean signal intensity in a box in the seam cell cytoplasm served as background. After background subtraction, all profiles from an individual cell were averaged, and resulting profiles from different cells were plotted as mean ± SEM.

Statistical analysis

Statistical analysis was performed with Prism 9.0 software (GraphPad). Statistical significance was determined by ordinary one-way ANOVA followed by Šídák's multiple comparison test, or by a two-sided Mann-Whitney test, where ****P < 0.0001, ***P < 0.001, **P < 0.01, *P < 0.05, and ns = not significant, P > 0.05. The analytical method is specified in the figure legends.

Results

An N-terminal deletion mutant of C. elegans dynein IC supports development but results in premature death of adults by epidermal rupture

In an effort to determine the functional significance of the dynein IC N-terminus, which binds the co-factors dynactin p150 and Nde1/Ndel1, we used CRISPR/Cas9-mediated genome editing to delete residues 4 to 36 in the *C. elegans* dynein IC homolog DYCI-1 (**Figure 10A; Supplementary Figure 1A**). Animals homozygous for the mutation, hereafter referred to as *dyci-1(ΔN)*, develop into fertile adults, which lay embryos that fail to hatch. This contrasts with animals homozygous for the null allele *dyci-1(tm4732)*, which become developmentally arrested between larval stages L2 and L3 (**Figure 10A, B**). These findings indicate that dynein maintains residual activity when the DYCI-1 subunit cannot bind to co-factors, and that this residual activity is sufficient to support development to adulthood and fertility. The hypomorphic nature of *dyci-1(ΔN)* therefore offers an opportunity to examine the roles of dynein at developmental stages that are inaccessible with dynein null mutants.

Surprisingly, we found that developmentally synchronized *dyci-1(ΔN)* animals started to die 3 days after being released from L1 arrest, and 90 % of animals were dead 3 days later (**Figure 10C**). *dyci-1(ΔN)* animals therefore die shortly after reaching adulthood. Closer inspection revealed that *dyci-1(ΔN)* animals overwhelmingly (92 %, n=212) died by rupturing (**Figure 10D**). Dynein is required for proper formation of the vulva (Celestino *et al.*, 2019), the weakest point in the cuticle, but differential interference contrast imaging showed that *dyci-1(ΔN)* animals did not rupture through the vulva (**Supplementary Figure 1B**). We conclude that *dyci-1(ΔN)* weakens cuticle integrity beyond the vulva, causing penetrant premature death by spontaneous epidermal rupture.

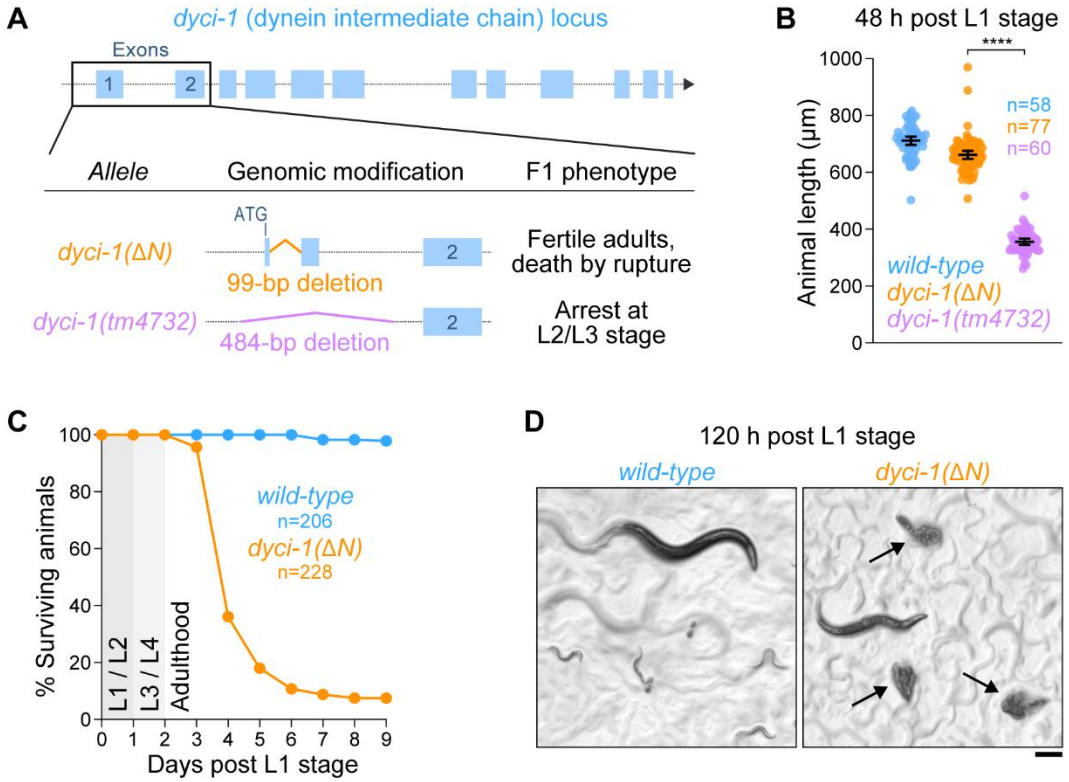

Figure 10 - An N-terminal deletion mutant of *C. elegans* dynein IC results in premature death by epidermal rupture.

(A) Schematic of the *dyci-1* locus and N-terminal deletion mutants. **(B)** Animal length measured 48 h after release from L1 arrest. Data points correspond to measurements in individual animals. *n* denotes the number of animals examined. Bars show mean ± 95% CI. Statistical significance was determined by the Mann-Whitney test. ****$P < 0.0001$. **(C)** Lifespan analysis after release from L1 arrest. *n* denotes the number of animals examined. **(D)** Images of animals on a plate with bacteria, 120 h after release from L1 arrest. Arrows point to adults that died by spontaneous epidermal rupture. Scale bar, 0.2 mm.

The dyci-1(ΔN) mutation compromises epidermal seam integrity

The penetrant rupture phenotype of *dyci-1(ΔN)* animals suggested that the mutation compromises cuticle integrity. Consistent with this idea, the cuticle of *dyci-1(ΔN)* animals was permeable to the normally excluded dye Hoechst 33342 when assayed 72 h after release from L1 arrest (**Figure 11A, B**). Cuticle formation requires secretion from epidermal cells (Chisholm and Xu, 2012). To test whether the cuticle integrity defect in *dyci-1(ΔN)* animals reflects compromised dynein function in the epidermis, we expressed wild-type *dyci-1* from a single-copy integrated transgene under the epidermal promoter P*dpy-7*. Epidermal expression of transgenic wild-type *dyci-1* in *dyci-1(ΔN)* animals rescued cuticle permeability and prevented premature death by rupture (**Figure 11C**). By contrast, *dyci-1(ΔN)* animals expressing transgenic *dyci-1(ΔN)* in the epidermis still ruptured (72 % of dead animals, n=158). These results show that dynein function in the epidermis is required for cuticle integrity.

To examine epidermal tissue morphology in *dyci-1(ΔN)* animals, we imaged the apical junction component DLG-1::GFP. In control L4 animals, DLG-1::GFP localized to two continuous parallel lines per lateral side, which mark the border between the seam syncytium and epidermal cells, primarily the large syncytial hyp7 cell (**Figure 11D, E**). In *dyci-1(ΔN)* animals, the seam was frequently disrupted by gaps and compartments of variable sizes. A similarly disorganized seam syncytium, as well as animal death by rupture, had previously been described for co-inhibition of the ninein-like protein NOCA-1 and the patronin homolog PTRN-1 (Wang *et al.*, 2015). Since co-inhibition of NOCA-1 and PTRN-1 perturbs the circumferential microtubule array in the hyp7 cell (Wang *et al.*, 2015), we asked whether aberrant seam morphology in *dyci-1(ΔN)* animals could be caused by a disorganized microtubule cytoskeleton. Visualization of epidermal microtubules with GFP::β-tubulin (TBB-2) showed that the *dyci-1(ΔN)* mutation, in contrast to co-inhibition of NOCA-1 and PTRN-1, did not perturb the regular arrangement of microtubule bundles in hyp7 (**Supplementary Figure 1C, D**). We conclude that *dyci-1(ΔN)* causes severe morphological defects in the seam without affecting epidermal microtubule organization.

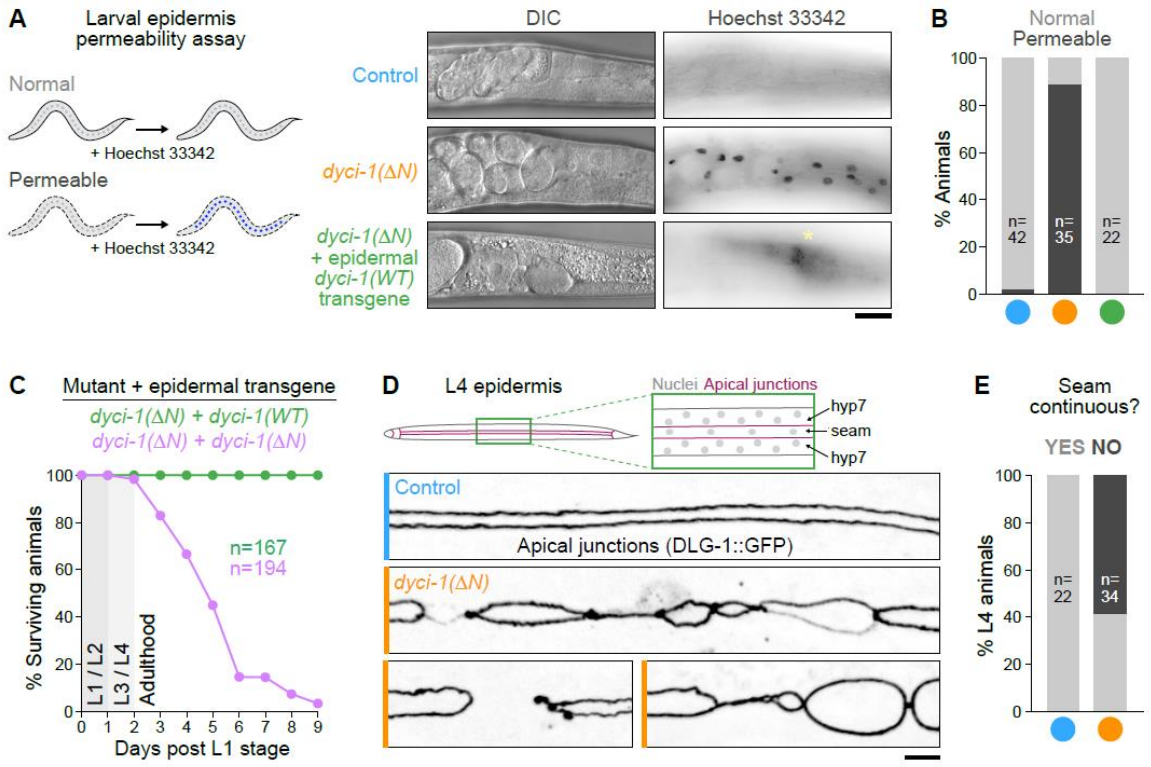

Figure 11 - The *dyci-1(ΔN)* mutation compromises epidermal seam integrity.

(A) *(left)* Schematic illustrating that the membrane–permeable dye Hoechst 33342 stains epidermal nuclei if the barrier function of the cuticle is compromised. *(right)* Differential interference contrast (DIC) and corresponding fluorescence images after Hoechst 33342 staining. Asterisk marks intestinal autofluorescence. Scale bar, 30 µm. **(B)** Quantification of epidermal permeability using the assay shown in *(A)*. *n* denotes the number of animals examined. **(C)** Lifespan analysis after release from L1 arrest. *n* denotes the number of animals examined. **(D)** *(top)* Schematic showing apical junctions in the late-L4 epidermis, which connect the syncytial hyp7 cell with the lateral seam syncytium. *(bottom)* Fluorescence images of late-L4 animals expressing the apical junction marker DLG-1::GFP. **(E)** Quantification of seam discontinuities based on images as shown in *(D)*. *n* denotes the number of animals examined.

The dyci-1(ΔN) mutation causes spindle mis-orientation during asymmetric seam cell division

To understand why *dyci-1(ΔN)* results in a disorganized seam, we monitored the last round of seam cell divisions at the L3 larval stage by time-lapse imaging in animals co-expressing GFP::TBB-2 and mCherry (mCh)-tagged histone H2B (HIS-11) (**Figure 12A**). Control cells proceeded from nuclear envelope breakdown (NEBD) to anaphase onset in 6.2 ± 0.5 min (mean ± 95 % CI) (**Figure 12B**), and divided along the A–P axis defined by the seam cell row. *dyci-1(ΔN)* cells assembled a bipolar spindle of normal size, which elongated in anaphase at the same rate as control spindles (**Figure 12C, D**). Chromosome

congression took slightly longer in *dyci-1(⊿N)* cells, which extended the NEBD–anaphase onset interval by 5 min on average (**Figure 12B**), but there was no discernible chromosome mis-segregation in anaphase. In contrast to control cells, metaphase spindles in *dyci-1(⊿N)* were occasionally severely mis-oriented (**Fig 12A**). Measurement of the angle between the spindle axis and the A–P (long) axis of cells in 3D image stacks revealed that spindle angles at anaphase onset were significantly increased in *dyci-1(⊿N)* cells (48 % of spindle angles above 15º versus 13 % in controls; *P* = 0.0002, Fisher's exact test) (**Figure 12E**). We conclude that dynein is required for proper spindle orientation in seam cells.

The dyci-1(⊿N) mutation perturbs positioning of prophase centrosomes along the A–P axis

To better understand how dynein contributes to spindle orientation, we examined prophase centrosome separation. At the beginning of prophase, the centrosome pair, marked by GFP::TBB-2, was positioned on A–P axis on one side of the mCh::HIS-11–marked nucleus, where the duplicated centrioles of the mitotic spindle pole had presumably come to rest at the end of the previous division. In 13 out of 14 control cells, we observed that prophase centrosomes subsequently separated along the A–P axis. One centrosome remained relatively stationary, while the other moved to the opposite side of the nucleus (**Figure 12F**). *dyci-1(⊿N)* did not inhibit centrosome separation *per se* but instead affected the path of centrosome migration such that the centrosome–centrosome axis was poorly aligned with the A–P axis at NEBD (**Figure 12C, F**). Quantitative analysis showed that centrosome–centrosome axis angles at NEBD were comparable to spindle axis angles at anaphase onset (**Figure 12E**). These results suggest that dynein sets up spindle orientation in prophase by directing centrosome migration along the A–P axis.

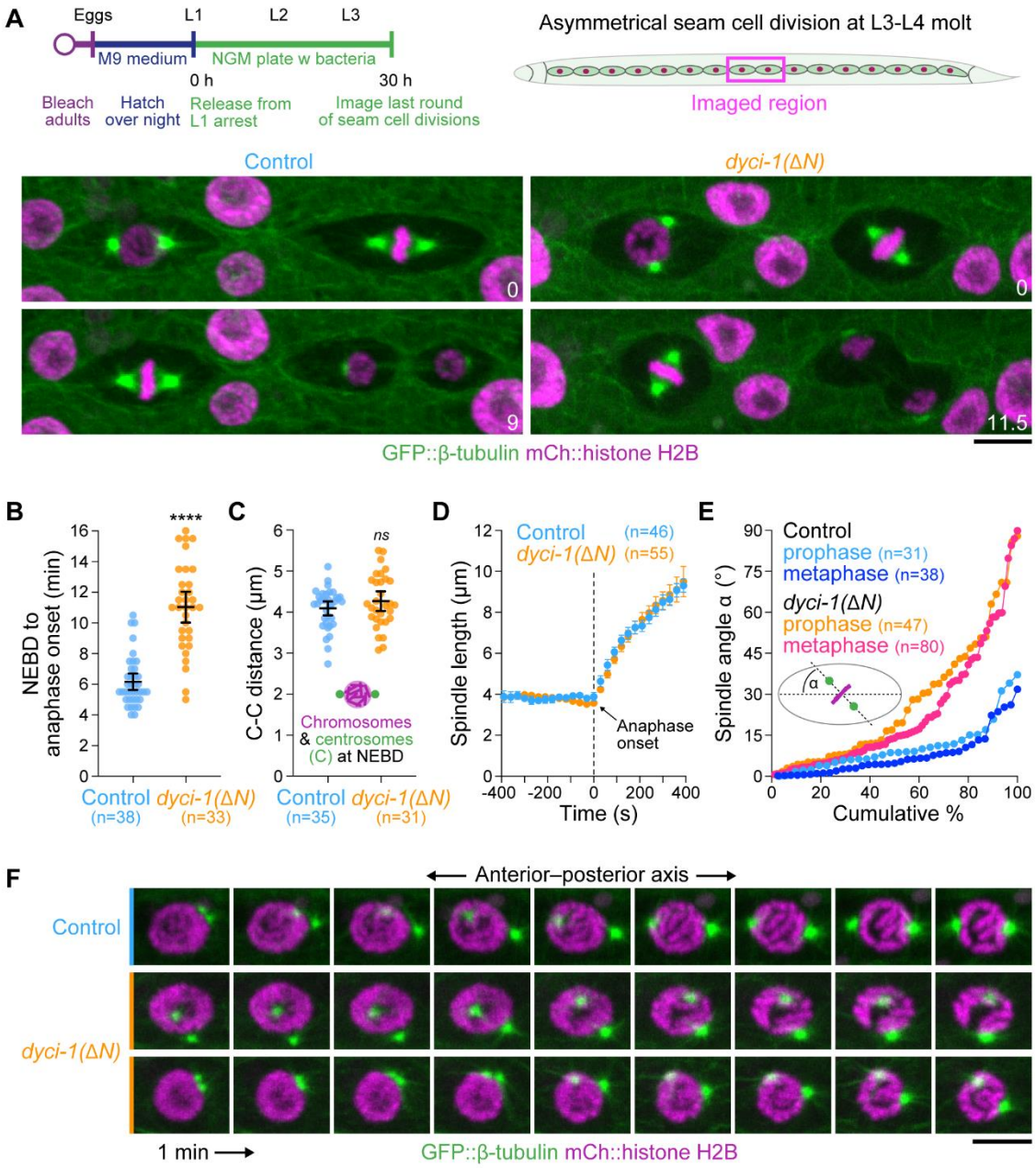

Figure 12 - The *dyci-1(ΔN)* mutation results in spindle mis-orientation during asymmetric seam cell division.

(A) *(top left)* Schematic of the experimental procedure followed for live imaging experiments. *(top right)* Schematic showing the epidermal region imaged in subsequent experiments. *(bottom)* Selected images from time-lapse movies of dividing seam cells co-expressing GFP::TBB-2 (β-tubulin) and mCh::HIS-11 (histone H2B). Time is indicated in minutes. Scale bar, 5 μm. **(B) – (E)** Quantification of seam cell mitosis. Data points in *(B)*, *(C)*, and *(E)* correspond to measurements in individual cells. Bars in *(B)* – *(D)* show the mean ± 95% CI. *n* denotes the total number of cells imaged in ≥ 20 animals. Statistical significance was determined by the Mann-Whitney test. ****$P < 0.0001$; *ns* = not significant, $P > 0.05$. **(F)** Successive frames (1 min apart) from time-lapse movies of cells as in *(A)*. Two examples are shown for the *dyci-1(ΔN)* mutant. Scale bar, 5 μm.

Dynein acts at the seam cell cortex downstream of LIN-5^{NuMA}

The observation that dynein contributes to spindle orientation in seam cells predicts that the motor is anchored at the cell cortex to generate pulling forces on astral microtubules. To test this, we examined the localization of dynein in larval L3-stage seam cells using endogenous GFP-tagged dynein HC (DHC-1), co-expressed with mCh::HIS-11 and the mCh-tagged pleckstrin homology (PH) domain of mammalian PLC1δ1 as a plasma membrane marker. During interphase and prophase, GFP::DHC-1 was highly concentrated near the apical junctions that connect neighboring seam cells and also exhibited a comparatively modest enrichment across the remaining regions of the cell cortex (**Figure 13A, B**).Line scan analysis of GFP::DHC-1 and mCh::PH showed that cortical dynein was enriched on the seam cell side of the seam-hyp7 boundary (**Figure 13D**), consistent with a role in cortical force generation in seam cells. GFP::DHC-1 also localized to mitotic centrosomes, spindle microtubules, and kinetochores, and became prominently enriched in the cleavage furrow at later stages of cytokinesis (**Figure 13A**). In the *dyci-1(ΔN)* mutant, GFP::DHC-1 was no longer noticeably enriched at subcellular sites (**Supplementary Figure 2A**).

We next examined the localization of dynein's cortical adaptor LIN-5^{NuMA} using an endogenous mNeonGreen (mNG) fusion (Heppert *et al.*, 2018). During early prophase, LIN-5::mNG was prominently enriched on the cortex but not at apical junctions between seam cells, where co-expressed mCh::DHC-1 was the most concentrated (**Figure 13C**). This suggests that dynein accumulates at seam cell contacts independently of LIN-5, and that this dynein pool is therefore unlikely to be involved in centrosome positioning. Instead, mCherry::DHC-1 and LIN-5::mNG were co-enriched at cortical sites away from seam cell contacts (**Figure 13C, D**), and line scan analysis with GFP::DHC-1 and mCh::PH confirmed that cortical dynein was enriched on the seam cell side of the seam-hyp7 boundary (**Figure 13D**), consistent with a role in cortical force generation in seam cells.

Close examination of LIN-5::mNG distribution in mitotic seam cells revealed that the anterior and posterior cortex had higher levels of LIN-5::mNG than the lateral cortex, and LIN-5::mNG tended to be displaced from the cortical region that was adjacent to separating centrosomes in early prophase (**Figure 13E, F; Supplementary Figure 2C**). Interestingly, cortical LIN-5::mNG levels decreased as cells progressed through prophase, concomitantly with an increase of LIN-5::mNG levels at centrosomes (**Supplementary Figure 2C**). LIN-5::mNG re-appeared on the cortex during prometaphase and exhibited a prominent bipolar distribution in metaphase before its cortical levels diminished again during anaphase. The bipolar distribution of LIN-5 is consistent with the idea that pulling forces generated by LIN-

5–associated dynein orient the spindle along the A–P axis, and that this cortical dynein cue already acts in early prophase to direct the migration of separating centrosomes.

To examine LIN-5 function in mitotic seam cells, we acutely inhibited LIN-5 at the larval L3 stage used the fast-acting temperature-sensitive mutant *lin-5(ev571)* (Lorson *et al.*, 2000). Rapid upshift to the non-permissive temperature (26 °C) in dividing seam cells co-expressing GFP::TBB-2 and mCh::HIS-11 resulted in centrosome separation failure (12 out of 14 cells versus 0 out of 10 in controls), while already assembled spindles became mis-oriented (7 out of 9 cells versus 3 out of 10 in controls) (**Figure 13G**). Furthermore, LIN-5 inhibition attenuated spindle elongation in anaphase (6 out of 6 cells versus 0 out of 10 in controls). RNAi-mediated depletion of LIN-5 in cells co-expressing GFP::DHC-1, mCh::HIS-11, and mCh::PH resulted in similar defects and confirmed that LIN-5 is required for GFP::DHC-1 recruitment to the cortex. By contrast, LIN-5 depletion did not affect the prominent GFP::DHC-1 concentration at seam cell contacts, consistent with the absence of LIN-5::mNG at this location (**Figure 13H, I**). These results support the idea that dynein contributes to spindle orientation in seam cells through its association with LIN-5.

Prior work demonstrated a role for the argonaute ALG-1 in seam cell spindle orientation (Wildwater *et al.*, 2011), raising the possibility that cortical dynein could be regulated by pathways involving ALG-1, such as the Wnt/β–catenin asymmetry pathway. GFP::DHC-1 accumulated robustly on the seam cell cortex in *alg-1(RNAi)* animals (**Supplementary Figure 2C, D**), which exhibited the seam defects described previously (Wildwater *et al.*, 2011). We conclude that ALG-1 is dispensable for cortical dynein recruitment.

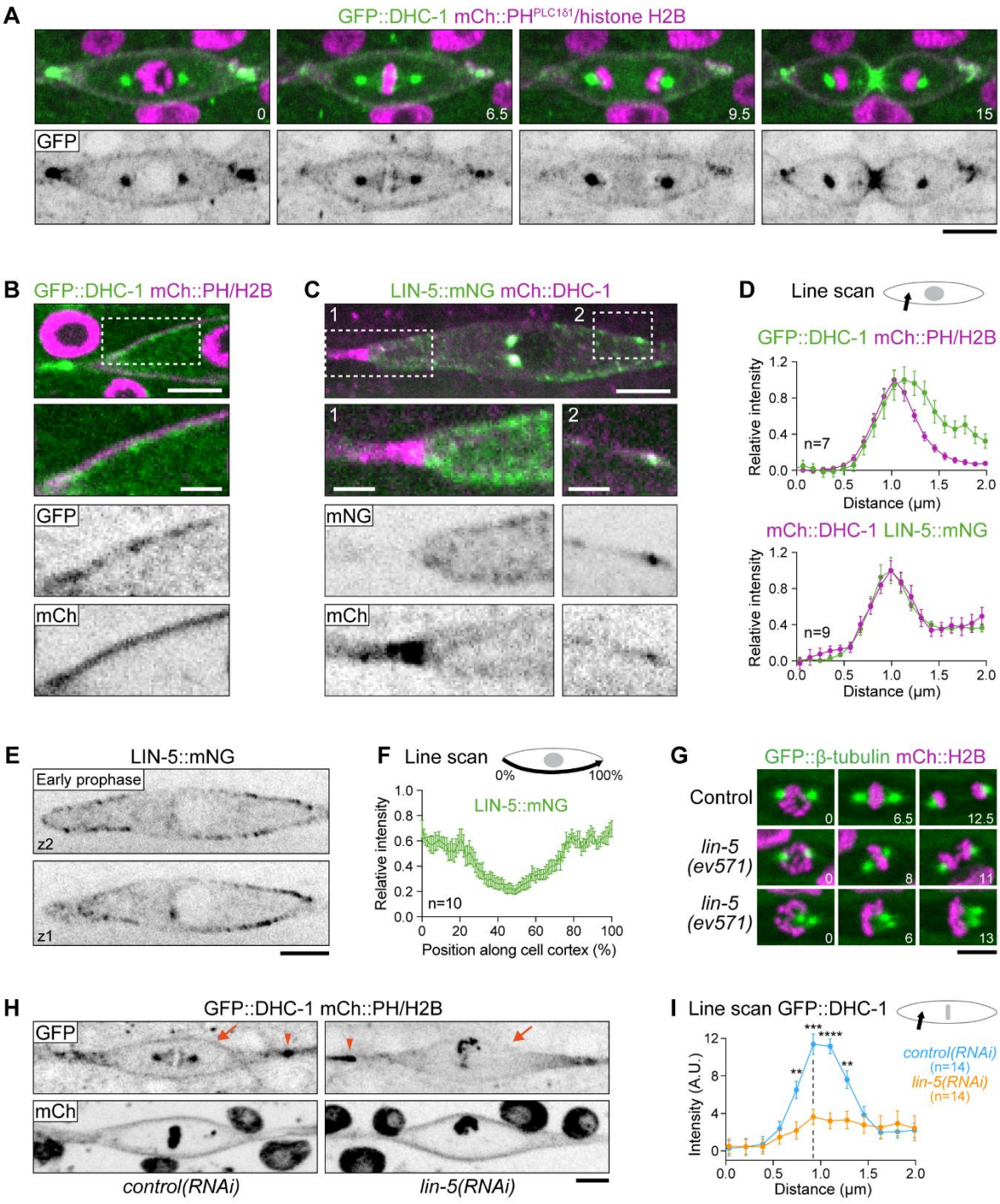
A
GFP::DHC-1 mCh::PH^PLC1δ1/histone H2B
0
6.5
9.5
15
GFP
B
GFP::DHC-1 mCh::PH/H2B
GFP
mCh
C
LIN-5::mNG mCh::DHC-1
1
2
mNG
mCh
D
Line scan
GFP::DHC-1 mCh::PH/H2B
Relative intensity
n=7
Distance (µm)
mCh::DHC-1 LIN-5::mNG
n=9
E
LIN-5::mNG
Early prophase
z2
z1
F
Line scan
0%
100%
LIN-5::mNG
n=10
Position along cell cortex (%)
G
GFP::β-tubulin mCh::H2B
Control
lin-5 (ev571)
lin-5 (ev571)
H
GFP::DHC-1 mCh::PH/H2B
GFP
mCh
control(RNAi)
lin-5(RNAi)
I
Line scan GFP::DHC-1
Intensity (A.U.)
control(RNAi) (n=14)
lin-5(RNAi) (n=14)
Distance (µm)

Figure 13 - Dynein acts at the seam cell cortex downstream of LIN-5^{NuMA}.
(A) Selected images from a time-lapse movie in a dividing seam cell co-expressing GFP::DHC-1 (dynein heavy chain), mCh::PH(PLC1δ1), and mCh::HIS-11 (histone H2B). Time is indicated in minutes. Scale bar, 5 µm. **(B)** Image of a cortical region in a prophase seam cell as in *(A)*. Scale bars, 5 µm *(top)* and 2 µm *(magnified region)*. **(C)** Image of a prophase seam cell co-expressing LIN-5::mNG and mCh::DHC-1. Scale bars, 5 µm *(top)* and 2 µm *(magnified region)*. **(D)** Line scan profiles across the seam cell cortex, as illustrated in the schematic (*top*), measured in images such as in *(B)* and *(C)*. Data is plotted as mean ± SEM. *n* denotes the total number of cells examined in ≥ 5 animals. **(E)** Single confocal z-section (z) images (0.5 µm apart) of the prophase seam cell in *(C)*. Scale bar, 5 µm. **(F)** Line scan profile of LIN-5::mNG along the early prophase cell cortex, as indicated in the schematic *(top)*, in cells such as in *(E)*. Data is plotted as mean ± SEM. *n* denotes the number of cells examined (one cell per animal). **(G)** Selected images from time-lapse movies of dividing seam cells co-expressing GFP::TBB-2 (β-tubulin) and mCh::HIS-11. Time is indicated in minutes. Scale bar, 5 µm. **(H)** Images of metaphase seam cells co-expressing GFP::DHC-1, mCh::PH(PLC1δ1), and mCh::HIS-11. Arrows and arrowheads point to GFP::DHC-1 at the cortex and seam cell contacts, respectively. Scale bar, 5 µm. **(I)** Line scan profiles across the seam cell cortex, as illustrated in the schematic (*top*), measured at metaphase in images such as in *(H)*. Dashed line indicates the peak of the mCh::PH(PLC1δ1) signal. Data is plotted as mean ± SEM with arbitrary units (A.U.) on the y-axis. *n* denotes the total number of cells examined in ≥ 10 animals. Statistical significance was determined by the Mann-Whitney test. ****P < 0.0001; ***P < 0.001, **P < 0.01.

GOA-1^{Gαi} is uniformly distributed on the seam cell cortex and is required for LIN-5 recruitment, prophase centrosome separation, and spindle orientation

Work in the early embryo identified the Gαi subunits GOA-1 and GPA-16 as the plasma membrane receptors for GPR-1/2, which in turn recruit LIN-5 (Colombo *et al.*, 2003; Gotta *et al.*, 2003; Srinivasan *et al.*, 2003). To determine whether this pathway operates in seam cells, we first asked whether GOA-1 is present in seam cells using a transgene that expresses functional GOA-1, internally tagged with GFP, from *goa-1* regulatory elements (Kumar *et al.*, 2021). Co-expression with mCh::HIS-11 and mCh::PH showed that GOA-1::GFP localizes uniformly to the seam cell plasma membrane at all stages of the cell cycle, which contrasts with the fluctuating levels and bipolar distribution of LIN-5::mNG (**Figure 14A, B; Supplementary Figure 2C**). RNAi-mediated depletion of GOA-1 in dividing seam cells reduced LIN-5::mNG localization at the cell cortex (**Figure 14C, D**), inhibited centrosome separation in prophase (**Figure 14E, F**), and resulted in spindle mis-orientation (31 % of spindle angles above 15º versus 0 % in controls; P = 0.0041, Fisher's exact test) (**Figure 14E, G**). Taken together, our results suggest that seam cells use the GOA-1^{Gαi}–LIN-5^{NuMA} pathway to recruit dynein to the cell cortex in early prophase to generate pulling

forces on astral microtubules that separate centrosomes and direct the path of centrosome migration along the A–P axis. The same force generation machinery subsequently maintains the spindle oriented during prometaphase and metaphase and promotes chromosome segregation by elongating the spindle in anaphase.

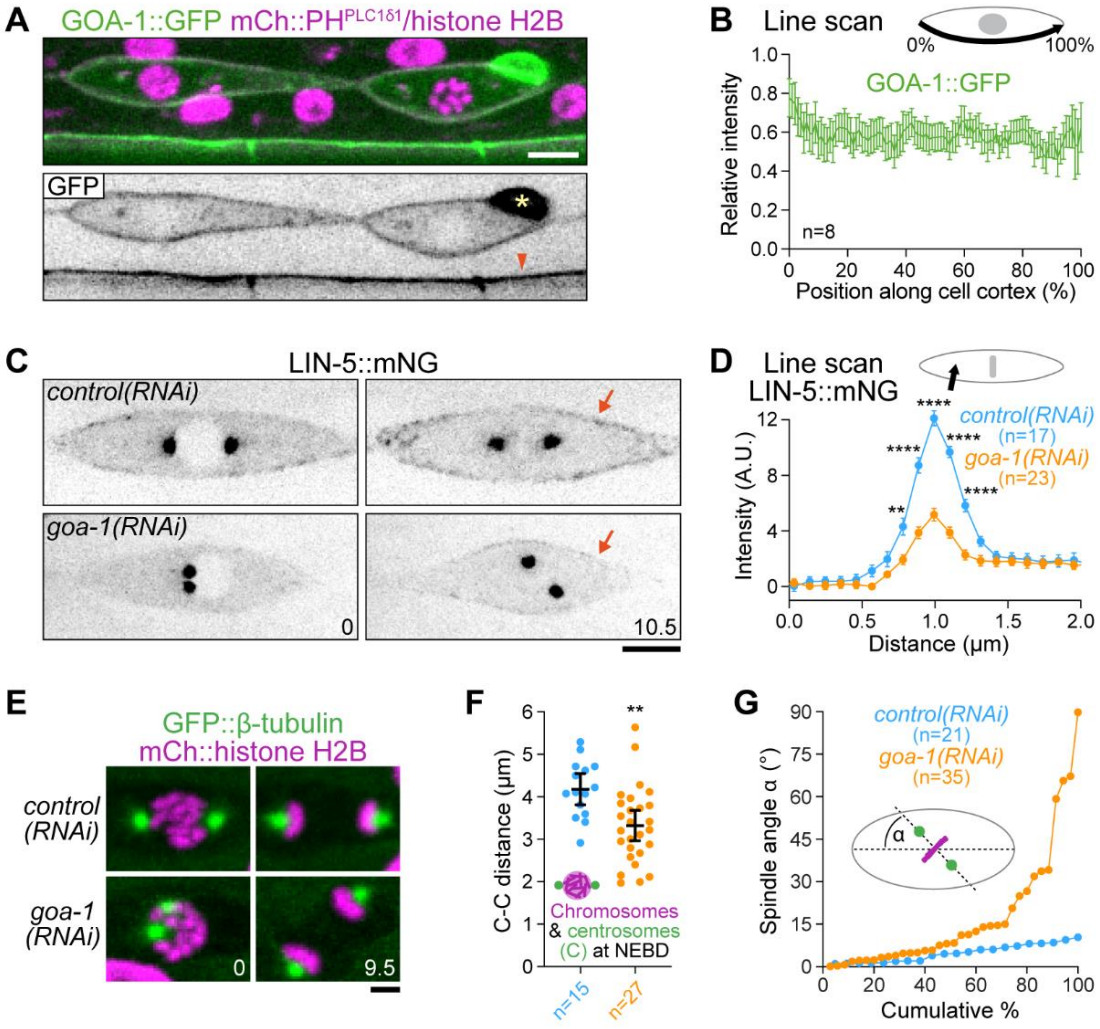

Figure 14 - GOA-1$^{G\alpha i}$ is uniformly distributed on the seam cell cortex and is required for LIN-5^{NuMA} recruitment, prophase centrosome separation, and spindle orientation.
(A) Image of adjacent seam cells in interphase *(left)* and prophase *(right)*, co-expressing GOA-1 internally tagged with GFP, the plasma membrane marker mCh::PH$^{PLC1\delta1}$, and mCh::HIS-11 (histone H2B). Asterisk and arrowhead point to a neuronal cell body and neurite, respectively. Scale bar, 5 µm. **(B)** Line scan profile of GOA-1::GFP along the early prophase cell cortex, as indicated in the schematic *(top)*, in cells such as in *(A)***.** Data is plotted as mean ± SEM. *n* denotes the number of cells examined (one cell per animal). **(C), (E)** Selected images from time-lapse movies of dividing seam cells expressing LIN-5::mNG *(C)* or co-expressing GFP::TBB-2 (β-tubulin) and mCh::HIS-11 *(E)*. Time is indicated in minutes. Arrows in *(C)* point to cortical LIN-5::mNG. Scale bars, 5 µm *(C)* and 2 µm *(E)*. **(D)** Line scan profiles across the seam cell cortex, as illustrated in the schematic (*top*), measured at metaphase in images such as in *(C)*. Data is plotted as mean ± SEM with arbitrary units (A.U.) on the y-axis. *n* denotes the total number of cells examined in ≥ 10 animals. Statistical significance was determined by the Mann-Whitney test. ****$P < 0.0001$; **$P < 0.01$. **F)** Quantification of centrosome–centrosome distance (mean ± 95% CI) at NEBD. Data points correspond to measurements in individual cells. *n* denotes the total number of cells imaged in ≥ 5 animals. Color scheme is the same as in *(E)*. Statistical significance was determined by the Mann-Whitney test. **$P < 0.01$. **(G)** Quantification of seam cell spindle orientation, measured at metaphase. Data points correspond to measurements in individual cells. *n* denotes the total number of cells examined in ≥ 15 animals.

Mis-oriented divisions in the dyci-1(ΔN) seam result in mis-placed daughter cells and generate anucleate membrane compartments due to aberrant cytokinesis

To understand how spindle mis-orientation caused by *dyci-1(ΔN)* impacts the formation, positioning, and fate of daughter cells, we performed time-lapse imaging in larval L3-stage seam cells co-expressing GFP::HIS-11 and GFP::PH. Seam cell row neighbors in both control and *dyci-1(ΔN)* animals remained connected to each other on the apical side during mitosis and therefore maintained an elongated shape. *dyci-1(ΔN)* cells whose spindle was mis-oriented at anaphase onset proceeded to divide along the spindle axis, even when the resulting division axis was dramatically skewed relative to the long axis of the cell (**Figure 15A**). Examination of cytokinesis using GFP::PH and the contractile ring marker TagRFP::ANI-1^{Anillin} revealed that the cleavage furrow in seam cells closes asymmetrically from the basal to the apical side (**Figure 15B**). In mis-oriented *dyci-1(ΔN)* divisions, the cleavage plane was no longer positioned perpendicularly to the long axis of seam cells, which interfered with formation of a compact contractile ring (**Figure 15C**). Occasionally, more than one region of the cortex became contractile (**Figure 15C**), and simultaneous constriction of two cleavage furrows created small apical membrane

compartments between daughter cells that lacked chromosomes (**Figure 15D**). These likely correspond to the small compartments observed with the apical junction marker GFP::DLG-1 (**Figure 11D**). We conclude that mis-oriented divisions produce daughter cells that are positioned outside the seam cell row while promoting formation of anucleate compartments within the seam cell row.

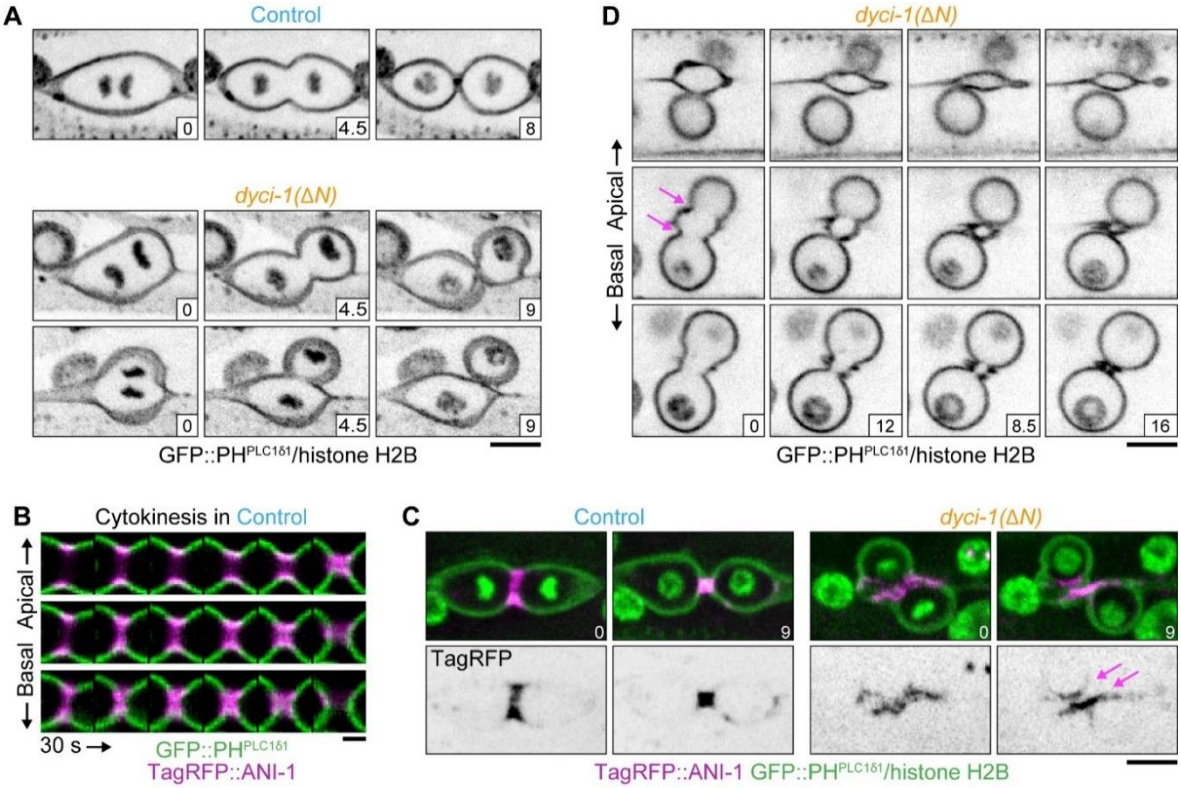

Figure 15 - Mis-oriented divisions in the *dyci-1(ΔN)* seam result in mis-placed daughter cells and anucleate membrane compartments.

(A), (D) Selected images from time-lapse movies of seam cells co-expressing GFP::PH(PLC1δ1) and GFP::HIS-11 (histone H2B). Projected confocal z-stacks *(A)* or single z-sections (1 µm apart) *(D)* are shown. Arrows in *(D)* point to ingressing cleavage furrows. Time is indicated in minutes. Scale bar, 5 µm. **(B)** Successive frames (30 s apart) from a time-lapse movie of cytokinesis in a seam cell co-expressing the cleavage furrow marker TagRFP::ANI-1^{Anillin}, GFP::PH(PLC1δ1), and GFP::HIS-11. Single confocal z-sections (0.5 µm apart) of the cleavage furrow region are shown. Scale bar, 2 µm. **(C)** Selected images from time-lapse movies of seam cells as in *(B)*. Arrows point to ingressing cleavage furrows. Time is indicated in minutes. Scale bar, 5 µm.

Mis-oriented divisions in the dyci-1(ΔN) seam result in incorrect inheritance of the Wnt/β–catenin asymmetry pathway component APR-1^{APC} and alter daughter cell fate

Following the last round of division at the L3 stage, seam cell daughters have different fates: the anterior daughter differentiates and fuses with the hyp7 cell, whereas the posterior

daughter maintains seam cell identify (**Figure 16A**). To examine how mis-oriented divisions impact cell fate, we first monitored the distribution of APR-1^{APC}, a component of the Wnt/β–catenin asymmetry pathway that is asymmetrically inherited by daughter cells (Mizumoto & Sawa, 2007). In control cells, endogenous GFP-tagged APR-1 was visible on the anterior cortex by metaphase and persisted there until the end of mitosis (**Figure 16B**). The anterior daughter therefore inherits the bulk of APR-1. In *dyci-1(ΔN)* cells with correctly oriented spindles, GFP::APR-1 localization was identical to that in control cells, showing that the *dyci-1(ΔN)* mutation does not affect APR-1 distribution *per se*. In *dyci-1(ΔN)* cells with mis-oriented spindles, GFP::APR-1 was still enriched on the anterior cortex at metaphase, but its distribution was skewed towards the lateral side on which the anterior spindle pole was located (**Figure 16B**), suggesting that APR-1 distribution is influenced by the orientation of the spindle. In cases where the cleavage plane was oriented nearly parallel to the seam cell row axis, GFP::APR-1 became enriched in the ingressing cleavage furrow (**Figure 16B**), thus ending up in both daughter cells. We conclude that mis-oriented divisions caused by *dyci-1(ΔN)* interfere with the correct asymmetric distribution of cell fate determinants.

To assess how mis-oriented divisions impact daughter cell fate, we constructed a strain co-expressing GFP with a nuclear localization signal (GFP::NLS) from the artificial *scm* promoter, which reports on seam cell identity (Terns *et al.*, 1997), and mCh::HIS-11 from the *wrt-2* promoter, which marks all epidermal nuclei (**Figure 16C**). The same *scm* and *wrt-2* promoters also drive expression of GFP::PH and mCh::PH from respective operons to mark the plasma membrane. In control L4 larvae, the seam syncytium contains 16 nuclei, which in our reporter strain were labeled with both GFP::NLS and mCh::HIS-11 (**Figure 16D – F**). Furthermore, the seam was clearly delimited by GFP::PH– and mCh::PH–labelled plasma membrane. Nuclei in the surrounding hyp7 cell, by contrast, were only labeled with mCh::HIS-11. This strain therefore allowed us to identify nuclei that are physically integrated within the seam (i.e., surrounded by plasma membrane) while simultaneously evaluating seam identity of these nuclei through the *scm* reporter.

When counting nuclei positive for the *scm* reporter, we found that 32 % of *dyci-1(ΔN)* L4 larvae had less than 16 nuclei, compared to 10 % of control larvae ($P = 0.0234$, Fisher's exact test) (**Figure 16F**). *dyci-1(ΔN)* animals with less than 16 *scm*-positive nuclei had gaps in the seam, and highly condensed mCh::HIS-11 signal was occasionally visible in these gaps (**Figure 16D**), suggesting that gaps form in part by seam cells undergoing apoptosis. When counting the total number of seam-associated nuclei (i.e. mCh::HIS-11-positive nuclei surrounded by plasma membrane), we found that only 5 % of control L4 larvae contained more than 16 seam-associated nuclei, and in all of these cases there was only a single extra nucleus in the seam syncytium. By contrast, 79 % of *dyci-1(ΔN)* L4 larvae contained

more than 16 nuclei ($P < 0.0001$, Fisher's exact test), with counts ranging from 17 to 22 (**Figure 16F**), and the extra nuclei corresponded to individual cells that were positioned outside the seam syncytium and were negative for the *scm* reporter (**Figure 16E**). These mis-positioned cells are likely to be anterior daughters that have correctly lost expression of the seam cell identity marker but are unable to fuse with the hyp7 syncytium.

We conclude that mis-oriented division of *dyci-1(ΔN)* seam cells at the L3 stage results in incorrect inheritance of cell fate determinants, which in conjunction with daughter cell mis-positioning interferes with the developmental program that generates the seam syncytium with 16 nuclei at the L4 stage.

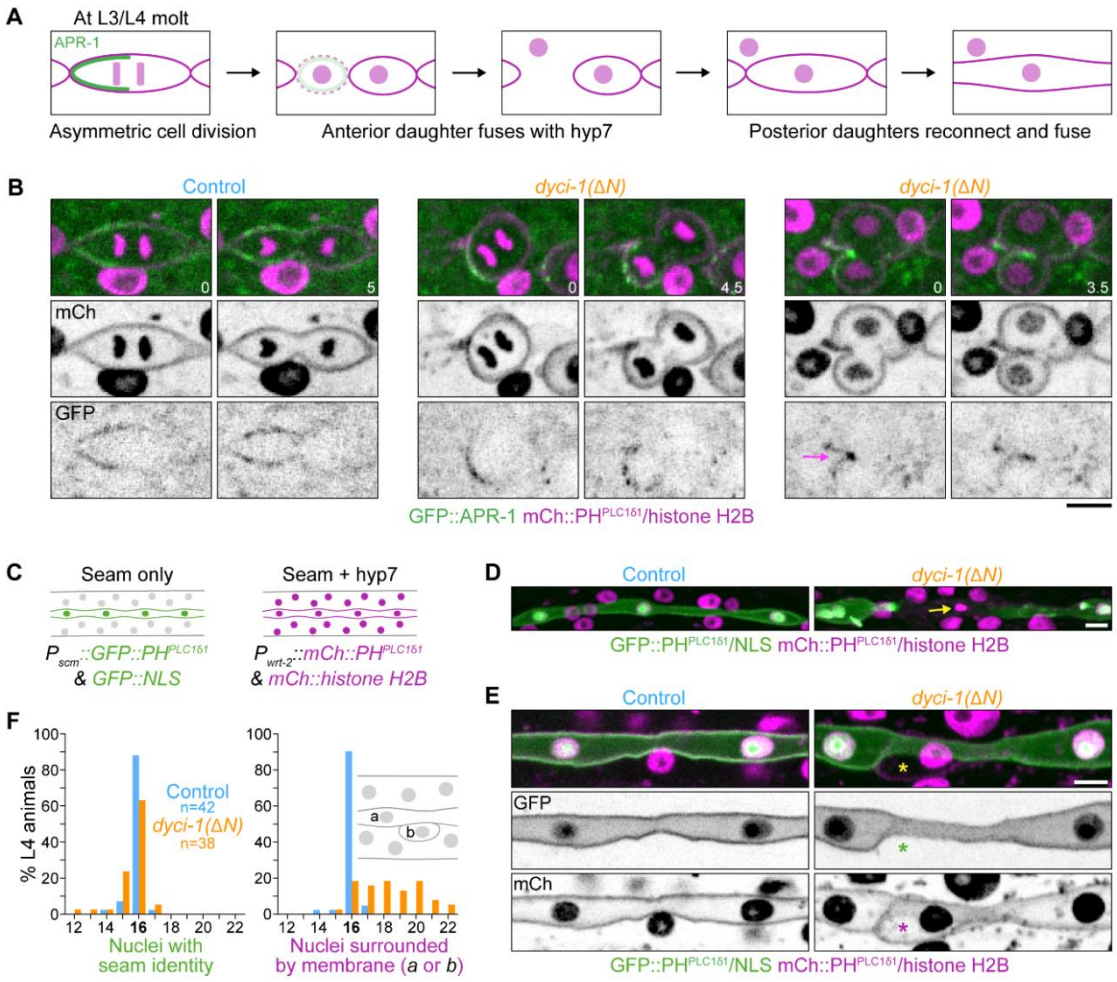

Figure 16 - Mis-oriented divisions in the *dyci-1(ΔN)* seam result in incorrect APR-1^{APC} inheritance and altered daughter cell fate.

(A) Schematic overview of asymmetric seam cell division at the L3/L4 molt and subsequent fate of anterior and posterior daughters. APR-1 is enriched on the anterior cortex. **(B)** Selected images from time-lapse movies of seam cells co-expressing GFP::APR-1, mCh::PH(PLC1δ1), and mCh::HIS-11 (histone H2B). Arrow points to enrichment of GFP::APR-1 in the cleavage furrow. Time is indicated in minutes. Scale bar, 5 μm. **(C)** Schematic describing the markers co-expressed in the cell fate

reporter strain used in *(D)* – *(F)* and in Figure 8. **(D), (E)** Images of the L4 seam in the strain described in *(C)*. Arrow in *(D)* points to a gap in the seam containing hyper-condensed (apoptotic) chromatin. Asterisks in *(E)* point to a seam–adjacent cell (mCh) that does not express the seam identity marker (GFP). Scale bars, 5 µm. **(F)** Seam nuclei count in L4 animals using the markers described in *(C)* and the criteria outlined in the schematics. *n* denotes the number of animals examined.

Elongating seam cells rescues spindle mis-orientation and aberrant nuclei number in the dyci-1(ΔN) seam.

A prior study demonstrated that the elongated shape of seam cells provides an important cue for correct spindle orientation (Wildwater *et al.*, 2011). We therefore set out to understand how spindle mis-orientation caused by inhibition of the dynein pathway is influenced by cell shape. We used the mutations *dpy-11(e224)* and *lon-1(e185)* that produce shorter and longer animals, respectively (**Figure 17A**), and result in corresponding changes in seam cell shape (Wildwater *et al.*, 2011), which we confirmed by measuring cell length and width with the GFP::PH marker (**Figure 17B**). This also revealed that *dyci-1(ΔN)* cells are rounder than controls. We then combined the *dpy-11(e224)* and *lon-1(e185)* mutations with *dyci-1(ΔN)* and determined the orientation of the metaphase plate, marked by GFP::HIS-11, as a proxy for spindle orientation. Spindle orientation in *dpy-11(e224)* and *lon-1(e185)* single mutants was indistinguishable from controls (**Figure 17C**), consistent with prior work (Wildwater *et al.*, 2011). Similarly, the *dpy-11(e224)*;*dyci-1(ΔN)* double mutant behaved the same as *dyci-1(ΔN)*. By contrast, combining the *lon-1(e185)* mutation with *dyci-1(ΔN)* improved spindle orientation (48 % of spindle angles below 15º in *dyci-1(ΔN)* versus 76 % in *lon-1(e185);dyci-1(ΔN)*; $P = 0.0129$, Fisher's exact test) (**Figure 17D**). When we counted the total number of seam-associated mCh::HIS-11–positive nuclei in L4 larvae, we found that the fraction of animals containing more than 16 nuclei was reduced from 95 % in *dyci-1(ΔN)* to 33 % in *lon-1(e185);dyci-1(ΔN)* ($P < 0.0001$, Fisher's exact test), compared to 10 % in controls and 5 % in *lon-1(e185)* (**Figure 17E**). We conclude that giving seam cells in the *dyci-1(ΔN)* mutant a more elongated shape partially rescues spindle mis-orientation and the resulting defects in seam morphology.

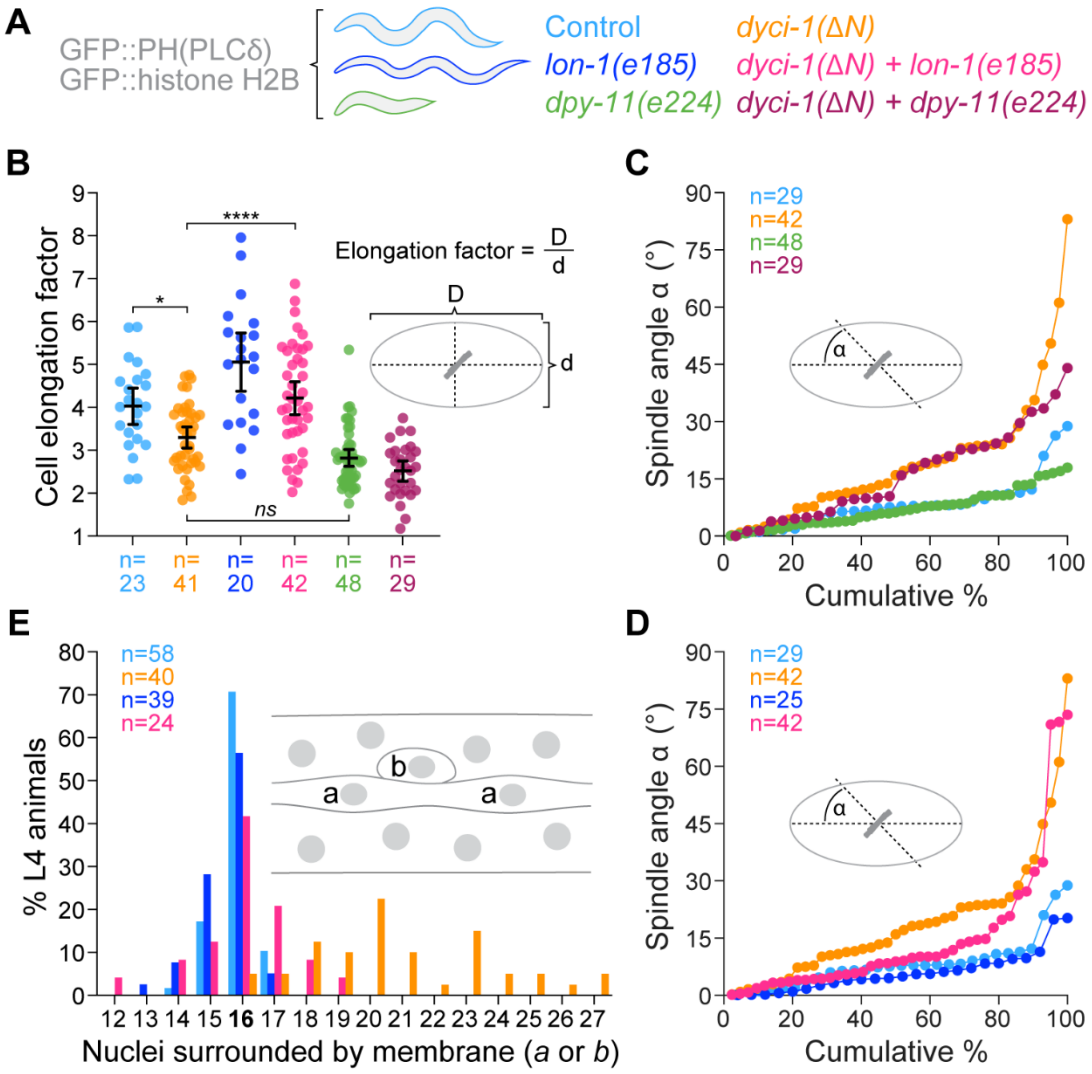

Figure 17 - Elongating seam cells rescues spindle mis-orientation and extra nuclei number in the *dyci-1(ΔN)* seam.

(A) Schematic illustrating the effect of *lon-1(e185)* and *dpy-11(e224)* mutations on animal length. **(B)** Quantification of the seam cell elongation factor at metaphase, calculated as shown in the schematic. Data points correspond to measurements in individual cells and bars show the mean ± 95% CI. *n* denotes the total number of cells examined in ≥ 10 animals. Statistical significance was determined by ordinary one-way ANOVA followed by Šídák's multiple comparison test. ****$P < 0.0001$; *$P < 0.05$; *ns* = not significant, $P > 0.05$. **(C), (D)** Quantification of seam cell spindle orientation, measured at metaphase. Data points correspond to measurements in individual cells. *n* denotes the total number of cells examined in ≥ 10 animals. **(E)** Seam nuclei count in L4 animals using the markers described in Figure 7C and the criteria outlined in the schematic. *n* denotes the number of animals examined.

Discussion

The *C. elegans* epidermis is a well-established model for the study of stem cell-like divisions in a simple epithelium. Here we characterized the role of the microtubule motor dynein during the last round of asymmetric seam cell divisions that give rise to the seam syncytium. Our results show that dynein acts together with elongated cell shape to ensure spindle assembly occurs along the A–P axis, and we demonstrate that this is crucial for developing a functional seam. We further show that dynein acts downstream of the conserved cortical Gai–LGN–NuMA pathway and contributes to spindle orientation by directing the trajectory followed by separating prophase centrosomes.

The importance of oriented division for seam development

The *dyci-1(ΔN)* mutant supports spindle assembly and error-free chromosome segregation of seam cells at the L3 stage but results in mis-orientated spindles. This hypomorphic phenotype enabled us to address the importance of oriented division for seam cell development. The immediate consequences of spindle mis-orientation are two–fold: daughter cells are placed outside the seam cell row, and anucleate compartments form due to aberrant cytokinesis, in which cleavage furrows are forced to close against the presumed axis of tension.

How are the defects caused by spindle mis-orientation at the L3 stage related to the subsequent defects observed in the mature seam syncytium at the L4 stage? The mature *dyci-1(ΔN)* seam contains extra seam–derived cells that persist adjacent to the seam syncytium but are negative for a seam identity marker. These cells are most likely anterior daughters unable to fuse with hyp7. This suggests mis-oriented division interferes with terminal differentiation of anterior daughters, consistent with the observation that the Wnt/β–catenin asymmetry pathway component APR-1^{APC} is inappropriately distributed to daughter cells during mis-oriented division. Support for a causal relationship between mis-oriented division and altered cell fate is provided by the observation that elongating *dyci-1(ΔN)* cells with the *lon-1(e185)* mutant not only rescues spindle mis-orientation in L3 larvae but also reduces the number of the extra seam-derived cells at the L4 stage.

The other major defects observed in the mature *dyci-1(ΔN)* seam are anucleate compartments and large gaps, which is predicted to be particularly detrimental since the seam secretes components that make up the cuticle to ensure impermeability of the epidermis (Chisholm & Xu, 2012). Gaps in the seam may form when anucleate compartments produced by mis-oriented divisions degenerate, or when mis-placed posterior daughters fail to re-connect after anterior daughters have fused with hyp7. Taken

together, our results show that seam development is highly sensitive to mis-oriented divisions, highlighting the importance of redundant mechanisms for spindle orientation, as discussed below.

Dynein's contribution to spindle orientation in the context of cell shape and Wnt signalling

Hertwig's rule states that spindles orient along the long axis of the cell, and a previous study established the importance of elongated cell shape for oriented seam cell division in the context of perturbed Wnt signalling (Wildwater *et al.*, 2011). Specifically, inhibition of the argonaut ALG-1 perturbed Wnt signalling and made cells rounder, and the resulting mis-oriented divisions could be rescued by elongating cells with the *lon-1(e185)* mutation. Furthermore, combining the *dpy-11(e224)* mutation, which makes seam cells rounder, with inhibition of Wnt signalling also resulted in mis-oriented divisions (Wildwater *et al.*, 2011). Our findings are analogous in that the *dyci-1(ΔN)* mutation produces L3 seam cells that are rounder than controls, and elongating *dyci-1(ΔN)* cells with *lon-1(e185)* partially rescues spindle mis-orientation. The *dpy-11(e224)* mutant also shows that roundness *per se* is not sufficient to induce spindle mis-orientation, in agreement with prior results (Wildwater *et al.*, 2011). Taken together, this suggests that spindle mis-orientation in *dyci-1(ΔN)* cells is a combined consequence of cortical dynein inhibition and increased cell roundness, re-enforcing the notion that redundant geometric and cortical cues exist to provide robust control over the cell division axis (Wildwater *et al.*, 2011).

Since both dynein (this study) and Wnt signaling (Wildwater *et al.*, 2011) contribute to spindle orientation in seam cells, the question arises whether Wnt signalling regulates cortical dynein. Wnt signaling directs dynein to the cortex in *D. melanogaster* and vertebrate cells, albeit in an LGN-independent manner (Lechler & Mapelli, 2021). We did not observe an obvious reduction of cortical LIN-5^{NuMA} levels after *alg-1(RNAi)*, which perturbs Wnt signaling (Wildwater *et al.*, 2011),and Wnt signalling in the four-cell embryo, while required for spindle orientation, is dispensable for LIN-5 enrichment at the P2–EMS cell boundary (Heppert *et al.*, 2018; Srinivasan *et al.*, 2003). Nevertheless, a more detailed examination is needed to clarify whether Wnt signaling contributes to spindle orientation in seam cells through the cortical dynein pathway or in a dynein–independent manner, for example through APR-1^{APC}–mediated microtubule stabilization (Sugioka *et al.*, 2011).

Dynein–dependent cortical force generation separates prophase centrosomes in seam cells

We find that RNAi-mediated depletion of GOA-1$^{G\alpha i}$ has a strong inhibitory effect on prophase centrosome separation. This contrasts with the situation in the one-cell embryo, where co-depletion of GOA-1 and GPA-16 slows but does not prevent prophase centrosome separation (De Simone *et al.*, 2016). In the one-cell embryo, cortex–associated dynein acts together with nucleus-associated dynein to separate centrosomes (De Simone *et al.*, 2016), whereas in seam cells dynein is not enriched at the nuclear envelope. The apparent lack of nucleus-associated dynein may explain why the cortical dynein pathway in seam cells plays a more prominent role in centrosome separation compared to the one-cell embryo.

Cortical dynein in seam cells directs prophase centrosome migration along the A–P axis

In the early embryo, prophase centrosomes migrate evenly to opposite sides of the nucleus, which gives rise to the orthogonal division pattern in AB blastomeres (Hyman & White, 1987). By contrast, the P0 blastomere and its descendants (P1, P2, and EMS) need to divide along the A–P axis. In these cells, the centrosome–nucleus complex is rotated into the correct position once centrosomes have separated (Hyman & White, 1987). We find that seam cells use a different strategy to ensure successive divisions along the A–P axis. Instead of rotating the centrosome–nucleus complex, the migration path of separating centrosomes is already directed along the A–P axis. This requires that one centrosome remains relatively stationary while the other migrates to the opposite side of the nucleus. The *dyci-1(⊿N)* mutant shows that dynein is responsible for the directionality of centrosome migration, which we speculate is facilitated by the cell–pole enriched distribution of LIN-5^{NuMA} in prophase, as discussed below.

Localization dynamics of the dynein force generation machinery at the seam cell cortex

To the best of our knowledge, mitotic Gαi localization has not been examined by live cell imaging in any organism. We took advantage of a recently generated functional GFP-tagged version of GOA-1 (Kumar *et al.*, 2021) to examine its localization in seam cells. This revealed that GOA-1 is uniformly distributed on the cortex throughout mitosis, which contrasts with the uneven distribution and fluctuating levels of LIN-5^{NuMA}. Similar observations were made by immunofluorescence in chick neuroepithelial and HeLa cells

(Kiyomitsu & Cheeseman, 2012; Peyre *et al.*, 2011), in which Gαi, but not LGN–NuMA, is uniformly distributed on the metaphase cortex. Since we can only observe the total GOA-1 pool, it is possible that GOA-1–GDP, the specific GOA-1 pool that interacts with GPR-1/2^{LGN} (Colombo *et al.*, 2003; Gotta *et al.*, 2003; Srinivasan *et al.*, 2003), exhibits a distribution similar to that of LIN-5. Another possibility is that GOA-1–GDP is uniformly distributed and the interaction between GOA-1–GDP and GPR-1/2 (for which we had no live imaging probe), or the interaction between GPR-1/2 and LIN-5, is subject to regulation.

In prophase, LIN-5 is depleted from the centrosome–proximal cortical region and preferentially localizes to the polar regions of the elongated seam cell. This cell pole–enriched distribution of LIN-5–dynein may help direct centrosome migration along the A–P axis. In HeLa cells, cortical dynein is displaced by the proximity of spindle poles, albeit downstream of NuMA, through the pole–localized kinase Plk1 (Kiyomitsu & Cheeseman, 2012). It is therefore conceivable that PLK-1 plays a role in displacing LIN-5–dynein from the centrosome–proximal seam cell cortex in prophase. Interestingly, the progressive increase of LIN-5 levels at centrosomes is accompanied by a reduction of cortical LIN-5 levels, suggesting LIN-5–dynein may remove itself from the prophase cortex through transport along astral microtubules. Removal along astral microtubules was previously documented for GPR-1/2 in the P2 cell of the four–cell embryo, although in this case removal occurs only once spindle orientation has completed and serves to prevent hyperaccumulation of GPR-1/2 (Werts *et al.*, 2011).

Additional roles of dynein in seam cells beyond cell division

Although spindle mis-orientation is significantly rescued by elongating *dyci-1(ΔN)* seam cells, *dyci-1(ΔN);lon-1(e185)* animals still have gaps in the seam and die prematurely by epidermal rupture (data not shown), indicating that dynein has additional important roles in the epidermis. In interphase and prophase, we find that dynein, but not its cortical adaptor LIN-5, accumulates prominently near apical junctions that connect neighboring seam cells, which is where microtubule minus-ends concentrate (Wang *et al.*, 2015). It is therefore possible that dynein–driven membrane trafficking directed to apical junctions plays a role in maintaining cell–cell adhesion within the seam cell row, which is presumably under considerable tension. Furthermore, dynein–driven membrane trafficking may be required for proper secretion of cuticle components. Consistent with this latter possibility, a null mutant of the small GTPase RAB-6.2, which marks golgi-derived exocytotic vesicles that are a known cargo of dynein, exhibits cuticle integrity defects (Kim *et al.*, 2019). It will be interesting to investigate these potential contributions of dynein to epidermal development in future work.

Acknowledgements

The authors thank Eurico Morais de Sá (i3S Porto) for critical reading of the manuscript; Michael Koelle (Yale University School of Medicine) and Karen Oegema (University of California San Diego) sharing strains; and WormBase for providing data and tools. Some strains were provided by the *Caenorhabditis* Genetics Center (CGC), which is funded by the NIH Office of Research Infrastructure Programs (P40 OD010440). This project was funded by the European Research Council under the European Union's Seventh Framework Programme (ERC-2013-StG-338410-DYNEINOME) and by the Fundação para a Ciência e a Tecnologia (FCT)/Ministério da Ciência, Tecnologia e Ensino Superior (PTDC/BIA-CEL/1321/2021). R. G. and A. C. are supported by FCT Principal Investigator positions (CEECIND/00333/2017 and CEECIND/01967/2017, respectively), D. J. B. is supported by an FCT Junior Researcher position (DL57/2016/CP1355/CT0007), and C. C. is supported by an FCT PhD fellowship (SFRH/BD/144877/2019). The authors declare no competing financial interests.

Supplementary Figures

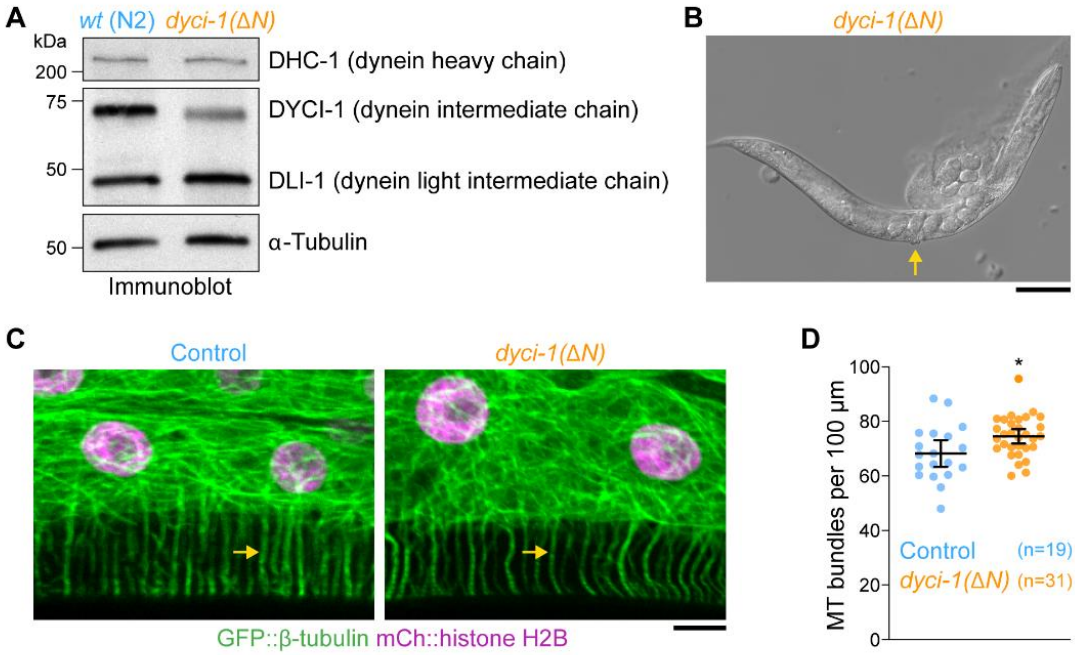

Supplementary Figure 1 - Related to Figures 10 and 11.

(A) Immunoblot of adult animals. Anti–α-tubulin antibody serves as the loading control. Molecular weight is indicated in kilodaltons (kDa). **(B)** Differential interference contrast image of a ruptured dyci-1(ΔN) adult with embryos. Arrow points at the intact vulva. Scale bar, 100 µm. **(C)** Images of hyp7 at the L4 stage in animals co-expressing GFP::TBB-2 α-tubulin) and mCh::HIS-11 (histone H2B). Arrows point to microtubule bundles. Scale bar, 5 µm. **(D)** Quantification of microtubule bundle density in hyp7, using images such as shown in **(C)**. Data points correspond to counts in individual animals with bars showing the mean ± 95% CI. n denotes the number of animals examined. Statistical significance was determined by the Mann-Whitney test. *P < 0.05.

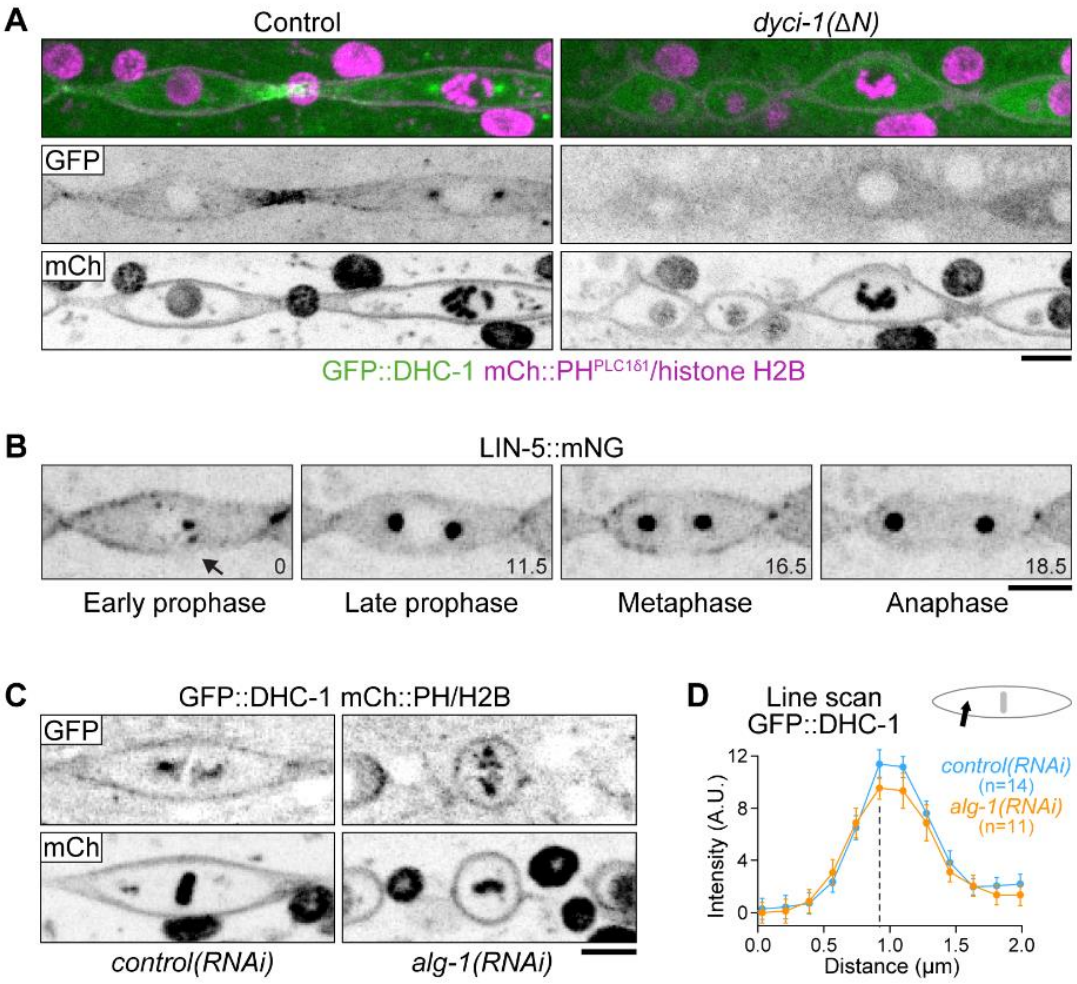

Supplementary Figure 2 - Related to Figures 13 and 14.

(A) Images of an interphase *(left)* and late prophase *(right)* seam cell co-expressing GFP::DHC-1 (dynein heavy chain), the plasma membrane marker mCh::PH(PLC1δ1), and mCh::HIS-11 (histone H2B). Scale bar, 5 μm. **(B)** Selected images from a time-lapse movie of a dividing seam cell expressing LIN-5::mNG. Arrows point to the absence of cortical LIN-5::mNG near prophase centrosomes. Time is indicated in minutes. Scale bar, 5 μm.**(C)** Images of metaphase seam cells co-expressing GFP::DHC-1, mCh::PH(PLC1δ1), and mCh::HIS-11. Scale bar, 5 μm. **(D)** Line scan profiles across the seam cell cortex, as illustrated in the schematic (*top*), measured at metaphase in images such as in ***(C)***. Dashed line indicates the peak of the mCh::PH(PLC1δ1) signal. Data is plotted as mean ± SEM with arbitrary units (A.U.) on the y-axis. *n* denotes the total number of cells examined in ≥ 10 animals.

Chapter IV. Distinct C-terminal domains in ZYG-12/Hook specify its dual function as a dynein adaptor for early endosomes and nuclei

Distinct C-terminal domains in ZYG-12/Hook specify its dual function as a dynein adaptor for early endosomes and nuclei

Manuscript in preparation.

Personal contribution: Cátia Carvalho participated in study design, performed all the described experiments, analysed the data, prepared the figures, and wrote the manuscript.

Abstract

The microtubule motor cytoplasmic dynein-1 (dynein) relies on adaptor proteins to transport diverse cargo, including various endomembrane compartments. Some adaptors can recruit dynein to more than one type of endomembrane, but the underlying mechanisms remains poorly understood. Hook family adaptors recruit dynein to early endosomes in fungi and human cells by forming a complex with FTS and FHIP (called the FHF complex), which in turn binds membrane-bound Rab5. By contrast, the only known function of the *C. elegans* Hook and KASH domain protein ZYG-12 is dynein recruitment to the nuclear envelope, which occurs in the germline and early embryo, and requires formation of a SUN-KASH complex. I demonstrate that, in epithelia, ZYG-12 performs a second distinct function as part of FHF. Deletion of a C-terminal region that precedes the KASH domain abrogates ZYG-12 recruitment to early endosomes without affecting its function at the nuclear envelope, and mutation of conserved motifs reveals the importance of ZYG-12's interaction with FTS and FHIP. This study delineates conserved molecular determinants governing dynein recruitment to early endosomes in animals and reveals alternative splicing of adaptors as a mechanism to generate diversity in dynein-cargo interactions.

Introduction

Hook proteins are activating cargo adaptors that mediate early endosome transport (Bielska *et al.*, 2014) and contribute to Golgi positioning, centrosome function, and endocytic cargo sorting (Dwivedi *et al.*, 2019; Maldonado-Baez *et al.*, 2013; Walenta *et al.*, 2001). Hook proteins were firstly described in flies, when mutations in *hook* resulted in defects in endocytic trafficking (Krämer & Phistry, 1998). In humans, the Hook family comprises three members: Hook1, Hook2, Hook3, that share similarities such as a central

coiled-coil motif that mediates homodimerization, a C-terminal domain involved in cargo binding and an N-terminal region that binds dynein (McKenney *et al.*, 2014; Olenick *et al.*, 2016; Walenta *et al.*, 2001), including a signature N-terminal Hook domain that binds DLIC (Celestino *et al.*, 2019; Lee *et al.*, 2018; Schroeder & Vale, 2016) .

Hook proteins were initially demonstrated to promote dynein recruitment to early endosomes in fungi (Bielska *et al.*, 2014; Zhang *et al.*, 2014). Both fungal and mammal Hooks are members of the FHF complex (Christensen *et al.*, 2021; Yao *et al.*, 2014), which links dynein to lyso-endosomal cargos. The complex consists of FHIP (FHF complex subunit Hook interacting protein), Hook, and FTS (Fused Toes) (Xiang *et al.*, 2015). In humans, besides having three Hook proteins, cells have one FTS and four FHIPs (FHIP1A, FHIP1B, FHIP2A, FHIP2B) (Christensen *et al.*, 2021). Christensen and colleagues (Christensen *et al.*, 2021) found that FHF complexes composed of different combinations of the three proteins is a mechanism that dynein uses to achieve cargo diversity (Christensen *et al.*, 2021). So far, FHF complexes have been associated with early endosome transport, with late endosomes/lysosome fusion in combination with the HOPS (homotypic fusion and protein sorting) complex, and with ER-to-Golgi vesicle transport (Christensen *et al.*, 2021; Xu *et al.*, 2008).

More recently, the struture of FHF (Hook3, FHIP1B and FTS) was resolved by cryo-EM showing that this complex includes four points of contact between its components (**Figure 18**) (Ali *et al.*, 2023). Hook3 binds FHIP1B through one contact in which one of the C-terminal extension of Hook is locked into a hydrophobic pocket within FHIP1B (Ali *et al.*, 2023). FTS binds to Hook in two different regions: one contact is between Hook3 coiled-coil 4 residues and the catalytically dead ubiquitin ligase domains of FTS; and one between the opposite side of Hook3 coiled-coil 4 and a C-terminal alpha-helix of FTS (Ali *et al.*, 2023). Finally, FTS binds directly to FHIP in a way that an FTS loop wraps around Hook3 and docks into a pocket on FHIP1B (Ali *et al.*, 2023). Authors also suggest that FHIP1B harbors the binding site for Rab5, completing the link between early endosomes and dynein.

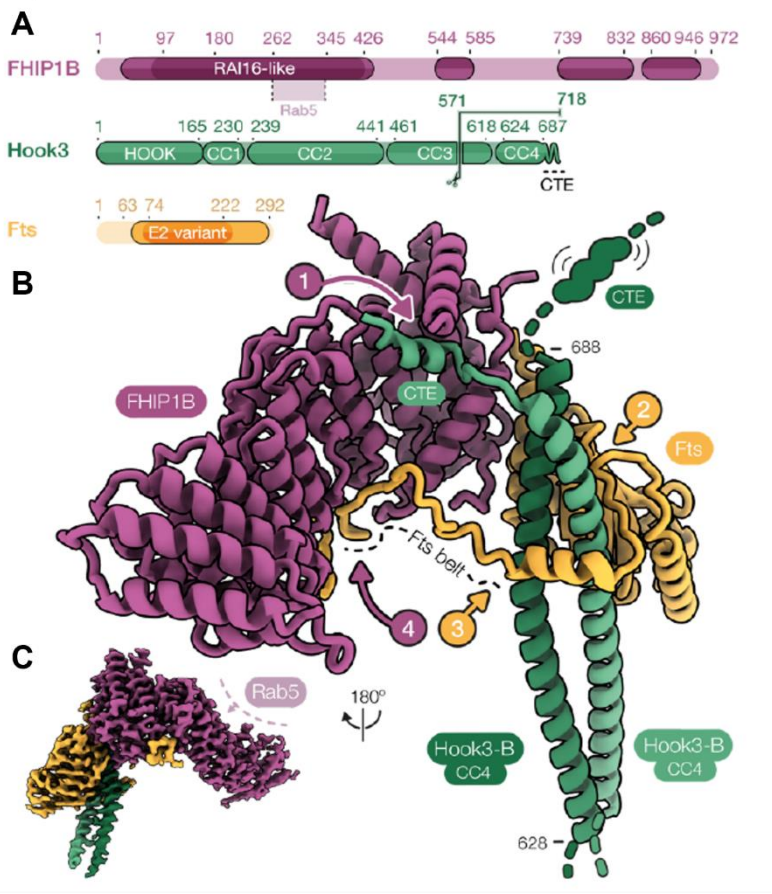

Figure 18 – Cryo-EM structure of the human FHF complex.
(**A**) Domain organization of human FHIP1B, Hook3 and Fts. (**B**) Atomic model of FHF complex, obtained by cryo-EM, indicating the four main interaction sites. (**C**) Cryo-EM density of FHF with AlphaFold2-predicted Rab5 binding site. Reproduced from (Ali *et al.*, 2023).

In *C. elegans*, ZYG-12 is the sole Hook homolog. Like other Hook proteins, ZYG-12 binds to the DLIC homolog DLI-1 (Malone *et al.*, 2003). In 2009, Minn and colleagues showed that ZYG-12 is part of the linker of nucleoplasm and cytoplasm (LINC) complex, which is conserved from nematodes to mammals (Lawrence *et al.*, 2016; Minn *et al.*, 2009). The LINC complex includes nuclear membrane proteins and cytoskeletal proteins, which form a bridge between the inner nuclear membrane and the outer nuclear membrane, connecting the nuclear interior with the cytoplasm (Lawrence *et al.*, 2016; Tapley & Starr, 2013). Key components of the LINC complex include SUN domain proteins (SUN-1 and UNC-84 in worms) in the inner nuclear membrane (INM) and KASH domain proteins (ZYG-12 and ANC-1 in worms) in the outer nuclear membrane (ONM) (Lawrence *et al.*, 2016; Luxton & Starr, 2014). These proteins interact to create the bridge that links the nucleus and the cytoskeleton. This process is particularly important during meiosis, where the LINC complex is involved in a variety of functions, including nuclear migration and anchoring, chromosome movements, and centrosome attachment (Luxton & Starr, 2014). The

canonical SUN protein SUN-1 is required to localize ZYG-12 at the ONM (Malone *et al.*, 2003). Additionally, both proteins recruit dynein to subtelomeric regions (pairing centres) that serve as telomeric attachment sites in meiosis (Luxton & Starr, 2014). Chromosome homologue pairing and synapsis is supported by the intranuclear chromosome movement, which is mediated by dynein extranuclear movement along microtubules (Sato *et al.*, 2009). This evidence makes ZYG-12 a likely functional equivalent of the human KASH5, a meiotic dynein activating adaptor (Agrawal *et al.*, 2022; Garner *et al.*, 2023; Sato *et al.*, 2009).

Here, I report that ZYG-12, besides being a KASH protein subunit of the LINC complex, also functions as a component of FHF at early endosomes. I identify and functionally characterize the *C. elegans* FHIP and FTS homologues, FHIP-1 and UBC-19, respectively, and I map the ZYG-12 domain responsible for the association with early endosomes, which is distinct from the KASH domain involved in LINC complex formation.

Materials and Methods

Caenorhabditis elegans

Strains (**Table 5**) were maintained at 20 ºC on standard nematode growth media (NGM) plates seeded with OP50 bacteria, as described on the previous chapter. Insertion of new *locus* was done using CRISPR-Cas9 system or single copy insertion of transgenes (MoSCi) as described below. All subsequent modifications were added by mating, as previsouly described.

Table 5 - Strains constructed and used on this chapter.

Strain	Genotype
N2	*N2 Bristol wild isolate*
GCP1373	*dhc-1(he250[N-terminal mCherry]) I; zyg-12(dha137; N-terminal gfp::AID) II*
GCP1479	*zyg-12(dha137[N-terminal gfp::AID]) II; prtSi260 [pRG1372; 1.38 kb Pdpy-7::mKate2::rab-5::tbb-2 3' UTR; cb-unc-119(+)] V; unc-119(ed3) III*
GCP1480	*zyg-12(dha137[N-terminal gfp::AID]) II; prtSi261 [pRG1373; 1.38 kb Pdpy-7::ctns-1::5 aa linker::mKate2::tbb-2 3' UTR; cb-unc-119(+)] V; unc-119(ed3) III*
GCP1482	*dhc-1(he264[N-terminal egfp]) I; prtSi260 [pRG1372; 1.38 kb Pdpy-7::mKate2::rab-5::tbb-2 3' UTR; cb-unc-119(+)] V; unc-119(ed3) III*
GCP1536	*fhip-1(prt257[knockout]) III; zyg-12(dha137[N-terminal gfp::AID]) II; prtSi260 [pRG1372; 1.38 kb Pdpy-7::mKate2::rab-5::tbb-2 3' UTR; cb-unc-119(+)] V*

GCP1591	*zyg-12(dha137[N-terminal gfp::AID]) II; ubc-19(prt279 [knockout]) V; prtSi260 [pRG1372; 1.38 kb Pdpy-7::mKate2::rab-5::tbb-2 3′ UTR; cb-unc-119(+)] V*
GCP1568	*zyg-12(dha137[N-terminal gfp::AID]) II; fhip-1(prt276 [N-terminal gfp]) III; prtSi260 [pRG1372; 1.38 kb Pdpy-7::mKate2::rab-5::tbb-2 3′ UTR; cb-unc-119(+)] V; unc-119(ed3) III*
GCP1634	*fhip-1(prt276 [C-terminal gfp]) unc-119(ed3) III, ubc-19(prt279 [knockout]) V; prtSi260 [pRG1372; 1.38 kb Pdpy-7::mKate2::rab-5::tbb-2 3' UTR; cb-unc-119(+)] V*
GCP1588	*zyg-12(dha137[N-terminal gfp]), (prt280 [6A fhip-1 binding mutant)] II, prtSi260 [pRG1372; 1.38 kb Pdpy-7::mKate2::rab-5::tbb-2 3′ UTR; cb-unc-119(+)] V; unc-119(ed3) III*
GCP1593	*zyg-12(dha137[N-terminal gfp]), (prt273 [∆aa686-730)] II, prtSi260 [pRG1372; 1.38 kb Pdpy-7::mKate2::rab-5::tbb-2 3′ UTR; cb-unc-119(+)] V; unc-119(ed3) III*
GCP1622	*zyg-12(dha137[N-terminal gfp]), (prt283 [6A ubc-19 binding mutant]) II; prtSi260 [pRG1372; 1.38 kb Pdpy-7::mKate2::rab-5::tbb-2 3′ UTR; cb-unc-119(+)] V; unc-119(ed3) III*
GCP1653	*zyg-12(dha137[N-terminal gfp]), (prt280[6A fhip-1 binding mutant]), (prt290 [6A ubc-19 binding mutant]) II, prtSi260 [pRG1372; 1.38 kb Pdpy-7::mKate2::rab-5::tbb-2 3′ UTR; cb-unc-119(+)] V; unc-119(ed3) III*
GCP1572	*zyg-12(dha137[N-terminal gfp], (prt280[6A fhip-1 binding mutant], II; ubc-19(prt279 [knockout]) V; prtSi260 [pRG1372; 1.38 kb Pdpy-7::mKate2::rab-5::tbb-2 3′ UTR; cb-unc-119(+)] V*

Genome engineering using the CRISPR-Cas9 system

All mutants (**Table 6**) were generated using a RNP-based strategy (Dokshin *et al.*, 2018). In this protocol, a mix consisting of crRNA/tracrRNA and home-made purified recombinant Cas9 protein is freshly prepared before the injection. To facilitate the identification of successfully injected animals, two different strategies were used: co-injection with PRF4::rol-6 (su1006) following (Dokshin *et al.*, 2018) and co-conversion protocol with dpy-10(cn64) (Arribere *et al.*, 2014).

Table 6 - CRISPR-Cas9 engineered mutations, locus, 5'-3 genomic sequences targeted by sgRNAs, type of repair templates and strategy used for genome editing.

Gene ID (Chr)	Mutation	Locus	Single-guide recognition region 5'-3'	Repair Template	Strategy
K546.1 (II)	*Δ686-730*	prt273	AAGGATTCGAACAAGAGAAT; AAATGAGTGGAGCACTTCCA	ssODN	PRF4::rol-6 (su1006)
	6A(fhip-1)	prt280	AAATGAGTGGAGCACTTCCA		
	6A(ubc-19)	prt283	AAGGATTCGAACAAGAGAAT		
C05D11.8 (III)	*fhip-1 ko*	prt257	ATGGATTCTCAATCTACAAT; ACAGTATGGGAACAACTATT	ssODN	dpy-10(cn64)
	fhip-1::gfp	prt276	ATGGATTCTCAATCTACAAT	dsDNA hybrid	
Y69H2.6 (V)	*ubc-19 ko*	prt279	GGCCCCACAAGACGGATTAT; GATCACCAAGTATGATGACG	ssODN	PRF4::rol-6 (su1006)

Single copy insertion of transgenes

A Mos1 transposon-based strategy (Frøkjær-Jensen *et al.*, 2008) was used to generate strains stably expressing transgenes under the control of the *dpy-7* promoter for expression in epidermal cells. This strategy was used to generate prtSi260 *(Pdpy-7::mKate2::rab-5::tbb-2 3' UTR)*, and prtSi261 (*Pdpy-7::ctns-1::5 aa linker::mKate2::tbb-2 3' UTR).* Transgenes were cloned into pCFJ151, as described on **Table 7**, for insertion on chromosome 5 (oxTi365), and transgene integration was confirmed by PCR.

Table 7 - Plasmids constructed for transgenic insertion into the *C. elegans* genome, related to the experiments on this chapter.

Plasmid	Backbone	Strategy	Description
pRG1373	pCFJ151	Gibson Assembly*	1.38 kb Pdpy-7::ctns-1::5aa linker::mKate2::tbb-2 3' UTR
pRG1372	pCFJ151	Gibson Assembly*	1.38 kb Pdpy-7::mKate2::5aa linker::rab-5::tbb-2 3' UTR

*Gibson Assembly was performed has described on the previous chapter.

Microscopy

Animals were immobilized with 5 mM levamisole for 10 min, mounted on a freshly prepared 2 % (w/v) agarose pad, and covered with an 18 mm × 18 mm coverslip (No. 1.5H, Marienfeld). Imaging was performed in L4-stage animals, at 20 ºC, using a Nikon Eclipse Ti

coupled to an Andor Revolution XD spinning disk confocal system, composed of an iXon Ultra 897 CCD camera (Andor Technology), a solid-state laser combiner (ALC-UVP 350i, Andor Technology), and a CSU-X1 confocal scanner (Yokogawa Electric Corporation), controlled by Andor IQ3 software (Andor Technology). A 60x NA 1.4 Plan-Apochromat objective was used to acquire a 4-µm z-stack (step size 0.1 µm). For each condition, more than 8 worms were imaged in at least 2 independent sessions.

Results

The Hook protein ZYG-12 recruits dynein to early endosomes in the C. elegans epidermis

ZYG-12 shows significant similarity (~22 % identity) with both Hook1 and Hook3, yet no canonical Hook protein functions for ZYG-12 have been described. Furthermore, ZYG-12 localization has only been assessed using transgenic reporters under the expression of the germline-specific *pie-1* promotor. In an effort to determine potential additional functions of ZYG-12 besides dynein recruitment to the NE, I used endogenously tagged GFP::ZYG-12 to assess its postembryonic expression pattern.

In the gonad of L4 stage animals, GFP::ZYG-12 was present on the NE with prominent ‘‘patches’’ in several nuclei (**Figure 19A, B**), as expected (Malone *et al.*, 2003; Sato *et al.*, 2009). In the same animals, GFP::ZYG-12 was also present in cytoplasmic puncta in the hyp7 cell and the epidermal seam, suggesting an association with membrane-bound organelles other than the nucleus (**Figure 19A, B**). mCh::DHC-1 co-localized with GFP::ZYG-12 in the gonad (**Figure 19B**), consistent with previous work showing that ZYG-12 recruits dynein to the NE (Malone *et al.*, 2003). In addition, mCh::DHC-1 co-localized with the ZYG-12 puncta in the epidermis, suggesting that ZYG-12 also acts as a dynein adaptor in this context (**Figure 19B**).

To determine the endomembrane identity of the GFP::ZYG-12 puncta, I constructed two transgenic strains: one expressing epidermal mKate2::RAB-5, homolog of human Rab5b and Rab5c, and the other expressing epidermal CTNS-1::mKate2, homolog of the human lysosomal transmembrane protein cystinosin. CTNS-1::mKate2-labelled structures were mostly tubular, whereas mKate2::RAB-5 showed a more vesicular pattern with several enlarged round compartments (**Figure 19C, D**). Co-expression of these membrane markers with GFP::ZYG-12 showed no co-localization with CTNS-1::mKate2 and very good co-localization with mKate2::RAB-5 (**Figure 19C, D**).

These results suggest that ZYG-12 recruits dynein to early endosomes in the epidermis, a hitherto unknown function that is distinct from its germline/early embryo function as a dynein adaptor for nuclei.

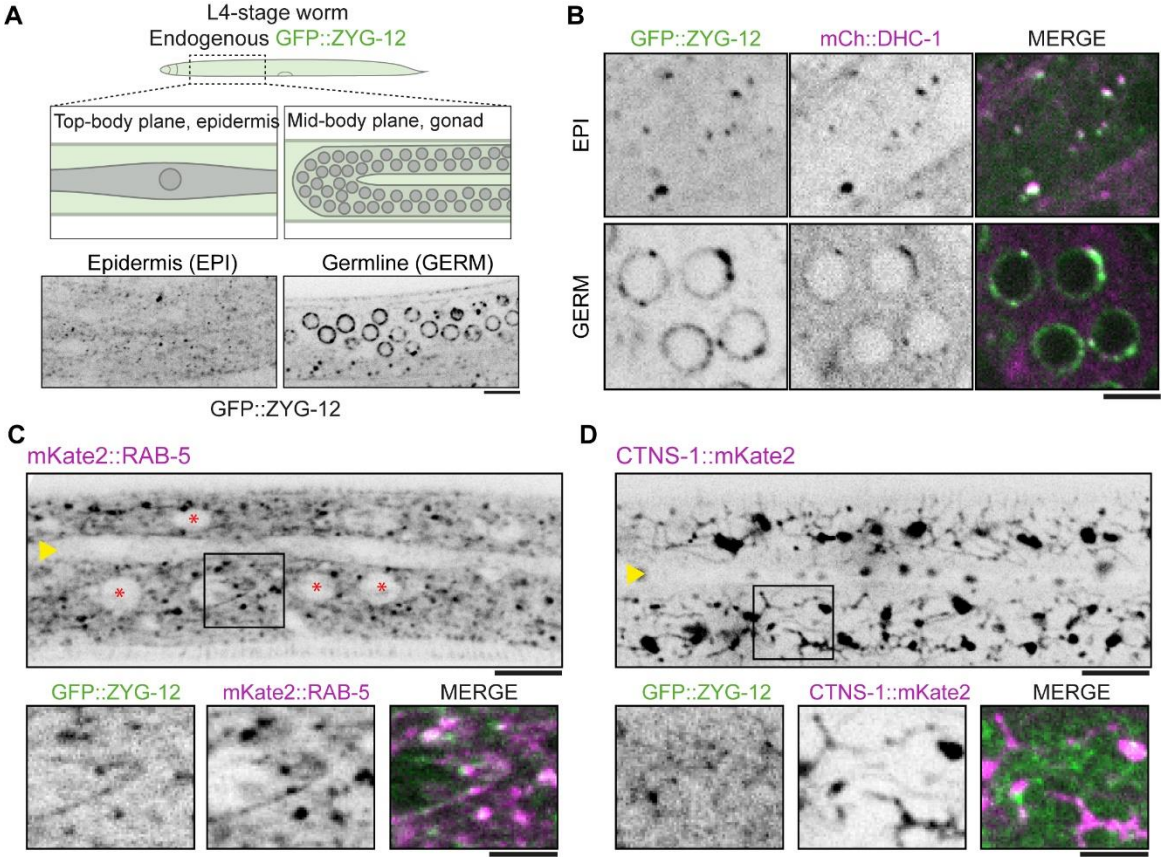

Figure 19 - Hook protein ZYG-12 associates with dynein and early endosomes in the *C. elegans* epidermis.

(A) (*top)* Schematic showing the epidermal and gonad region imaged in subsequent experiments. (*bottom)* Selected images from both epidermis (EPI) and germline (GERM) showing expression of GFP::ZYG-12. Scale bar, 20 µm. **(B)** Selected images from the epidermis and germline of the same animal co-expressing GFP::ZYG-12 and mCh::DHC-1 (dynein heavy chain). Scale bar, 5 µm. **(C)** *(top)* Selected image from L4-animal epidermis expressing transgenic mKate2::RAB-5 under *dpy-7* promotor. Scale bar, 10 µm *(bottom)* Zoom images of the same animal co-expressing GFP::ZYG-12 and mKate2::RAB-5. Scale bar, 5 µm. **(D)** *(top)* Selected image from L4-animal epidermis expressing transgenic CTNS-1::mKate2 under *dpy-7* promotor. Scale bar, 10 µm *(bottom)* Zoom images of the same animal co-expressing GFP::ZYG-12 and CTNS-1::mKate2. Scale bar, 5 µm.

ZYG-12 recruitment to early endosomes requires FHIP-1 but not UBC-19

Both Hook1 and 3 bind to early endosomes through the formation of an FHF complex (Christensen *et al.*, 2021). Human FHIP1A and FHIP1B show significant similarity (29.49 % and 31.10 % identity, respectively) with *C. elegans* C05D11.8, making it the likely FHIP

homolog. I will therefore refer to C05D11.8 as FHIP-1. To assess its function, I generated an *fhip-1* null mutant by deleting 3 kb using CRISPR/Cas9-mediated genome editing (**Figure 20A**). Knocking out FHIP-1 resulted in delocalization of GFP::ZYG-12 from mKate2::RAB-5 in the epidermis (**Figure 20B**) but did not perturb GFP::ZYG-12 localization at the NE in the gonad (**Figure 20C**). This implied that ZYG-12 localizes to nuclei and early endosomes through distinct mechanisms.

I next constructed endogenously tagged FHIP-1::GFP by inserting GFP into an internal loop. Combining this tagged version with mKate2::RAB-5 showed that FHIP-1::GFP is enriched on early endosomes (**Figure 20D**). In contrast, no FHIP-1::GFP signal was detectable in the gonad (data not shown). These results further support the idea that FHIP-1 functions at early endosomes as part of FHF.

Besides Hook and FHIP proteins, the FHF complex also includes FTS (Xu *et al.*, 2008). Human FTS shows significant identity (36.13 %) with *C. elegans* UBC-19, making it

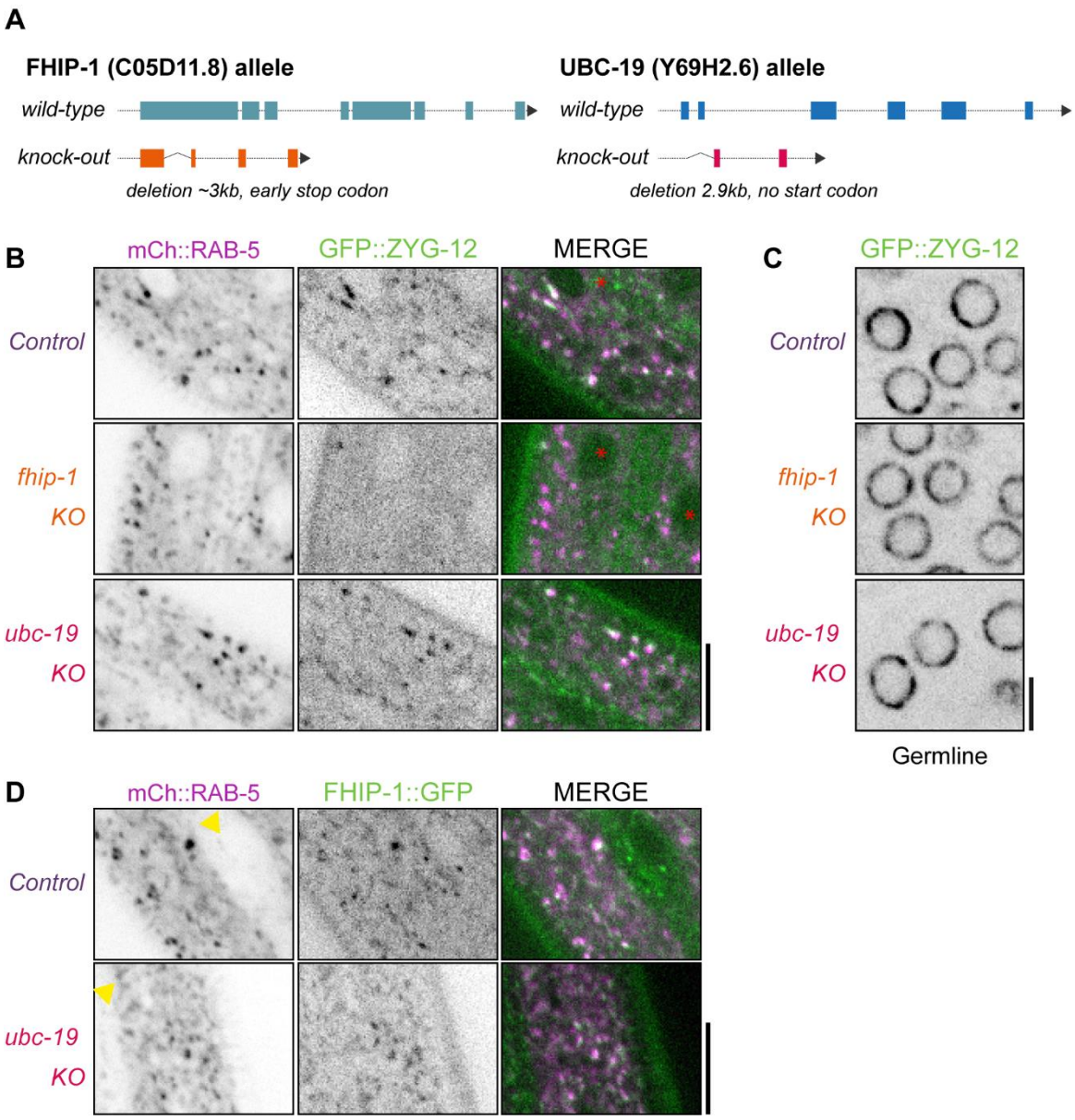

Figure 20 - ZYG-12 recruitment to early endosomes, but not to the nuclear envelope, is mediated by the FHF complex subunit FHIP-1.
(A) (*left)* Schematics showing the ORF from the wild-type FHIP-1 gene and the constructed *knock-out* upon a approximatly 3kb base pairs deletion that results in a early stop codon. *(right)* Schematics showing the ORF from the wild-type UBC-19 gene and the constructed *knock-out* upon a 2.9kb base pairs deletion that included the start codon. **(B)** Selected images from the L4-animals epidermis co-expressing GFP::ZYG-12 and transgenic mKate2::RAB-5 under *dpy-7* promotor. Scale bar, 10 µm. **(C)** Selected images from the L4-animals gonad expressing GFP::ZYG-12. Scale bar, 10 µm. **(D)** Selected images from the L4-animals epidermis co-expressing FHIP-1::GFP and transgenic mKate2::RAB-5 under *dpy-7* promotor. Yellow arrowheads correspond to the seam cell syncytium. Scale bar, 10 µm.

the likely FTS homolog. To assess whether *C. elegans* FHF function requires FTS, I deleted 2.9 kb, including the start codon, from *ubc-19* (**Figure 20A**). In *ubc-19 null* animals, GFP::ZYG-12 still localized to mKate2::RAB-5 puncta in the epidermis (**Figure 20B**) and to the NE in the gonad (**Figure 20C**). This result shows that UBC-19 is dispensable for ZYG-12 recruitment to early endosomes. FHIP-1::GFP localization was also not perturbed in *ubc-19* null animals, showing that FHIP-1 recruitment to early endosomes is independent of UBC-19 (**Figure 20D**).

A ZYG-12 mutant defective in FHIP/FTS binding cannot target to early endosomes but preserves its targeting to the nuclear envelope

Recently, the cryo-EM structure of the human FHF complex revealed that Hook3 interacts with both FTS and FHIP using three sites: a Hook3 helix that fits onto a hydrophobic pocket in FHIP (site 1); a span of ~30 residues of the Hook3 coiled-coil packed against the catalytically dead ubiquitin ligase domain of FTS (site 2); and, within the ~30 residues of site 2, a shorter span of 8 residues that binds to a C-terminal helix of FTS (site 3) (Ali *et al.*, 2023). AlphaFold2 makes similar predictions for *C. elegans* FHF (data not shown).

Sequence alignments of vertebrate and nematode Hook proteins revealed a conserved region before the C-terminal KASH domain of ZYG-12, which contains the 3 binding sites sites for FHIP/FTS (Ali *et al.*, 2023). To evaluate whether this region is important for ZYG-12 association with early endosomes, I deleted residues 686 to 730 by genome editing. The localization of GFP::ZYG-12(∆686-730) to germline nuclei was unperturbed and the animals are viable, indicating that the LINC complex functions of ZYG-12 were unaffected by this mutation (**Figure 21B, C**). In contrast, GFP::ZYG-12(∆686-730)

no longer co-localized with mKate2::RAB-5 puncta in the epidermis (**Figure 21B,C**), showing that this region is essential for ZYG-12 association with early endosomes.

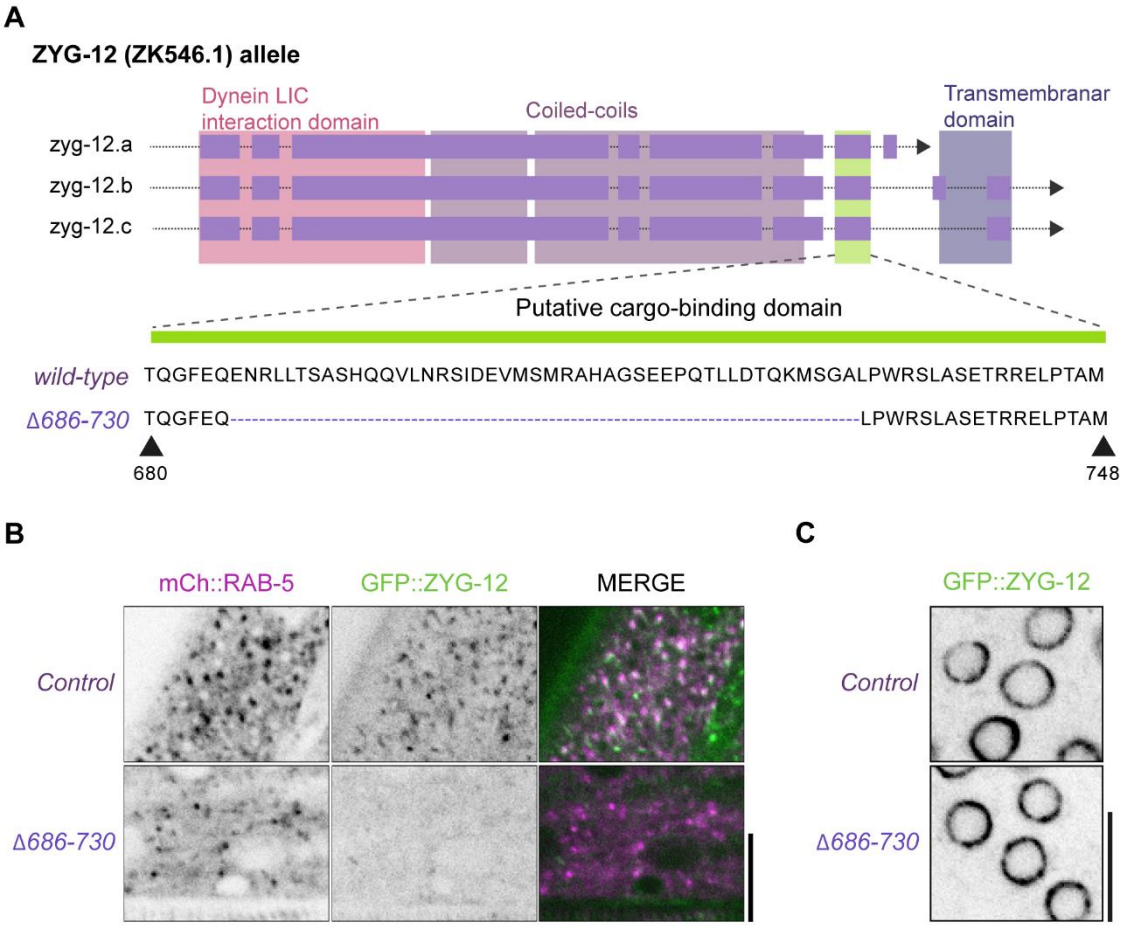

Figure 21 – Deletion of a putatuve cargo-binding domain impedes ZYG-12 targetting to early endosomes but preserves its targetting to the nuclear envelope.
(A) (*top)* Schematic showing the three ORF correspondent to the three ZYG-12 isoforms. Shaded regions correspond to the predicted domains. (*bellow)* Nucleotide sequence of the predicted cargo-binding domain with identification of the residues deleted in the *zyg-12 Δ686-730* mutant. **(B)** Selected images from the L4-animals epidermis co-expressing GFP::ZYG-12 and transgenic mKate2::RAB-5 under *dpy-7* promotor. Scale bar, 10 µm. **(C)** Selected images from the L4-animals gonad expressing GFP::ZYG-12. Scale bar, 10 µm.

The region encompassing ZYG-12 residues 686 to 730 contains two separate short stretches of residues that are highly conserved and correspond to the FHIP binding site (i.e., site 1 in Ali *et al.*, 2023), and the FTS binding sites (sites 2 and 3 in Ali *et al.*, 2023). To determine the functional significance of these sites, I constructed three mutants: the ZYG-12 mutant *6A(ubc-19*) consists of E686A, R688A, L689A, L690A, T691A, and S692A, and is expected to disrupt the binding between ZYG-12 and UBC-19 at sites 2 and 3; the ZYG-12 mutant *6A(fhip-1*) consists of T720A, L721A, L722A, Q725A, K726A, and L731A, and disrupts the binding of ZYG-12 to FHIP-1 (site 1); and the ZYG-12 mutant *12A*, which

combines the two 6A mutations and is therefore expected to disrupt the binding to both UBC-19 and FHIP-1.

None of the mutations affected localization to the NE (**Figure 22B**), reinforcing the observation that the FHIP/FTS interaction domain is dispensable for the LINC complex function of ZYG-12. Surprisingly, none of the mutations de-localized GFP::ZYG-12 from mKate2::RAB-5 puncta (**Figure 22A**). Considering that the extended interaction surface between UBC-19 and ZYG-12 at site 2 may not be fully perturbed in the 12A mutant, I combined the *6A(fhip-1)* mutant with the *ubc-19 null* mutant. This combination resulted in displacement of GFP::ZYG-12 from mKate2::RAB-5 puncta (**Figure 22A**). Given that the *ubc-19 null* mutant on its own has no effect (**Figure 20D**), these results indicate that the interaction between UBC-19 and ZYG-12 is dispensable for ZYG-12 recruitment to early endosomes as long as ZYG-12 can bind to FHIP-1. The fact that the 12A mutant localizes

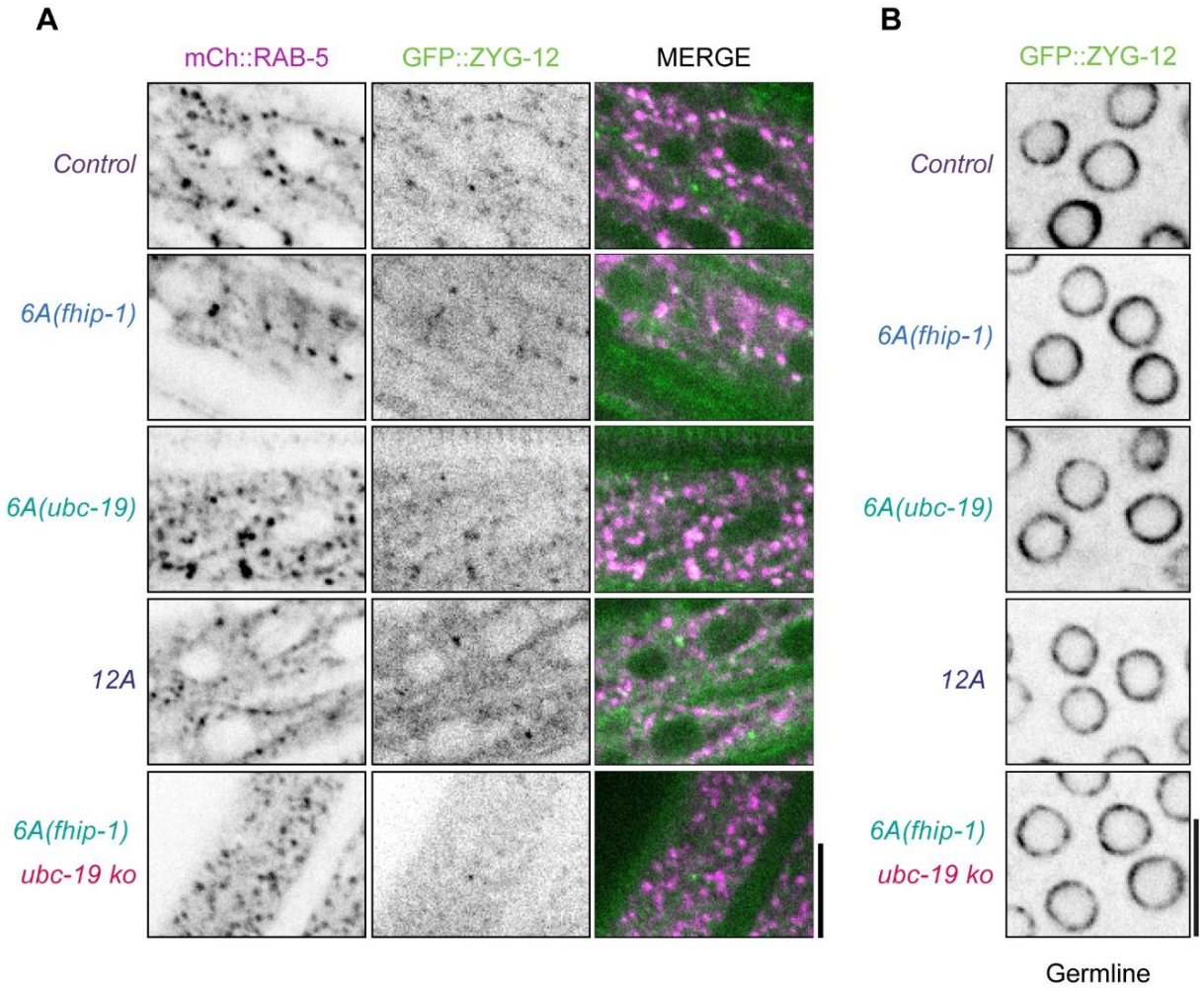

Figure 22 - UBC-19^{FTS} becomes essential for early endosome recruitment of ZYG-12 when it is defective for FHIP-1 binding.

(B) Selected images from the L4-animals epidermis co-expressing GFP::ZYG-12 and transgenic mKate2::RAB-5 under *dpy-7* promotor. Scale bar, 10 µm. **(C)** Selected images from the L4-animals gonad expressing GFP::ZYG-12. Scale bar, 10 µm.

to early endosomes also indicates that there are additional residues that participate in the binding of ZYG-12 to UBC-19 at site 2, and that this residual interaction is sufficient for FHF complex formation.

Discussion and future perspectives

ZYG-12 is the well-established Hook homolog in *C. elegans*. However, ZYG-12 has never been associated with early endosome transport, in contrast to Hook proteins in fungi and vertebrates. Here, I constructed and characterized a separation-of-function mutant that disrupts ZYG-12 recruitment to early endosomes but retains its meiotic and mitotic activity in the germline and early embryo. I identified the conserved motifs responsible for ZYG-12 interactions with FTS and FHIP, as well as defined the hierachy of interactions needed for the FHF complex assembly in *C. elegans.* In this initial analysis, I used a qualitative approach to describe the results obtained. The inclusion of a quantitative analysis should be considered to further reinforce these conclusions and improve this study.

ZYG-12 recruits dynein to early endosomes in the epidermis

Malone and colleagues first described that the ZYG-12 N-terminal region shares sequence identity with proteins of the Hook family (Malone *et al.*, 2003). However, ZYG-12 also features a transmembrane KASH domain at its C-terminus, which is not found in Hook proteins (Walenta *et al.*, 2001). ZYG-12 uses the KASH domain to form the LINC complex with SUN-1 (Minn *et al.*, 2009). Because this LINC complex is required to anchor centrosomes to the NE during early embryonic divisions, inhibition of ZYG-12, either by RNAi-mediated depletion or *null* mutations, is lethal (Malone *et al.*, 2003).

Intriguingly, as research on ZYG-12's meiotic and mitotic roles was progressing, Hook proteins in other species were established as important adaptors for early endosome transport (Bielska *et al.*, 2014; Christensen *et al.*, 2021; Kendrick *et al.*, 2018; Olenick *et al.*, 2016; Schroeder & Vale, 2016; Xu *et al.*, 2008; Zhang *et al.*, 2014). Evidence coming from *C. elegans* showed that disrupting retrograde transport impairs Rab5-marked organelle trafficking in neurons (Celestino *et al.*, 2022; Celestino *et al.*, 2019), indicating a potentially conserved mechanism for cargo-adaptor binding in worms. Still, in contrast to the other Hook proteins, ZYG-12 was never shown to be associated with Rab5-positive vesicles.

The CRISPR/Cas9 revolution represents a tremendous technical advance for cell biological studies, in particular because it facilitates fluorescent tagging of endogenous proteins (Chen *et al.*, 2016; Dickinson & Goldstein, 2016; Dokshin *et al.*, 2018; Heppert *et al.*, 2018; Paix *et al.*, 2017). The use of endogenously labelled ZYG-12 allowed me to

explore ZYG-12 localization in different tissues, which led to the detection of the punctate pattern in the epidermis. This observation immediately suggested that ZYG-12 has a canonical Hook protein function in this tissue.

By combining different fluorescent markers, I showed that ZYG-12 in the epidermis colocalizes with RAB-5 and DHC-1, indicating the presence of both the motor and the adaptor on early endosomes. Hook proteins bind to dynein through its essential subunit DLIC (DLI-1 in *C. elegans*) (Schroeder & Vale, 2016). The ZYG-12 N-terminal region comprises a conserved domain for DLI-1 binding (Malone *et al.*, 2003; Zhou *et al.*, 2009) followed by a long stretch of coiled-coil. DLI-1 binding to ZYG-12 occurs through the C-terminal region of DLI-1 (Malone *et al.*, 2003). The C-terminal helix1 of DLIC is responsible for the binding of all the described adaptors to dynein (Celestino *et al.*, 2019; Lee *et al.*, 2020; Lee *et al.*, 2018). It remains to be explored if perturbation of the DLI-1 helix1 would be sufficient to delocalize dynein from ZYG-12.

I have not explored whether perturbation of ZYG-12 results in defects in early endosome motility. The use of transgenic mKate2::RAB-5, expressed from a strong epidermal promotor, is likely not ideal to assess early endosome motility. Most of the RAB-5 structures detected are enlarged and mostly stationary, which may be a consequence of RAB-5 over-expression (Bucci *et al.*, 1992; Roberts *et al.*, 1999; Stenmark *et al.*, 1994). Additionally, this transgenic strategy only allows to assess RAB-5 motility in the epidermis. To clarify the relevance of ZYG-12 for early endosome motility in *C. elegans*, an endogenously tagged RAB-5 version would be preferable.

ZYG-12, FHIP-1 and UBC-19 form the C. elegans FHF complex

Prior to my study, the *C. elegans* FHF complex had not been described. My work identified C05D11.8 as the FHIP homolog, which I therefore propose to be named FHIP-1. I conclude from my results that FHIP-1 acts together with UBC-19, the homolog of FTS, to recruit dynein to early endosomes via ZYG-12. In 2014, a study in *Aspergillus nidulans* used genetic screening to find proteins involved in the distribution of organelles, including early endosomes (Yao *et al.*, 2014). This screen identified *fhip*A (homolog of FHIP) and *ftsA* (homolog of FTS). Both proteins were shown to be essential for dynein-mediated early endosome transport (Yao *et al.*, 2014). In addition, tagged-versions of FhipA and FtsA colocalized with Rab5 (*Aspergillus* RabA)-marked endosomes (Yao *et al.*, 2014), similar to what I observed with for GFP-tagged FHIP-1.

Furthermore, both FtsA or FhipA *knock-out* resulted in delocalization of HookA, the *Aspergillus* Hook protein, from RabA particles (Yao *et al.*, 2014). This is consistent with my observation that knocking out FHIP-1 delocalizes ZYG-12 from RAB-5 puncta, indicating

that FHIP-1 has a conserved function in establishing the connection between FHF and early endosomes. In contrast, knocking out UBC-19 neither affects ZYG-12 nor FHIP-1 localization to RAB-5 puncta, indicating a comparatively minor role for UBC-19 in the formation of the FHF complex. This contrasts with results described in fungi, where FtsA depletion significantly decreased the levels of HookA and FhipA on RabA particles (Yao *et al.*, 2014)**.**

ZYG-12 recruitment to the NE was not impaired by knocking out FHIP-1 or UBC-19, and GFP-tagged FHIP-1 was neither detected in the germline nor in the zygote. These results demonstrate that the essential roles of ZYG-12 during meiosis and embryogenesis are independent of FHF.

In fungi, HookA depletion impacts FhipA protein levels but not FtsA protein levels (Yao *et al.*, 2014). In mammals, evidence shows that Hook3 is the central element for the formation of the complex, since FTS and FHIP cannot form a subcomplex on their own (Ali *et al.*, 2023). It would be interesting to check whether the ZYG-12(∆686-730) mutant, in which the binding sites for FHIP-1 and UBC-19 are deleted, shows reduced FHIP-1 and/or UBC-19 protein levels.

Distinct domains in ZYG-12 mediate its recruitment to early endosomes and the NE

The *C. elegans* ZYG-12 protein consists of an a N-terminal domain responsible for DLIC binding, followed by a long coiled-coil and a C-terminal transmembrane domain. A recent cryo-EM study of the human FHF complex revealed how its subunits interact with each other (Ali *et al.*, 2023). The binding sites for FHIP and FTS in Hook3 are conserved in ZYG-12, and my work shows that deletion of this region prevents ZYG-12 recruitment to early endosomes without affecting its recruitment to the NE. This demonstrates that ZYG-12 participates in LINC and FHF complex formation through distinct domains.

Surprisingly, mutating six residues of the FHIP-1 binding region and six residues of the UBC-19 binding region (i.e., the 12A mutant) was insufficient to delocalize ZYG-12 from mKate2::RAB-5 puncta. It is important to note that the binding interface between UBC-19 and ZYG-12 likely involves additional residues that are part of the extended interaction surface of site 2. The observation that the Hook3 C-terminus is positioned between FHIP and FTS, which also directly interact with each other (Ali *et al.*, 2023), may explain why residual contacts between ZYG-12 and UBC-19 in the 12A mutant are sufficient for FHF formation. The fact that multiple contacts contribute to the stability of the FHF complex also helps explain why UBC-19 is not mandatory for ZYG-12 recruitment to early endosomes but becomes essential when FHIP-1 binding to ZYG-12 is unperturbed.

ZYG-12 isoforms may have a decisive role in defining its functions

The *zyg-12* ORF produces three different isoforms through alternative spicing, denoted A, B and C. All share the first 730 residues (DLIC binding and the coiled coil) but only two isoforms (B and C) have an extension of 29 amino acids that comprise the transmembrane KASH domain that forms the LINC complex at the NE. Previous studies used a transgene-based approach to examine the localization patterns of the three isoforms in the germline and early embryo (Malone *et al.*, 2003; Minn *et al.*, 2009). In the *C. elegans* zygote, ZYG-12B and C were shown to decorate both the NE and centrosomes, whereas ZYG-12A was only present at centrosomes (Malone *et al.*, 2003). In that study, the authors also used this transgenic approach to rescue the severe embryonic phenotype of mutant *zyg-12*. Transgenic expression of ZYG-12A was unable to rescue (Malone *et al.*, 2003), confirming the importance of the KASH domain.

An interesting question is whether ZYG-12's dual role at early endosomes and nuclei is regulated by tissue-specific expression of splice isoforms. Consistent with this idea, ZYG-12 is only detected at the NE in the germline and during embryonic divisions. It would be informative to use genome editing to restrict ZYG-12 expression to specific isoforms (in a GFP::ZYG-12 background). Such an approach may reveal whether ZYG-12A, which lacks the KASH domain but retains the FTS/FHIP binding domain, is the main isoform in the epidermis.

Apart from tissue-specific expression of ZYG-12 isoforms, additional mechanisms could influence whether ZYG-12 is recruited to early endosomes or the NE. ZYG-12B and C are expressed in the germline and the early embryo, and both contain the FTS/FHIP binding domain in addition to the KASH domain. Nevertheless, ZYG-12 and RAB-5 do not detectably colocalize in these tissues (data not shown). One likely reason is that the FHF complex cannot form because FHIP-1 is not expressed. It is conceivable that the lack of FHIP-1 expression in the gonad and early embryo facilitates ZYG-12 enrichment at the NE by avoiding competition for ZYG-12 binding that would occur if ZYG-12 was also recruited to early endosomes.

Acknowledgements

The authors thank to the Dhanya Cheerambathur (University of Edinburgh) for sharing strains; and WormBase for providing data and tools. This project was funded by the Fundação para a Ciência e a Tecnologia (FCT)/Ministério da Ciência, Tecnologia e Ensino Superior (PTDC/BIA-CEL/1321/2021).

Chapter V. Final Remarks

Conclusions and outlooks

After the discovery of cytoplasmic dynein 1 almost four decades ago, it was quickly realized that its functional diversity is associated with multiple layers of regulation. In this thesis, I took advantage of the powerful animal model *C. elegans* to study dynein regulation in two distinct functional contexts. The genetic tractability of *C. elegans* allowed me to construct a hypomorphic dynein mutant to characterize dynein's roles in the assembly and position of the mitotic spindle during stem cell-like divisions and to insert precise mutations in a gene that codes for a dynein adaptor.

In the first part of this thesis, I adapted several microscopy protocols to study the postembryonic development of the epidermis. This allowed me to explore how dynein's roles during cell division impact tissue morphogenesis. So far, few studies have directly characterized the impact of mis-oriented division on epidermal tissue architecture and cell fate decisions. By perturbatig spindle positioning mechanically without interfering with polarity signalling, I was able to demonstrate that mis-oriented divisions lead to significant alterations in cell fate. Additionally, I demonstrate that spindle orientation and position is regulated through the canonical LIN-5/dynein pathway in seam cells, and I identify a novel role for dynein in directed centrosome migration during prophase, which is important for correct spindle orientation.

In the second part of this thesis, I uncovered that the Hook domain protein ZYG-12 is associated with early endosomes in the epidermis. I showed that besides being part of the LINC complex through its KASH domain, as described by others, ZYG-12 is part of the FHF complex. Using CRISPR/Cas9-mediated genome editing, AlphaFold2-based structure prediction, and live imaging, I identified the domains in ZYG-12 responsible for early endosome association and succeded in constructing a separation-of-function mutant that selectively perturbed early endosome recruitment of ZYG-12. My study illustrates how a single type of adaptor can allow dynein to bind multiple distinct cargos.

The work presented in this thesis was aided by the recent *in vitro* reconstitution of the dynein transport machine (Ali *et al.*, 2023; Singh *et al.*, 2023), and it is my expectation that in the future cryo-EM and structure prediction will remain crucial tools in understanding dynein and its regulators.

Finally, the work performed in this thesis highlights that *C. elegans* is a versatile animal model to uncover new knowledge about molecular motors in different tissues and cellular enviroments. The combination of established models and innovative methods is vital for probing deeper into biological mechanisms, transcending species boundaries for insightful discoveries.

Chapter VI. Reference List

Afshar, K., Willard, F. S., Colombo, K., Siderovski, D. P., & Gonczy, P. (2005). Cortical localization of the Galpha protein GPA-16 requires RIC-8 function during C. elegans asymmetric cell division. *Development*, *132*(20), 4449-4459. https://doi.org/10.1242/dev.02039

Agrawal, R., Gillies, J. P., Zang, J. L., Zhang, J., Garrott, S. R., Shibuya, H., Nandakumar, J., & DeSantis, M. E. (2022). The KASH5 protein involved in meiotic chromosomal movements is a novel dynein activating adaptor. *Elife*, *11*. https://doi.org/10.7554/elife.78201

Ai, E., & Skop, A. R. (2009). Endosomal recycling regulation during cytokinesis. *Communicative & Integrative Biology*, *2*(5), 444-447. https://doi.org/10.4161/cib.2.5.8931

Ali, F. A., Zwetsloot, A. J., Stone, C. E., Morgan, T. E., Wademan, R. F., Carter, A. P., & Straube, A. (2023). KIF1C activates and extends dynein movement through the FHF cargo adaptor. *bioRxiv*. https://doi.org/10.1101/2023.10.26.564242

Almeida, A. C., Soares-de-Oliveira, J., Drpic, D., Cheeseman, L. P., Damas, J., Lewin, H. A., Larkin, D. M., Aguiar, P., Pereira, A. J., & Maiato, H. (2022). Augmin-dependent microtubule self-organization drives kinetochore fiber maturation in mammals. *Cell Reports*, *39*(1), 110610. https://doi.org/10.1016/j.celrep.2022.110610

Amos, L. A. (1989). Brain dynein crossbridges microtubules into bundles. *Journal of Cell Science*, *93*(1), 19-28. https://doi.org/10.1242/jcs.93.1.19

Aniento, F., Emans, N., Gareth Grittiths, & Gruenberg, J. (1993). Cytoplasmic dynein-dependent vesicular transport from early to late endosomes *The Journal of Cell Biology*, *123*(6), 1373-1387. https://doi.org/10.1083/jcb.123.6.1373

Arimoto, M., Koushika, S. P., Choudhary, B. C., Li, C., Matsumoto, K., & Hisamoto, N. (2011). The Caenorhabditis elegans JIP3 protein UNC-16 functions as an adaptor to link kinesin-1 with cytoplasmic dynein. *Journal of Neurosciences*, *31*(6), 2216-2224. https://doi.org/10.1523/JNEUROSCI.2653-10.2011

Arribere, J. A., Bell, R. T., Fu, B. X., Artiles, K. L., Hartman, P. S., & Fire, A. Z. (2014). Efficient marker-free recovery of custom genetic modifications with CRISPR/Cas9 in Caenorhabditis elegans. *Genetics*, *198*(3), 837-846. https://doi.org/10.1534/genetics.114.169730

Baravalle, G., Schober, D., Huber, M., Bayer, N., Murphy, R. F., & Fuchs, R. (2005). Transferrin recycling and dextran transport to lysosomes is differentially affected by bafilomycin, nocodazole, and low temperature. *Cell and Tissue Research*, *320*(1), 99-113. https://doi.org/10.1007/s00441-004-1060-x

Barbosa, D. J., Duro, J., Prevo, B., Cheerambathur, D. K., Carvalho, A. X., & Gassmann, R. (2017). Dynactin binding to tyrosinated microtubules promotes centrosome centration in *C. elegans* by enhancing dynein-mediated organelle transport. *PLOS Genetics*, *13*(7), e1006941. https://doi.org/10.1371/journal.pgen.1006941

Barlan, K., & Gelfand, V. I. (2017). Microtubule-Based Transport and the Distribution, Tethering, and Organization of Organelles. *Cold Spring Harbor Perspectives in Biology 9*(5). https://doi.org/10.1101/cshperspect.a025817

Bergstralh, D. T., & St Johnston, D. (2014). Spindle orientation: what if it goes wrong? *Seminars in Cell & Developmental Biology*, *34*, 140-145. https://doi.org/10.1016/j.semcdb.2014.06.014

Bielli, A., Thornqvist, P. O., Hendrick, A. G., Finn, R., Fitzgerald, K., & McCaffrey, M. W. (2001). The small GTPase Rab4A interacts with the central region of cytoplasmic dynein light intermediate chain-1. *Biochemical and Biophysical Research Communications*, *281*(5), 1141-1153. https://doi.org/10.1006/bbrc.2001.4468

Bielska, E., Schuster, M., Roger, Y., Berepiki, A., Soanes, D. M., Talbot, N. J., & Steinberg, G. (2014). Hook is an adapter that coordinates kinesin-3 and dynein cargo attachment on early endosomes. *Journal of Cell Biology*, *204*(6), 989-1007. https://doi.org/10.1083/jcb.201309022

Bouissou, A., Verollet, C., de Forges, H., Haren, L., Bellaiche, Y., Perez, F., Merdes, A., & Raynaud-Messina, B. (2014). gamma-Tubulin Ring Complexes and EB1 play antagonistic roles in microtubule dynamics and spindle positioning. *EMBO Journal*, *33*(2), 114-128. https://doi.org/10.1002/embj.201385967

Bowman, S. K., Neumuller, R. A., Novatchkova, M., Du, Q., & Knoblich, J. A. (2006). The Drosophila NuMA Homolog Mud regulates spindle orientation in asymmetric cell division. *Developmental Cell*, *10*(6), 731-742. https://doi.org/10.1016/j.devcel.2006.05.005

Box, K., Joyce, B. W., & Devenport, D. (2019). Epithelial geometry regulates spindle orientation and progenitor fate during formation of the mammalian epidermis. *Elife*, *8*. https://doi.org/10.7554/eLife.47102

Brenner, S. (1974). The Genetics of Caenorhabditis elegans. *Genetics*, *77*(1), 71-94. https://doi.org/doi: 10.1093/genetics/77.1.71

Bucci, C., Parton, R. G., Mather, I. H., Stunnenberg, H., Simons, K., Hoflack, B., & Zerial, M. (1992). The small GTPase rab5 functions as a regulatory factor in the early endocytic pathway. *Cell*, *70*(5), 715-728.

Byrd, D. T., & Kimble, J. (2009). Scratching the niche that controls Caenorhabditis elegans germline stem cells. *Seminars in Cell & Developmental Biology*, *20*(9), 1107-1113. https://doi.org/10.1016/j.semcdb.2009.09.005

Cantalupo, G., Alifano, P., Roberti, V., B.Bruni, C., & Bucci, C. (2001). Rab-interactinglysosomal protein (RILP): the Rab7 effector required for transport to lysosomes. *The EMBO Journal*.

Canty, J. T., Hensley, A., Aslan, M., Jack, A., & Yildiz, A. (2023). TRAK adaptors regulate the recruitment and activation of dynein and kinesin in mitochondrial transport. *Nature Communications*, *14*(1), 1376. https://doi.org/10.1038/s41467-023-36945-8

Carter, A. P., Diamant, A. G., & Urnavicius, L. (2016). How dynein and dynactin transport cargos: a structural perspective. *Current Opinion in Structural Biology*, *37*, 62-70. https://doi.org/10.1016/j.sbi.2015.12.003

Carvalho, C., Barbosa, D. J., Celestino, R., Zanin, E., Xavier Carvalho, A., & Gassmann, R. (2024). Dynein directs prophase centrosome migration to control the stem cell division axis in the developing C. elegans epidermis. *Genetics*. https://doi.org/10.1093/genetics/iyae005

Cason, S. E., Carman, P. J., Van Duyne, C., Goldsmith, J., Dominguez, R., & Holzbaur, E. L. F. (2021). Sequential dynein effectors regulate axonal autophagosome motility in a maturation-dependent pathway. *Journal of Cell Biology*, *220*(7). https://doi.org/10.1083/jcb.202010179

Caussinus, E., & Gonzalez, C. (2005). Induction of tumor growth by altered stem-cell asymmetric division in Drosophila melanogaster. *Nature Genetics*, *37*, 1125-1129. https://doi.org/https://doi.org/10.1038/ng1632

Celestino, R., Gama, J. B., Castro-Rodrigues, A. F., Barbosa, D. J., Rocha, H., d'Amico, E. A., Musacchio, A., Carvalho, A. X., Morais-Cabral, J. H., & Gassmann, R. (2022). JIP3 interacts with dynein and kinesin-1 to regulate bidirectional organelle transport. *Journal of Cellular Biology*, *221*(8). https://doi.org/10.1083/jcb.202110057

Celestino, R., Henen, M. A., Gama, J. B., Carvalho, C., McCabe, M., Barbosa, D. J., Born, A., Nichols, P. J., Carvalho, A. X., Gassmann, R., & Vogeli, B. (2019). A transient helix in the disordered region of dynein light intermediate chain links the motor to structurally diverse adaptors for cargo transport. *PLoS Biology*, *17*(1), e3000100. https://doi.org/10.1371/journal.pbio.3000100

Chaaban, S., & Carter, A. P. (2022). Structure of dynein-dynactin on microtubules shows tandem adaptor binding. *Nature*, *610*(7930), 212-216. https://doi.org/10.1038/s41586-022-05186-y

Chen, X., Feng, X., & Guang, S. (2016). Targeted genome engineering in *Caenorhabditis elegans*. *Cell Biosciences*, *6*, 60. https://doi.org/10.1186/s13578-016-0125-3

Chisholm, A. D., & Hsiao, T. I. (2012). The Caenorhabditis elegans epidermis as a model skin. I: development, patterning, and growth. *Wiley Interdiscip Rev Dev Biol*, *1*(6), 861-878. https://doi.org/10.1002/wdev.79

Chisholm, A. D., & Xu, S. (2012). The Caenorhabditis elegans epidermis as a model skin. II: differentiation and physiological roles. *Wiley Interdisciplinary Reviews: Developmental Biology*, *1*(6), 879-902. https://doi.org/10.1002/wdev.77

Christensen, J. R., Kendrick, A. A., Truong, J. B., Aguilar-Maldonado, A., Adani, V., Dzieciatkowska, M., & Reck-Peterson, S. L. (2021). Cytoplasmic dynein-1 cargo diversity is mediated by the combinatorial assembly of FTS-Hook-FHIP complexes. *Elife*, *10*. https://doi.org/10.7554/eLife.74538

Collins, E. S., Balchand, S. K., Faraci, J. L., Wadsworth, P., & Lee, W. L. (2012). Cell cycle-regulated cortical dynein/dynactin promotes symmetric cell division by differential pole motion in anaphase. *Molecular Biology of the Cell*, *23*(17), 3380-3390. https://doi.org/10.1091/mbc.E12-02-0109

Colombo, K., Grill, S. W., Kimple, R. J., Willard, F. S., Siderovski, D. P., & Gönczy, P. (2003). Translation of Polarity Cues into Asymmetric Spindle Positioning in Caenorhabditis

elegans Embryos. *Science*, *300*(5627), 1957-1961. https://doi.org/10.1126/science.1084146

Conklin, E. G. (1905). *The organization and cell-lineage of the ascidian egg* (Vol. 13). Academy of Natural Sciences. https://doi.org/https://doi.org/10.5962/bhl.title.4801

Couwenbergs, C., Labbé, J.-C., Goulding, M., Marty, T., Bowerman, B., & Gotta, M. (2007). Heterotrimeric G protein signaling functions with dynein to promote spindle positioning in *C. elegans*. *The Journal of Cell Biology*, *179*(1), 15-22. https://doi.org/10.1083/jcb.200707085

Culetto, E., & Sattelle, D. B. (2000). A role for Caenorhabditiselegansin understanding the function and interactions of human disease genes [Review]. *Human Molecular Genetics*, *9*, 869–877. https://doi.org/https://doi.org/10.1093/hmg/9.6.869

De Simone, A., Nédélec, F., & Gönczy, P. (2016). Dynein Transmits Polarized Actomyosin Cortical Flows to Promote Centrosome Separation. *Cell Reports*, *14*(9), 2250-2262. https://doi.org/10.1016/j.celrep.2016.01.077

Dehmelt, L., & Halpain, S. (2004). The MAP2/Tau family of microtubule-associated proteins. *Genome Biology*, *6*(1), 204. https://doi.org/10.1186/gb-2004-6-1-204

Deng, Q., & Wang, H. (2022). Re-visiting the principles of apicobasal polarity in Drosophila neural stem cells. *Development Biology*, *484*, 57-62. https://doi.org/10.1016/j.ydbio.2022.02.006

Dewey, E., Taylor, D., & Johnston, C. (2015). Cell Fate Decision Making through Oriented Cell Division. *Journal of Developmental Biology*, *3*(4), 129-157. https://doi.org/10.3390/jdb3040129

Dickinson, D. J., & Goldstein, B. (2016). CRISPR-Based Methods for Caenorhabditis elegans Genome Engineering. *Genetics*, *202*(3), 885-901. https://doi.org/10.1534/genetics.115.182162

Dimitriadi, M., Derdowski, A., Kalloo, G., Maginnis, M. S., O'Hern, P., Bliska, B., Sorkaç, A., Nguyen, K. C. Q., Cook, S. J., Poulogiannis, G., Atwood, W. J., Hall, D. H., & Hart, A. C. (2016). Decreased function of survival motor neuron protein impairs endocytic pathways. *Proceedings of the National Academy of Sciences*, *113*(30), E4377-E4386. https://doi.org/10.1073/pnas.1600015113

Dokshin, G. A., Ghanta, K. S., Piscopo, K. M., & Mello, C. C. (2018). Robust Genome Editing with Short Single-Stranded and Long, Partially Single-Stranded DNA Donors in Caenorhabditis elegans. *Genetics*, *210*(3), 781-787. https://doi.org/10.1534/genetics.118.301532

Driskell, O. J., Mironov, A., Allan, V. J., & Woodman, P. G. (2007). Dynein is required for receptor sorting and the morphogenesis of early endosomes. *Nature Cell Biology*, *9*, 113-120. https://doi.org/https://doi.org/10.1038/ncb1525

Dwivedi, D., Kumari, A., Rathi, S., Mylavarapu, S. V. S., & Sharma, M. (2019). The dynein adaptor Hook2 plays essential roles in mitotic progression and cytokinesis. *Journal of Cellular Biology*, *218*(3), 871-894. https://doi.org/10.1083/jcb.201804183

Echard, A., Jollivet, F., Martinez, O., Lacapere, J.-J., Rousselet, A., Janoueix-Lerosey, I., & Goud, B. (1998). Interaction of a Golgi-Associated Kinesin-Like Protein with Rab6. *Science*, *279*(5350), 580-585. https://doi.org/10.1126/science.279.5350.580

Edgley, M. L., Baillie, D. L., Riddle, D. L., & Rose, A. M. (2006). Genetic balancers. *WormBook*, 1-32. https://doi.org/10.1895/wormbook.1.89.1

Endow, S. A., Kull, F. J., & Liu, H. (2010). Kinesins at a glance. *Journal of Cell Science*, *123*(Pt 20), 3420-3424. https://doi.org/10.1242/jcs.064113

Fellows, A. D., Bruntraeger, M., Burgold, T., Bassett, A. R., & Carter, A. P. (2023). Dynein and dynactin move long-range but are delivered separately to the axon tip. *bioRxiv*. https://doi.org/10.1101/2023.07.03.547521

Fielmich, L. E., Schmidt, R., Dickinson, D. J., Goldstein, B., Akhmanova, A., & van den Heuvel, S. (2018). Optogenetic dissection of mitotic spindle positioning in vivo. *Elife*, *7*. https://doi.org/10.7554/eLife.38198

Flemming, A. J., Shen, Z.-Z., Cunha, A., Emmons, S. W., & Leroi, A. M. (2000). Somatic polyploidization and cellular proliferationdrive body size evolution in nematodes. *Proceedings of the National Academy of Sciences*, *97*, 5285–5290.

Flemming, W. (1965). Contributions to the knowledge of the cell and its vital processes. *Journal of Cell Biology*, *25*, 3 - 69.

Frøkjær-Jensen, C., Wayne Davis, M., Hopkins, C. E., Newman, B. J., Thummel, J. M., Olesen, S.-P., Grunnet, M., & Jorgensen, E. M. (2008). Single-copy insertion of

transgenes in Caenorhabditis elegans. *Nature Genetics*, *40*(11), 1375-1383. https://doi.org/10.1038/ng.248

Gama, J. B., Pereira, C., Simoes, P. A., Celestino, R., Reis, R. M., Barbosa, D. J., Pires, H. R., Carvalho, C., Amorim, J., Carvalho, A. X., Cheerambathur, D. K., & Gassmann, R. (2017). Molecular mechanism of dynein recruitment to kinetochores by the Rod-Zw10-Zwilch complex and Spindly. *Journal of Cellular Biology*, *216*(4), 943-960. https://doi.org/10.1083/jcb.201610108

Garner, K. E. L., Salter, A., Lau, C. K., Gurusaran, M., Villemant, C. M., Granger, E. P., McNee, G., Woodman, P. G., Davies, O. R., Burke, B. E., & Allan, V. J. (2023). The meiotic LINC complex component KASH5 is an activating adaptor for cytoplasmic dynein. *Journal of Cellular Biology 222*(5). https://doi.org/10.1083/jcb.202204042

Gassmann, R. (2023). Dynein at the kinetochore. *Journal of Cell Science*, *136*(5). https://doi.org/10.1242/jcs.220269

Gleason, J. E., & Eisenmann, D. M. (2010). Wnt signaling controls the stem cell-like asymmetric division of the epithelial seam cells during C. elegans larval development. *Developmental Biology*, *348*(1), 58-66. https://doi.org/10.1016/j.ydbio.2010.09.005

Gönczy, P., Pichler, S., Kirkham, M., & Hyman, A. A. (1999). Cytoplasmic Dynein Is Required for Distinct Aspects of MTOC Positioning, Including Centrosome Separation, in the One Cell Stage Caenorhabditis elegans Embryo. *The Journal of Cell Biology*.

Goodson, H. V., & Jonasson, E. M. (2018). Microtubules and Microtubule-Associated Proteins. *Cold Spring Harbor Perspectives in Biology 10*(6). https://doi.org/10.1101/cshperspect.a022608

Goody, R. S., Müller, M. P., & Wu, Y.-W. (2017). Mechanisms of action of Rab proteins, key regulators of intracellular vesicular transport. *Biological Chemistry*, *398*(5-6), 565-575. https://doi.org/10.1515/hsz-2016-0274

Gotta, M., & Ahringer, J. (2001). Distinct roles for Gα and Gβγ in regulating spindle position and orientation in Caenorhabditis elegans embryos. *Nature Cell Biology 1*, 297–300. https://doi.org/doi.org/10.1038/35060092

Gotta, M., Dong, Y., Peterson, Y. K., Lanier, S. M., & Ahringer, J. (2003). Asymmetrically distributed *C. elegans* homologs of AGS3/PINS control spindle position in the early

embryo. *Current Biology*, *13*(12), 1029-1037. https://doi.org/10.1016/s0960-9822(03)00371-3

Green, R. A., Paluch, E., & Oegema, K. (2012). Cytokinesis in animal cells. *Annual Review of Cell and Developmental Biology 28*, 29-58. https://doi.org/10.1146/annurev-cellbio-101011-155718

Grill, S. W., Gönczy, P., Stelzer, E. H. K., & Hyman, A. A. (2001). Polarity controls forces governing asymmetric spindle positioning in the Caenorhabditis elegans embryo. *Polarity controls forces governing asymmetric spindle positioning in the Caenorhabditis elegans embryo*, *409*, 630-633. https://doi.org/https://doi.org/10.1038/35054572

Grill, S. W., Howard, J., Schäffer, E., Stelzer, E. H. K., & Hyman, A. A. (2003). The Distribution of Active Force Generators Controls Mitotic Spindle Position. *Science*, *301*, 518-521. https://doi.org/10.1126/science.108656

Grotjahn, D. A., Chowdhury, S., Xu, Y., McKenney, R. J., Schroer, T. A., & Lander, G. C. (2018). Cryo-electron tomography reveals that dynactin recruits a team of dyneins for processive motility. *Nature Structural & Molecular Biology*, *25*(3), 203-207. https://doi.org/10.1038/s41594-018-0027-7

Guo, X., Farias, G. G., Mattera, R., & Bonifacino, J. S. (2016). Rab5 and its effector FHF contribute to neuronal polarity through dynein-dependent retrieval of somatodendritic proteins from the axon. *Proceedings of the National Academy of Sciences*, *113*(36), E5318-5327. https://doi.org/10.1073/pnas.1601844113

Gusnowski, E. M., & Srayko, M. (2011). Visualization of dynein-dependent microtubule gliding at the cell cortex: implications for spindle positioning. *Journal of Cell Biology*, *194*(3), 377-386. https://doi.org/10.1083/jcb.201103128

Hehnly, H., & Doxsey, S. (2014). Rab11 Endosomes Contribute to Mitotic Spindle Organization and Orientation. *Developmental Cell*, *28*(5), 497-507. https://doi.org/10.1016/j.devcel.2014.01.014

Heppert, J. K., Pani, A. M., Roberts, A. M., Dickinson, D. J., & Goldstein, B. (2018). A CRISPR Tagging-Based Screen Reveals Localized Players in Wnt-Directed Asymmetric Cell Division. *Genetics*, *208*(3), 1147-1164. https://doi.org/10.1534/genetics.117.300487

Hernandez-Perez, I., Rubio, J., Baumann, A., Girao, H., Ferrando, M., Rebollo, E., Aragay, A. M., & Geli, M. I. (2023). Kazrin promotes dynein/dynactin-dependent traffic from early to recycling endosomes. *Elife*, *12*. https://doi.org/10.7554/elife.83793

Hertwig, O. (1884). *Das Problem der Befruchtung und der Isotropie des Eies, eine Theorie der Vererbung*. Jena.

Hoepfner, S., Severin, F., Cabezas, A., Habermann, B., Runge, A., Gillooly, D., Stenmark, H., & Zerial, M. (2005). Modulation of receptor recycling and degradation by the endosomal kinesin KIF16B. *Cell*, *121*(3), 437-450. https://doi.org/10.1016/j.cell.2005.02.017

Hoogenraad, C. C., Wulf, P., Schiefermeier, N., Stepanova, T., Galjart, N., Small, J. V., Grosveld, F., Zeeuw, C. I. d., & Akhmanova, A. (2003). Bicaudal D induces selective dynein-mediated microtubule minus end-directed transport. *The EMBO Journal*.

Horgan, C. P., Hanscom, S. R., Jolly, R. S., Futter, C. E., & McCaffrey, M. W. (2010). Rab11-FIP3 links the Rab11 GTPase and cytoplasmic dynein to mediate transport to the endosomal-recycling compartment. *Journal of Cell Science*, *123*(Pt 2), 181-191. https://doi.org/10.1242/jcs.052670

Horgan, C. P., & McCaffrey, M. W. (2011). Rab GTPases and microtubule motors. *Biochemical Society Transactions*, *39*(5), 1202-1206. https://doi.org/10.1042/BST0391202

Huang, J., Roberts, A. J., Leschziner, A. E., & Reck-Peterson, S. L. (2012). Lis1 acts as a "clutch" between the ATPase and microtubule-binding domains of the dynein motor. *Cell*, *150*(5), 975-986. https://doi.org/10.1016/j.cell.2012.07.022

Hueschen, C. L., Kenny, S. J., Xu, K., & Dumont, S. (2017). NuMA recruits dynein activity to microtubule minus-ends at mitosis. *Elife*, *6*. https://doi.org/10.7554/eLife.29328

Huotari, J., & Helenius, A. (2011). Endosome maturation. *EMBO Journal*, *30*(17), 3481-3500. https://doi.org/10.1038/emboj.2011.286

Hyman, A. A., & White, J. G. (1987). Determination of cell division axes in the early embryogenesis of Caenorhabditis elegans. *The Journal of Cell Biology*, *105*(5), 2123-2135. https://doi.org/10.1083/jcb.105.5.2123

Jankele, R., Jelier, R., & Gonczy, P. (2021). Physically asymmetric division of the C. elegans zygote ensures invariably successful embryogenesis. *Elife*, *10*. https://doi.org/10.7554/eLife.61714

Jovic, M., Sharma, M., Rahajeng, J., & Caplan, S. (2010). The early endosome: a busy sorting station for proteins at the crossroads. *Histology and Histopathology*, *1*(25), 99-112. https://doi.org/10.14670/hh-25.99

Kamath, R. S., Fraser, A. G., Dong, Y., Poulin, G., Durbin, R., Gotta, M., Kanapin, A., Le Bot, N., Moreno, S., Sohrmann, M., Welchman, D. P., Zipperlen, P., & Ahringer, J. (2003). Systematic functional analysis of the Caenorhabditis elegans genome using RNAi. *Nature*, *421*(6920), 231-237. https://doi.org/10.1038/nature01278

Karki, S., & Holzbaur, E. L. F. (1995). Affinity Chromatography Demonstrates a Direct Binding between Cytoplasmic Dynein and the Dynactin Complex. *The Journal of Biological Chemistry*.

Kendrick, A. A., Redwine, W. B., Tran, P. T., Vaites, L. P., Dzieciatkowska, M., Harper, J. W., & Reck-Peterson, S. L. (2018). HOOK3 is a scaffold for the opposite-polarity microtubule-based motors cytoplasmic dynein and KIF1C. *bioRxiv*. https://doi.org/10.1101/508887

Kim, A. J., & Endow, S. A. (2000). A kinesin family tree. *Journal of Cell Science*, *113*(21), 3681-3682. https://doi.org/10.1242/jcs.113.21.3681

Kim, J. D., Chun, A. Y., Mangan, R. J., Brown, G., Pacheco, B. M., Doyle, H., Leonard, A., & El Bejjani, R. (2019). A conserved retromer-independent function for RAB-6.2/RAB6 in *C. elegans* epidermis integrity. *Journal of Cell Science*, *132*(5), jcs223586. https://doi.org/10.1242/jcs.223586

Kimble, J., & Hirsh, D. (1979). The postembryonic cell lineages of the hermaphrodite and male gonads in Caenorhabditis elegans. *Developmental Biology*, *2*, 396-417. https://doi.org/10.1016/0012-1606(79)90035-6

Kimura, K., & Kimura, A. (2011). Intracellular organelles mediate cytoplasmic pulling force for centrosome centration in the Caenorhabditis elegans early embryo. *Proceedings of the National Academy of Sciences*, *108*(1), 137-142. https://doi.org/10.1073/pnas.1013275108

King, S. J., Brown, C. L., Maier, K. C., Quintyne, N. J., & Schroer, T. A. (2003). Analysis of the dynein-dynactin interaction in vitro and in vivo. *Molecular Biology of the Cell*, *14*(12), 5089-5097. https://doi.org/10.1091/mbc.e03-01-0025

Kingsley, E. P., Chan, X. Y., Duan, Y., & Lambert, J. D. (2007). Widespread RNA segregation in a spiralian embryo. *Evolution & Development*, *9*(6), 527-539. https://doi.org/10.1111/j.1525-142x.2007.00194.x

Kiyomitsu, T. (2019). The cortical force-generating machinery: how cortical spindle-pulling forces are generated. *Current Opinion of Cellular Biology*, *60*, 1-8. https://doi.org/10.1016/j.ceb.2019.03.001

Kiyomitsu, T., & Cheeseman, I. M. (2012). Chromosome- and spindle-pole-derived signals generate an intrinsic code for spindle position and orientation. *Nature Cell Biology*, *14*(3), 311-317. https://doi.org/10.1038/ncb2440

Kiyomitsu, T., & Cheeseman, I. M. (2013). Cortical dynein and asymmetric membrane elongation coordinately position the spindle in anaphase. *Cell*, *154*(2), 391-402. https://doi.org/10.1016/j.cell.2013.06.010

Knoblich, J. A. (2010). Asymmetric cell division: recent developments and their implications for tumour biology. *Nature Reviews Molecular Cell Biology*, *11*(12), 849-860. https://doi.org/10.1038/nrm3010

Konno, D., Shioi, G., Shitamukai, A., Mori, A., Kiyonari, H., Miyata, T., & Matsuzaki, F. (2008). Neuroepithelial progenitors undergo LGN-dependent planar divisions to maintain self-renewability during mammalian neurogenesis. *Nature Cell Biology*, *10*(1), 93-101. https://doi.org/10.1038/ncb1673

Kotak, S. (2019). Mechanisms of Spindle Positioning: Lessons from Worms and Mammalian Cells. *Biomolecules*, *9*(2). https://doi.org/10.3390/biom9020080

Kotak, S., Busso, C., & Gonczy, P. (2012). Cortical dynein is critical for proper spindle positioning in human cells. *Journal of Cell Biology*, *199*(1), 97-110. https://doi.org/10.1083/jcb.201203166

Kotak, S., & Gonczy, P. (2013). Mechanisms of spindle positioning: cortical force generators in the limelight. *Current Opinion in Cell Biology*, *25*(6), 741-748. https://doi.org/10.1016/j.ceb.2013.07.008

Koushika, S. P., Schaefer, A. M., Vincent, R., Willis, J. H., Bowerman, B., & Nonet, M. L. (2004). Mutations in Caenorhabditis elegans cytoplasmic dynein components reveal specificity of neuronal retrograde cargo. *Journal of Neurosciences*, *24*(16), 3907-3916. https://doi.org/10.1523/JNEUROSCI.5039-03.2004

Krämer, H., & Phistry, M. (1998). Genetic Analysis of hook, a Gene Required for Endocytic Trafficking in Drosophila. *Genetics*, 675 - 684. https://doi.org/10.1093/genetics/151.2.675

Kumar, S., Olson, A. C., & Koelle, M. R. (2021). The neural G protein Gαo tagged with GFP at an internal loop is functional in Caenorhabditis elegans. *G3*, *11*(8). https://doi.org/10.1093/g3journal/jkab167

Lancaster, M. A., & Knoblich, J. A. (2012). Spindle orientation in mammalian cerebral cortical development. *Current Opinion in Neurobiology*, *22*(5), 737-746. https://doi.org/10.1016/j.conb.2012.04.003

Lau, C. K., O'Reilly, F. J., Santhanam, B., Lacey, S. E., Rappsilber, J., & Carter, A. P. (2021). Cryo-EM reveals the complex architecture of dynactin's shoulder region and pointed end. *EMBO Journal 40*(8), e106164. https://doi.org/10.15252/embj.2020106164

Lawrence, K. S., Tapley, E. C., Cruz, V. E., Li, Q., Aung, K., Hart, K. C., Schwartz, T. U., Starr, D. A., & Engebrecht, J. (2016). LINC complexes promote homologous recombination in part through inhibition of nonhomologous end joining. *Journal of Cell Biology*, *215*(6), 801-821. https://doi.org/10.1083/jcb.201604112

Lazetic, V., & Fay, D. S. (2017). Molting in *C. elegans*. *Worm*, *6*(1), e1330246. https://doi.org/10.1080/21624054.2017.1330246

Lechler, T., & Mapelli, M. (2021). Spindle positioning and its impact on vertebrate tissue architecture and cell fate. *Nature Reviews of Molecular and Cellular Biology*. https://doi.org/10.1038/s41580-021-00384-4

Lee, I. G., Cason, S. E., Alqassim, S. S., Holzbaur, E. L. F., & Dominguez, R. (2020). A tunable LIC1-adaptor interaction modulates dynein activity in a cargo-specific manner. *Nature Communications*, *11*(1), 5695. https://doi.org/10.1038/s41467-020-19538-7

Lee, I. G., Olenick, M. A., Boczkowska, M., Franzini-Armstrong, C., Holzbaur, E. L. F., & Dominguez, R. (2018). A conserved interaction of the dynein light intermediate chain

with dynein-dynactin effectors necessary for processivity. *Nature Communications*, *9*(1), 986. https://doi.org/10.1038/s41467-018-03412-8

Liang, X., Dong, X., Moerman, D. G., Shen, K., & Wang, X. (2015). Sarcomeres Pattern Proprioceptive Sensory Dendritic Endings through UNC-52/Perlecan in *C. elegans*. *Developmental Cell*, *33*(4), 388-400. https://doi.org/10.1016/j.devcel.2015.03.010

Lim, Y. W., Wen, F. L., Shankar, P., Shibata, T., & Motegi, F. (2021). A balance between antagonizing PAR proteins specifies the pattern of asymmetric and symmetric divisions in C. elegans embryogenesis. *Cell Reports*, *36*(1), 109326. https://doi.org/10.1016/j.celrep.2021.109326

Lock, J. G., & Stow, J. L. (2005). Rab11 in recycling endosomes regulates the sorting and basolateral transport of E-cadherin. *Molecular Biology of the Cell*, *16*(4), 1744-1755. https://doi.org/10.1091/mbc.e04-10-0867

Loubery, S., Wilhelm, C., Hurbain, I., Neveu, S., Louvard, D., & Coudrier, E. (2008). Different microtubule motors move early and late endocytic compartments. *Traffic*, *9*(4), 492-509. https://doi.org/10.1111/j.1600-0854.2008.00704.x

Lough, K. J., Byrd, K. M., Descovich, C. P., Spitzer, D. C., Bergman, A. J., Beaudoin, G. M., 3rd, Reichardt, L. F., & Williams, S. E. (2019). Telophase correction refines division orientation in stratified epithelia. *Elife*, *8*. https://doi.org/10.7554/eLife.49249

Loyer, N., & Januschke, J. (2020). Where does asymmetry come from? Illustrating principles of polarity and asymmetry establishment in Drosophila neuroblasts. *Current Opinion on Cellular Biology*, *62*, 70-77. https://doi.org/10.1016/j.ceb.2019.07.018

Luiro, K., Yliannala, K., Ahtiainen, L., Maunu, H., Jarvela, I., Kyttala, A., & Jalanko, A. (2004). Interconnections of CLN3, Hook1 and Rab proteins link Batten disease to defects in the endocytic pathway. *Human Molecular Genetics*, *13*(23), 3017-3027. https://doi.org/10.1093/hmg/ddh321

Luxton, G. G., & Starr, D. A. (2014). KASHing up with the nucleus: novel functional roles of KASH proteins at the cytoplasmic surface of the nucleus. *Current Opinion in Cell Biology*, *28*, 69-75. https://doi.org/10.1016/j.ceb.2014.03.002

Maday, S., Twelvetrees, A. E., Moughamian, A. J., & Holzbaur, E. L. (2014). Axonal transport: cargo-specific mechanisms of motility and regulation. *Neuron*, *84*(2), 292-309. https://doi.org/10.1016/j.neuron.2014.10.019

Maldonado-Baez, L., Cole, N. B., Kramer, H., & Donaldson, J. G. (2013). Microtubule-dependent endosomal sorting of clathrin-independent cargo by Hook1. *Journal of Cell Biology*, *201*(2), 233-247. https://doi.org/10.1083/jcb.201208172

Malone, C. J., Misner, L., Bot, N. L., Tsai, M.-C., Campbell, J. M., Ahringer, J., & White, J. G. (2003). The C. elegans Hook Protein, ZYG-12, Mediates the Essential Attachment between the Centrosome and Nucleus. *Cell*, *115*, 825-836.

Markus, S. M., Marzo, M. G., & McKenney, R. J. (2020). New insights into the mechanism of dynein motor regulation by lissencephaly-1. *Elife*, *9*. https://doi.org/10.7554/eLife.59737

Mauser, J. F., & Prehoda, K. E. (2012). Inscuteable regulates the Pins-Mud spindle orientation pathway. *PLoS One*, *7*(1), e29611. https://doi.org/10.1371/journal.pone.0029611

McIntosh, J. R. (2016). Mitosis. *Cold Spring Harbor Perspectives in Biology*, *8*(9). https://doi.org/10.1101/cshperspect.a023218

McIntosh, J. R., & Hays, T. (2016). A Brief History of Research on Mitotic Mechanisms. *Biology*, *5*(4). https://doi.org/10.3390/biology5040055

McKenney, R. J., Huynh, W., Tanenbaum, M. E., Bhabha, G., & Vale, R. D. (2011). Activation of cytoplasmic dynein motility by dynactin-cargo adapter complexes. *Biochemical Society Transactions*, *39*(5), 1169-1178. https://doi.org/10.1042/BST0391169

McKenney, R. J., Huynh, W., Tanenbaum, M. E., Bhabha, G., & Vale, R. D. (2014). Activation of cytoplasmic dynein motility by dynactin-cargo adapter complexes. *Science*.

McKenney, R. J., Vershinin, M., Kunwar, A., Vallee, R. B., & Gross, S. P. (2010). LIS1 and NudE induce a persistent dynein force-producing state. *Cell*, *141*(2), 304-314. https://doi.org/10.1016/j.cell.2010.02.035

McKenney, R. J., Weil, S. J., Scherer, J., & Vallee, R. B. (2011). Mutually exclusive cytoplasmic dynein regulation by NudE-Lis1 and dynactin. *Journal of Biological Chemistry*, *286*(45), 39615-39622. https://doi.org/10.1074/jbc.M111.289017

McNally, F. J. (2013). Mechanisms of spindle positioning. *Journal of Cell Biology*, *200*(2), 131-140. https://doi.org/10.1083/jcb.201210007

Meraldi, P. (2016). Centrosomes in spindle organization and chromosome segregation: a mechanistic view. *Chromosome Research*, *24*(1), 19-34. https://doi.org/10.1007/s10577-015-9508-2

Middelkoop, T. C., Neipel, J., Cornell, C. E., Naumann, R., Pimpale, L. G., Jülicher, F., & Grill, S. W. (2023). A cytokinetic ring-driven cell rotation achieves Hertwig's rule in early development. *bioRxiv*. https://doi.org/10.1101/2023.06.23.546115

Miller, K. G., Emerson, M. D., McManus, J. R., & Rand, J. B. (2000). RIC-8 (Synembryn): A Novel Conserved Protein that Is Required for Gqα Signaling in the C. elegans Nervous System. *Neuron*, *27*(2), 289-299. https://doi.org/10.1016/s0896-6273(00)00037-4

Minn, I. L., Rolls, M. M., Hanna-Rose, W., & Malone, C. J. (2009). SUN-1 and ZYG-12, mediators of centrosome-nucleus attachment, are a functional SUN/KASH pair in *Caenorhabditis elegans*. *Molecular Biology of the Cell* *20*(21), 4586-4595. https://doi.org/10.1091/mbc.e08-10-1034

Mizumoto, K., & Sawa, H. (2007). Cortical beta-catenin and APC regulate asymmetric nuclear beta-catenin localization during asymmetric cell division in *C. elegans*. *Developmental Cell*, *12*(2), 287-299. https://doi.org/10.1016/j.devcel.2007.01.004

Moreci, R. S., & Lechler, T. (2021). KIF18B is a cell-type specific regulator of spindle orientation in the epidermis. *Molecular Biology of the Cell*. https://doi.org/10.1101/2021.06.03.446990

Morena, J., Gupta, A., & Hoyle, J. C. (2019). Charcot-Marie-Tooth: From Molecules to Therapy. *International Journal of Molecular Sciences*, *20*(14), 3419. https://doi.org/10.3390/ijms20143419

Morgan, J. L., Yeager, A., Estelle, A. B., Gsponer, J., & Barbar, E. (2021). Transient Tertiary Structures of Disordered Dynein Intermediate Chain Regulate its Interactions with Multiple Partners. *Journal of Molecular Biology* 167152. https://doi.org/10.1016/j.jmb.2021.167152

Morin, X., Jaouen, F., & Durbec, P. (2007). Control of planar divisions by the G-protein regulator LGN maintains progenitors in the chick neuroepithelium. *Nature Neuroscience*, *10*, 1440-1448. https://doi.org/doi.org/10.1038/nn1984

Nguyen-Ngoc, T., Afshar, K., & Gonczy, P. (2007). Coupling of cortical dynein and G alpha proteins mediates spindle positioning in Caenorhabditis elegans. *Nature Cell Biology*, *9*(11), 1294-1302. https://doi.org/10.1038/ncb1649

Noatynska, A., Gotta, M., & Meraldi, P. (2012). Mitotic spindle (DIS)orientation and DISease: cause or consequence? *Journal of Cell Biology*, *199*(7), 1025-1035. https://doi.org/10.1083/jcb.201209015

Ohkura, H. (2015). Meiosis: an overview of key differences from mitosis. *Cold Spring Harbor Perspectives in Biology*, *7*(5). https://doi.org/10.1101/cshperspect.a015859

Okada, K., Iyer, B. R., Lammers, L. G., Gutierrez, P., Li, W., Markus, S. M., & McKenney, R. J. (2023). Conserved Roles for the Dynein Intermediate Chain and Ndel1 in Assembly and Activation of Dynein. *bioRxiv*. https://doi.org/10.1101/2023.01.13.523097

Olenick, M. A., Tokito, M., Boczkowska, M., Dominguez, R., & Holzbaur, E. L. (2016). Hook Adaptors Induce Unidirectional Processive Motility by Enhancing the Dynein-Dynactin Interaction. *Journal of Biological Chemistry*, *291*(35), 18239-18251. https://doi.org/10.1074/jbc.M116.738211

Oliferenko, S., Chew, T. G., & Balasubramanian, M. K. (2009). Positioning cytokinesis. *Genes & Development*, *23*(6), 660-674. https://doi.org/10.1101/gad.1772009

Page, A. P., & Johnstone, I. L. (2007). The cuticle. *WormBook*, 1-15. https://doi.org/10.1895/wormbook.1.138.1

Paix, A., Folkmann, A., & Seydoux, G. (2017). Precision genome editing using CRISPR-Cas9 and linear repair templates in *C. elegans*. *Methods*, *121-122*, 86-93. https://doi.org/10.1016/j.ymeth.2017.03.023

Paix, A., Wang, Y., Smith, H. E., Lee, C.-Y. S., Calidas, D., Lu, T., Smith, J., Schmidt, H., Krause, M. W., & Seydoux, G. (2014). Scalable and Versatile Genome Editing Using Linear DNAs with Microhomology to Cas9 Sites in Caenorhabditis elegans. *Genetics*, *198*. https://doi.org/10.1534/genetics.114.170423

Park, D. H., & Rose, L. S. (2008). Dynamic localization of LIN-5 and GPR-1/2 to cortical force generation domains during spindle positioning. *Developmental Biology*, *315*(1), 42-54. https://doi.org/10.1016/j.ydbio.2007.11.037

Paschal, B. M., Shpetner, H. S., & Vallee, R. (1987). MAP 1C is a microtubule-activated ATPase which translocates microtubules in vitro and has dynein-like properties. *Journal of Cell Biology*. https://doi.org/10.1083/jcb.105.3.1273

Pasti, G., & Labouesse, M. (2014). Epithelial junctions, cytoskeleton, and polarity. *WormBook*, 1-35. https://doi.org/10.1895/wormbook.1.56.2

Petzold, J., & Gentleman, E. (2021). Intrinsic Mechanical Cues and Their Impact on Stem Cells and Embryogenesis. *Frontiers in Cell and Developmental Biology*, *9*, 761871. https://doi.org/10.3389/fcell.2021.761871

Peyre, E., Jaouen, F., Saadaoui, M., Haren, L., Merdes, A., Durbec, P., & Morin, X. (2011). A lateral belt of cortical LGN and NuMA guides mitotic spindle movements and planar division in neuroepithelial cells. *Journal of Cell Biology*, *193*(1), 141-154. https://doi.org/10.1083/jcb.201101039

Pfister, K. K., & Lo, K. W. H. (2012). Cytoplasmic Dynein Function Defined by Subunit Composition. In *Dyneins* (pp. 424-439). https://doi.org/10.1016/b978-0-12-382004-4.10015-9

Pietro, F., Echard, A., & Morin, X. (2016). Regulation of mitotic spindle orientation: an integrated view. *EMBO reports*, *17*(8), 1106-1130. https://doi.org/10.15252/embr.201642292

Polit, A., Mystek, P., & Błasiak, E. (2021). Every Detail Matters. That Is, How the Interaction between Gα Proteins and Membrane Affects Their Function. *Membranes*, *11*(3), 222. https://doi.org/10.3390/membranes11030222

Pollard, T. D., & Goldman, R. D. (2018). Overview of the Cytoskeleton from an Evolutionary Perspective. *Cold Spring Harbor Perspectives in Biology* *10*(7). https://doi.org/10.1101/cshperspect.a030288

Portegijs, V., Fielmich, L.-E., Galli, M., Schmidt, R., Muñoz, J., Van Mourik, T., Akhmanova, A., Heck, A. J. R., Boxem, M., & Van Den Heuvel, S. (2016). Multisite Phosphorylation of NuMA-Related LIN-5 Controls Mitotic Spindle Positioning in *C.*

elegans. *PLOS Genetics*, *12*(10), e1006291. https://doi.org/10.1371/journal.pgen.1006291

Pupo, E., Avanzato, D., Scianna, M., Oldani, A., Serini, G., & Lanzetti, L. (2018). Kinesin-2 Controls the Motility of RAB5 Endosomes and Their Association with the Spindle in Mitosis. *International Journal of Molecular Sciences*, *19*(9), 2575. https://doi.org/10.3390/ijms19092575

Pylypenko, O., Hammich, H., Yu, I. M., & Houdusse, A. (2018). Rab GTPases and their interacting protein partners: Structural insights into Rab functional diversity. *Small GTPases*, *9*(1-2), 22-48. https://doi.org/10.1080/21541248.2017.1336191

Quintin, S., Gally, C., & Labouesse, M. (2016). Noncentrosomal microtubules in *C. elegans* epithelia. *Genesis*, *54*(4), 229-242. https://doi.org/10.1002/dvg.22921

Raaijmakers, J. A., & Medema, R. H. (2014). Function and regulation of dynein in mitotic chromosome segregation. *Chromosoma*, *123*(5), 407-422. https://doi.org/10.1007/s00412-014-0468-7

Reck-Peterson, S. L. (2015). Dynactin revealed. *Nature Structural & Molecular Biology*, *22*(5), 359-360. https://doi.org/10.1038/nsmb.3022

Reck-Peterson, S. L., Redwine, W. B., Vale, R. D., & Carter, A. P. (2018). The cytoplasmic dynein transport machinery and its many cargoes. *Nature Reviews of Molecular and Cellular Biology*, *19*(6), 382-398. https://doi.org/10.1038/s41580-018-0004-3

Redemann, S., Pecreaux, J., Goehring, N. W., Khairy, K., Stelzer, E. H., Hyman, A. A., & Howard, J. (2010). Membrane invaginations reveal cortical sites that pull on mitotic spindles in one-cell C. elegans embryos. *PLoS One*, *5*(8), e12301. https://doi.org/10.1371/journal.pone.0012301

Redpath, G. M. I., & Ananthanarayanan, V. (2023). Endosomal sorting sorted - motors, adaptors and lessons from in vitro and cellular studies. *Journal of Cell Science*, *136*(5). https://doi.org/10.1242/jcs.260749

Redpath, G. M. I., Betzler, V. M., Rossatti, P., & Rossy, J. (2020). Membrane Heterogeneity Controls Cellular Endocytic Trafficking. *Frontiers in Cell and Developmental Biology*, *8*, 757. https://doi.org/10.3389/fcell.2020.00757

Redwine, W. B., DeSantis, M. E., Hollyer, I., Htet, Z. M., Tran, P. T., Swanson, S. K., Florens, L., Washburn, M. P., & Reck-Peterson, S. L. (2017). The human cytoplasmic dynein interactome reveals novel activators of motility. *Elife*, *6*. https://doi.org/10.7554/eLife.28257

Renna, C., Rizzelli, F., Carminati, M., Gaddoni, C., Pirovano, L., Cecatiello, V., Pasqualato, S., & Mapelli, M. (2020). Organizational Principles of the NuMA-Dynein Interaction Interface and Implications for Mitotic Spindle Functions. *Structure*, *28*(7), 820-829 e826. https://doi.org/10.1016/j.str.2020.04.017

Roberts, A. J. (2018). Emerging mechanisms of dynein transport in the cytoplasm versus the cilium. *Biochemical Society Transactions*, *46*(4), 967-982. https://doi.org/10.1042/BST20170568

Roberts, A. J., Kon, T., Knight, P. J., Sutoh, K., & Burgess, S. A. (2013). Functions and mechanics of dynein motor proteins. *Nature Reviews Molecular Cell Biology*, *14*(11), 713-726. https://doi.org/10.1038/nrm3667

Roberts, R. L., Barbieri, M. A., Pryse, K. M., Chua, M., Morisaki, J. H., & Stahl, P. D. (1999). Endosome fusion in living cells overexpressing GFP-rab5. *Journal of Cell Science*, *112*(21), 3367 - 3675. https://doi.org/doi.org/10.1242/jcs.112.21.3667

Rocha, H. (2019). *Identification of Novel Conserved Dynein Pathway Genes Using a Genome-wide Synthetic Lethal Screen in C. elegans* Universidade do Porto].

Rodriguez-Garcia, R., Chesneau, L., Pastezeur, S., Roul, J., Tramier, M., & Pecreaux, J. (2018). The polarity-induced force imbalance in Caenorhabditis elegans embryos is caused by asymmetric binding rates of dynein to the cortex. *Molecular Biology of the Cell*, *29*(26), 3093-3104. https://doi.org/10.1091/mbc.E17-11-0653

Saadaoui, M., Machicoane, M., Di Pietro, F., Etoc, F., Echard, A., & Morin, X. (2014). Dlg1 controls planar spindle orientation in the neuroepithelium through direct interaction with LGN. *Journal of Cell Biology*, *206*(6), 707-717. https://doi.org/10.1083/jcb.201405060

Sanchez-Huertas, C., Freixo, F., Viais, R., Lacasa, C., Soriano, E., & Luders, J. (2016). Non-centrosomal nucleation mediated by augmin organizes microtubules in post-mitotic neurons and controls axonal microtubule polarity. *Nature Communications*, *7*, 12187. https://doi.org/10.1038/ncomms12187

Sato, A., Isaac, B., Phillips, C. M., Rillo, R., Carlton, P. M., Wynne, D. J., Kasad, R. A., & Dernburg, A. F. (2009). Cytoskeletal forces span the nuclear envelope to coordinate meiotic chromosome pairing and synapsis. *Cell*, *139*(5), 907-919. https://doi.org/10.1016/j.cell.2009.10.039

Sawa, H. (2012). Control of cell polarity and asymmetric division in C. elegans. *Current Topics in Developmental Biology*, *101*, 55-76. https://doi.org/10.1016/B978-0-12-394592-1.00003-X

Schlager, M. A., Hoang, H. T., Urnavicius, L., Bullock, S. L., & Carter, A. P. (2014). In vitro reconstitution of a highly processive recombinant human dynein complex. *EMBO Journal*, *33*(17), 1855-1868. https://doi.org/10.15252/embj.201488792

Schlager, M. A., Serra-Marques, A., Grigoriev, I., Gumy, L. F., da Silva, M. E., Wulf, P. S., Akhmanova, A., & Hoogenraad, C. C. (2014). Bicaudal d family adaptor proteins control the velocity of Dynein-based movements. *Cell Reports*, *8*(5), 1248-1256. https://doi.org/10.1016/j.celrep.2014.07.052

Schmidt, D. J., Rose, D. J., Saxton, W. M., & Strome, S. (2005). Functional analysis of cytoplasmic dynein heavy chain in Caenorhabditis elegans with fast-acting temperature-sensitive mutations. *Molecular Biology of the Cell*, *16*(3), 1200-1212. https://doi.org/10.1091/mbc.e04-06-0523

Schroeder, C. M., Ostrem, J. M., Hertz, N. T., & Vale, R. D. (2014). A Ras-like domain in the light intermediate chain bridges the dynein motor to a cargo-binding region. *Elife*, *3*, e03351. https://doi.org/10.7554/eLife.03351

Schroeder, C. M., & Vale, R. D. (2016). Assembly and activation of dynein-dynactin by the cargo adaptor protein Hook3. *Journal of Cell Biology*, *214*(3), 309-318. https://doi.org/10.1083/jcb.201604002

Schroer, T. A. (2004). Dynactin. *Annual Review of Cell and Developmental Biology*, *20*, 759-779. https://doi.org/10.1146/annurev.cellbio.20.012103.094623

Schroer, T. A., & Sheetz, M. P. (1991). Two activators of microtubule-based vesicle transport. *The Journal of Cell Biology*, *115*(5), 1309-1318. https://doi.org/10.1083/jcb.115.5.1309

Schuster, M., Kilaru, S., Fink, G., Collemare, J., Roger, Y., & Steinberg, G. (2011). Kinesin-3 and dynein cooperate in long-range retrograde endosome motility along a

nonuniform microtubule array. *Molecular Biology of the Cell*, *22*(19), 3645-3657. https://doi.org/10.1091/mbc.e11-03-0217

Shaye, D. D., & Greenwald, I. (2011). OrthoList: a compendium of C. elegans genes with human orthologs. *PLoS One*, *6*(5), e20085. https://doi.org/10.1371/journal.pone.0020085

Shearer, L. J., & Petersen, N. O. (2019). Distribution and Co-localization of endosome markers in cells. *Heliyon*, *5*(9), e02375. https://doi.org/10.1016/j.heliyon.2019.e02375

Short, B., Preisinger, C., Schaletzky, J., Kopajtich, R., & Barr, F. A. (2002). The Rab6 GTPase Regulates Recruitment of the Dynactin Complex to Golgi Membranes. *Current Biology*, *12*(20), 1792-1795. https://doi.org/10.1016/s0960-9822(02)01221-6

Siegrist, S. E., & Doe, C. Q. (2006). Extrinsic cues orient the cell division axis in Drosophila embryonic neuroblasts. *Development*, *133*(3), 529-536. https://doi.org/10.1242/dev.02211

Simões, P. A., Celestino, R., Carvalho, A. X., & Gassmann, R. (2018). NudE regulates dynein at kinetochores but is dispensable for other dynein functions in the *C. elegans* early embryo. *Journal of Cell Science*, *131*(1). https://doi.org/10.1242/jcs.212159

Simon, G. C., & Prekeris, R. (2008). The role of FIP3-dependent endosome transport during cytokinesis. *Communicative & Integrative Biology*, *1*(2), 132-133. https://doi.org/10.4161/cib.1.2.6864

Singh, K., Lau, C. K., Manigrasso, G., Gama, J. B., Gassmann, R., & Carter, A. P. (2023). Molecular mechanism of dynein-dynactin activation by JIP3 and LIS1. *bioRxiv*. https://doi.org/10.1101/2022.08.17.504273

Sladewski, T. E., Billington, N., Ali, M. Y., Bookwalter, C. S., Lu, H., Krementsova, E. B., Schroer, T. A., & Trybus, K. M. (2018). Recruitment of two dyneins to an mRNA-dependent Bicaudal D transport complex. *Elife*, *7*. https://doi.org/10.7554/eLife.36306

Spronsen, M. v., Mikhaylova, M., Lipka, J., Schlager, M. A., Heuvel, D. J. v. d., Kuijpers, M., Wulf, P. S., Keijzer, N., Demmers, J., Kapitein, L. C., Jaarsma, D., Gerritsen, H. C.,

Akhmanova, A., & Hoogenraad, C. C. (2013). TRAK/Milton Motor-Adaptor Proteins Steer Mitochondrial Trafficking to Axons and Dendrites. *Neuron*, *77*(3), 485-502. https://doi.org/10.1016/j.neuron.2012.11.027

Srinivasan, D. G., Fisk, R. M., Xu, H., & Van Den Heuvel, S. (2003). A complex of LIN-5 and GPR proteins regulates G protein signaling and spindle function inC. elegans. *Genes & Development*, *17*(10), 1225-1239. https://doi.org/10.1101/gad.1081203

Stenmark, H., Parton, R. G., Steele-Mortimer, O., Lutcke, A., Gruenberg, J., & Zerial, M. (1994). Inhibition of rab5 GTPase activity stimulates membrane fusion in endocytosis. *EMBO J*, *13*(6), 1287-1296. https://doi.org/10.1002/j.1460-2075.1994.tb06381.x

Strauss, B., Adams, R. J., & Papalopulu, N. (2006). A default mechanism of spindle orientation based on cell shape is sufficient to generate cell fate diversity in polarisedXenopusblastomeres. *Development*, *133*(19), 3883-3893. https://doi.org/10.1242/dev.02578

Su, W.-H., Mruk, D. D., Wong, E. W. P., Lui, W.-Y., & Cheng, C. Y. (2013). Polarity Protein Complex Scribble/Lgl/Dlg And Epithelial Cell Barriers. *Advances in Experimental Medicine and Biology*, 149-170. https://doi.org/10.1007/978-1-4614-4711-5_7

Sugioka, K., Mizumoto, K., & Sawa, H. (2011). Wnt regulates spindle asymmetry to generate asymmetric nuclear beta-catenin in C. elegans. *Cell*, *146*(6), 942-954. https://doi.org/10.1016/j.cell.2011.07.043

Sulston, J. E., & Horvitz, H. R. (1977). Post-embryonic cell lineages of the nematode, Caenorhabditis elegans. *Developmental Biology*, *56*(1), 110-156. https://doi.org/https://doi.org/10.1016/0012-1606(77)90158-0

Sunchu, B., & Cabernard, C. (2020). Principles and mechanisms of asymmetric cell division. *Development*, *147*(13). https://doi.org/10.1242/dev.167650

Sweeney, H. L., & Holzbaur, E. L. F. (2018). Motor Proteins. *Cold Spring Harbor Perspectives in Biology 10*(5). https://doi.org/10.1101/cshperspect.a021931

Tabassum, D. P., & Polyak, K. (2015). Tumorigenesis: it takes a village. *Nature Reviews Cancer*, *15*, 473-483. https://doi.org/https://doi.org/10.1038/nrc3971

Tanenbaum, M. E., & Medema, R. H. (2010). Mechanisms of centrosome separation and bipolar spindle assembly. *Developmental Cell*, *19*(6), 797-806. https://doi.org/10.1016/j.devcel.2010.11.011

Tapley, E. C., & Starr, D. A. (2013). Connecting the nucleus to the cytoskeleton by SUN–KASH bridges across the nuclear envelope. *Current Opinion in Cell Biology*, *25*(1), 57-62. https://doi.org/10.1016/j.ceb.2012.10.014

Terns, R. M., Kroll-Conner, P., Zhu, J., Chung, S., & Rothman, J. H. (1997). A Deficiency Screen for Zygotic Loci Required for Establishment and Patterning of the Epidermis in Caenorhabditis elegans. *Genetics*, *146*(1), 185-206. https://doi.org/10.1093/genetics/146.1.185

Thawani, A., & Petry, S. (2021). Molecular insight into how γ-TuRC makes microtubules. *Journal of Cell Science*, *134*(14). https://doi.org/10.1242/jcs.245464

Torisawa, T., Ichikawa, M., Furuta, A., Saito, K., Oiwa, K., Kojima, H., Toyoshima, Y. Y., & Furuta, K. y. (2014). Autoinhibition and cooperative activation mechanisms of cytoplasmic dynein. *Nature Cell Biology*(16), 1118-1124. https://doi.org/https://doi.org/10.1038/ncb3048

Toropova, K., Zou, S., Roberts, A. J., Redwine, W. B., Goodman, B. S., Reck-Peterson, S. L., & Leschziner, A. E. (2014). Lis1 regulates dynein by sterically blocking its mechanochemical cycle. *Elife*, *3*. https://doi.org/10.7554/eLife.03372

Tripathy, S. K., Weil, S. J., Chen, C., Anand, P., Vallee, R. B., & Gross, S. P. (2014). Autoregulatory mechanism for dynactin control of processive and diffusive dynein transport. *Nature Cell Biology*, *16*(12), 1192-1201. https://doi.org/10.1038/ncb3063

Trokter, M., Mucke, N., & Surrey, T. (2012). Reconstitution of the human cytoplasmic dynein complex. *Proc Natl Acad Sci U S A*, *109*(51), 20895-20900. https://doi.org/10.1073/pnas.1210573110

Trokter, M., Mücke, N., & Surrey, T. (2012). Reconstitution of the human cytoplasmic dynein complex. *Proceedings of the National Academy of Sciences*, *109*(51), 20895-20900. https://doi.org/10.1073/pnas.1210573110

Tsou, M.-F. B., Hayashi, A., & Rose, L. S. (2003). LET-99 opposes Gα/GPR signaling to generate asymmetry for spindle positioning in response to PAR and MES-1/SRC-1 signaling. *Development*, *130*(23), 5717-5730. https://doi.org/10.1242/dev.00790

Ueno, H., Huang, X., Tanaka, Y., & Hirokawa, N. (2011). KIF16B/Rab14 molecular motor complex is critical for early embryonic development by transporting FGF receptor. *Developmental Cell*, *20*(1), 60-71. https://doi.org/10.1016/j.devcel.2010.11.008

Urnavicius, L., Lau, C. K., Elshenawy, M. M., Morales-Rios, E., Motz, C., Yildiz, A., & Carter, A. P. (2018). Cryo-EM shows how dynactin recruits two dyneins for faster movement. *Nature*, *554*(7691), 202-206. https://doi.org/10.1038/nature25462

Urnavicius, L., Zhang, K., Diamant, A. G., Motz, C., Schlager, M. A., Yu, C. J., Patel, N. A., Robinson, C. V., & Carter, A. P. (2015). The structure of the dynactin complex and its interaction with dynein. *Science*.

Valdez, V. A., Neahring, L., Petry, S., & Dumont, S. (2023). Mechanisms underlying spindle assembly and robustness. *Nature Reviews Molecular Cell Biology*, *24*, 523-542. https://doi.org/https://doi.org/10.1038/s41580-023-00584-0

Van Ijzendoorn, S. C. D. (2006). Recycling endosomes. *Journal of Cell Science*, *119*(9), 1679-1681. https://doi.org/10.1242/jcs.02948

Vaughan, K. T., & Vallee, R. B. (1995). Cytoplasmic dynein binds dynactin through a direct interaction between the intermediate chains and p150Glued. *Journal of Cell Biology*, *131*(6), 1507-1516. https://doi.org/10.1083/jcb.131.6.1507

Villari, G., Enrico Bena, C., Del Giudice, M., Gioelli, N., Sandri, C., Camillo, C., Fiorio Pla, A., Bosia, C., & Serini, G. (2020). Distinct retrograde microtubule motor sets drive early and late endosome transport. *EMBO Journal*, *39*(24), e103661. https://doi.org/10.15252/embj.2019103661

Wagers, A. J., Christensen, J. L., & Weissman, I. L. (2002). Cell fate determination from stem cells. *Gene Therapy*, *9*, 606-612. https://doi.org/https://doi.org/10.1038/sj.gt.3301717

Walczak, C. E., Gayek, S., & Ohi, R. (2013). Microtubule-depolymerizing kinesins. *Annual Review of Cell and Developmental Biology*, *29*, 417-441. https://doi.org/10.1146/annurev-cellbio-101512-122345

Walenta, J. H., Didier, A. J., Liu, X., & Krämer, H. (2001). The Golgi-Associated Hook3 Protein Is a Member of a Novel Family of Microtubule-Binding Proteins. *The Journal of Cell Biology*, *152*(5), 923-934. https://doi.org/10.1083/jcb.152.5.923

Wandinger-Ness, A., & Zerial, M. (2014). Rab proteins and the compartmentalization of the endosomal system. *Cold Spring Harbor Perspectives in Biology*, *6*(11), a022616. https://doi.org/10.1101/cshperspect.a022616

Wang, S., Ketcham, S. A., Schon, A., Goodman, B., Wang, Y., Yates, J., 3rd, Freire, E., Schroer, T. A., & Zheng, Y. (2013). Nudel/NudE and Lis1 promote dynein and dynactin interaction in the context of spindle morphogenesis. *Molecular Biology of the Cell*, *24*(22), 3522-3533. https://doi.org/10.1091/mbc.E13-05-0283

Wang, S., Wu, D., Quintin, S., Green, R. A., Cheerambathur, D. K., Ochoa, S. D., Desai, A., & Oegema, K. (2015). NOCA-1 functions with gamma-tubulin and in parallel to Patronin to assemble non-centrosomal microtubule arrays in C. elegans. *Elife*, *4*, e08649. https://doi.org/10.7554/eLife.08649

Wang, Y., Huynh, W., Skokan, T. D., & Vale, R. D. (2018). A new calcium-activated dynein adaptor protein, CRACR2a, regulates clathrinindependent endocytic traffic in T cells. *bioRxiv*. https://doi.org/10.1101/354498

Wanschers, B., Van De Vorstenbosch, R., Wijers, M., Wieringa, B., King, S. M., & Fransen, J. (2008). Rab6 family proteins interact with the dynein light chain protein DYNLRB1. *Cell Motility and the Cytoskeleton*, *65*(3), 183-196. https://doi.org/10.1002/cm.20254

Werts, A. D., Roh-Johnson, M., & Goldstein, B. (2011). Dynamic localization of C. elegans TPR-GoLoco proteins mediates mitotic spindle orientation by extrinsic signaling. *Development*, *138*(20), 4411-4422. https://doi.org/10.1242/dev.070979

Wildwater, M., Sander, N., de Vreede, G., & van den Heuvel, S. (2011). Cell shape and Wnt signaling redundantly control the division axis of C. elegans epithelial stem cells. *Development*, *138*(20), 4375-4385. https://doi.org/10.1242/dev.066431

Williams, S. E., & Fuchs, E. (2013). Oriented divisions, fate decisions. *Current Opinion in Cell Biology*, *25*(6), 749-758. https://doi.org/10.1016/j.ceb.2013.08.003

Xiang, X., Qiu, R., Yao, X., Arst, H. N., Jr., Penalva, M. A., & Zhang, J. (2015). Cytoplasmic dynein and early endosome transport. *Cellular and Molecular Life Sciences*, *72*(17), 3267-3280. https://doi.org/10.1007/s00018-015-1926-y

Xu, L., Sowa, M. E., Chen, J., Li, X., Gygi, S. P., & Harper, J. W. (2008). An FTS/Hook/p107(FHIP) complex interacts with and promotes endosomal clustering

by the homotypic vacuolar protein sorting complex. *Molecular Biology of the Cell*, *19*(12), 5059-5071. https://doi.org/10.1091/mbc.e08-05-0473

Yamamoto, Y., Takeshita, H., & Sawa, H. (2011). Multiple Wnts Redundantly Control Polarity Orientation in Caenorhabditis elegans Epithelial Stem Cells. *PLOS Genetics*, *7*(10), e1002308. https://doi.org/10.1371/journal.pgen.1002308

Yao, X., Wang, X., & Xiang, X. (2014). FHIP and FTS proteins are critical for dynein-mediated transport of early endosomes in Aspergillus. *Molecular Biology of the Cell*, *25*(14), 2181-2189. https://doi.org/10.1091/mbc.e14-04-0873

Yap, C. C., Digilio, L., McMahon, L. P., Wang, T., & Winckler, B. (2022). Dynein Is Required for Rab7-Dependent Endosome Maturation, Retrograde Dendritic Transport, and Degradation. *Journal of Neurosciences*, *42*(22), 4415-4434. https://doi.org/10.1523/JNEUROSCI.2530-21.2022

Yildiz, A., & Zhao, Y. (2023). Dyneins. *Current Biology*, *33*(24), R1274-R1279. https://doi.org/10.1016/j.cub.2023.10.064

Yuan, W., & Song, C. (2020). The Emerging Role of Rab5 in Membrane Receptor Trafficking and Signaling Pathways. *Biochemistry Research International*, *2020*, 1-10. https://doi.org/10.1155/2020/4186308

Zhang, H., Skop, A. R., & White, J. G. (2008). Src and Wnt signaling regulate dynactin accumulation to the P2-EMS cell border in C. elegans embryos. *Journal of Cell Science*, *121*(Pt 2), 155-161. https://doi.org/10.1242/jcs.015966

Zhang, H., Squirrell, J. M., & White, J. G. (2008). RAB-11 permissively regulates spindle alignment by modulating metaphase microtubule dynamics in Caenorhabditis elegans early embryos. *Molecular Biology of the Cell*, *19*(6), 2553-2565. https://doi.org/10.1091/mbc.E07-09-0862

Zhang, J., Qiu, R., Arst, H. N., Jr., Penalva, M. A., & Xiang, X. (2014). HookA is a novel dynein-early endosome linker critical for cargo movement in vivo. *Journal of Cell Biology*, *204*(6), 1009-1026. https://doi.org/10.1083/jcb.201308009

Zhang, K., Fishel Ben Kenan, R., Osakada, Y., Xu, W., Sinit, R. S., Chen, L., Zhao, X., Chen, J. Y., Cui, B., & Wu, C. (2013). Defective axonal transport of Rab7 GTPase results in dysregulated trophic signaling. *Journal of Neurosciences*, *33*(17), 7451-7462. https://doi.org/10.1523/JNEUROSCI.4322-12.2013

Zhang, M. L., Ti, H. Y., Wang, P. Y., & Li, H. (2021). Intracellular transport dynamics revealed by single-particle tracking. *Biophysic Reports*, *7*(5), 413-427. https://doi.org/10.52601/bpr.2021.210035

Zhou, C., Brian, Jay, Eldakak, A., Rubinstein, B., & Li, R. (2011). Motility and Segregation of Hsp104-Associated Protein Aggregates in Budding Yeast. *Cell*, *147*(5), 1186-1196. https://doi.org/10.1016/j.cell.2011.11.002

Zhou, K., Rolls, M. M., Hall, D. H., Malone, C. J., & Hanna-Rose, W. (2009). A ZYG-12–dynein interaction at the nuclear envelope defines cytoskeletal architecture in the C. elegans gonad. *Journal of Cell Biology*, *186*(2), 229-241. https://doi.org/10.1083/jcb.200902101